The kinematics and mechanics of muscle's myofilament lattice

Sage Arlene Malingen

A dissertation
submitted in partial fulfillment of the
requirements for the degree of

Doctor of Philosophy

University of Washington

2020

Reading Committee:

Thomas Daniel, Chair

Michael Regnier

Julie Theriot

Program Authorized to Offer Degree:
Biology

University of Washington

Abstract

The kinematics and mechanics of muscle's myofilament lattice

Sage Arlene Malingen

Chair of the Supervisory Committee:
Thomas Daniel
Department of Biology

By integrating the actions of millions of molecular motors, muscle cells power the movements of entire organisms. This multiscale system is tuned both by the geometry of the lattice of sub-cellular molecular machinery and by the interactions of the body with the environment. In this thesis, we review the structure of the molecular machinery and the seminal theories of muscle contractility. We document the movements of the molecular machinery using x-ray diffraction in a naturally functioning organism, where multiscale interactions remain intact, revealing how the lattice changes shape as a result of nervous activation. And guided by the observed structure and motions of the lattice of molecular machinery, we use a finite element model to investigate the flow of fluid and the viscous drag forces between the molecular machinery and the surrounding cytosol. These studies are a window into the elegant sub-cellular mechanisms that give rise to diverse functions at the organism scale.

TABLE OF CONTENTS

ACKNOWLEDGEMENTS

Completing a Ph.D. was made possible by a host of people whom I could never thank enough. I am so grateful to Tom Daniel for accepting one more graduate student. I thought my goal in grad school was to finally focus on one thing, but instead you encouraged my curiosity to expand. You made this journey meaningful and fun. Members of the Daniel lab, my cohort and the third floor: I cannot imagine more intelligent and kind people to have spent these years with. My committee members, Julie Theriot, Mike Regnier, Clemens Cabernard and Jim Riley encouraged me to think broadly and provided timely advice. The Biology department as a whole is filled with warm and brilliant individuals, and in particular, Bing Brunton, Alison Mehravari and David Perkel, I am grateful for your candor. Before coming to UW my advisors Seppi and David Carroll pushed me to pursue opportunities beyond my wildest hopes – I wouldn't have tried without you.

I am grateful for an ARCS Foundation fellowship and the support of the ARCS community. The Bioengineering Training Grant provided helpful training opportunities, and the Summer School in Computational Physiology broadened my perspective.

I am thankful for the friends who filled my free time with laughter, pastries, and walks. My housemates, Marcello, Andrey, Sarah, and Gail, made each day happier. Jon, thank you for living vibrantly with me. Auntie Ri, for reminding me how capable I am. Grandpa Dale and Grandma Marian, I am so grateful for your love and encouragement. Shane, your passion for STEM has inspired me since you brought me with you to a computer science class. Dad, Mom, and Bree, you were there at every step, laughing along with the sitcom – you fill my life with delight, and I could never thank each of you enough for your love and support.

DEDICATION

to my family.

INTRODUCTION

Muscles create the forces that propel organisms through space. The molecular machinery that powers movement is remarkably conserved both across the tree of life and a diverse array of functional roles, from microscopic insects (Polilov 2015) to great blue whales and land-dwelling vertebrates that hop, walk, slither and fly. For instance, midges boast flight muscle contraction frequencies of 1,000 Hz (Sotavalta 1953). Meanwhile, the fastest recorded vertebrate muscles are all used for sonication. They include the muscles of the swim bladder of the toadfish midshipmen (200 Hz) (Rome et al. 1996), those bats use for echolocation (220 Hz) (Elemans et al. 2011, Ratcliffe et al. 2013) and the muscles which shake the rattle of the rattlesnake (90 Hz) (Rome et al. 1996). At another extreme, molluscan catch muscle is specialized to hold high forces long after muscle activation (Andruchov et al. 2006). The muscles of the barnacle *Balanus nubulis* are another striking example of muscle diversity, with diameters up to 3mm (Hoyle et al. 1973), which is much larger than entire microscopic insects that contain multiple muscle cells. What function does this extreme form serve, and what physical constraints does such a large size impose? These examples are only a small sliver of the diversity in muscle form and function across taxa. Additionally, individual muscles perform multiple functional roles for an organism under different operating conditions. For instance, human skeletal muscle can be observed at turns braking the body's fall, powering its rise, and stabilizing its motion (Dickinson et al. 2000). How does muscle's elegant molecular architecture enable such a vast array of specialized functions?

At its most fundamental level, muscle's contractile machinery integrates the actions of millions of molecular motors, each generating piconewton-scale forces, to produce large forces that culminate in finely tuned body movements. In contrast to a reductionist portrayal, it is increasingly recognized that organism scale factors influence the contractile machinery.

This means that forces at the organism scale feedback and affect the function of individual molecular motors residing within a highly structured, compliant latticework of proteins. The observation that muscle is a multiscale system has driven research forward along multiple lines, from nervous activation to the functional impact of fiber orientation and linkages between muscles, tendons, and skeletal components, to the motions of single motor molecules. However, integrating these snapshots of function at multiple scales into a cohesive whole remains an exciting vista. Ultimately, understanding muscle's multiscale interactions may contribute significantly to our understanding of how it accomplishes diverse functions using relatively conserved molecular machinery (Williams & Holt 2018).

Each muscle cell is composed of bundles of contractile machinery called myofibrils that, in the case of skeletal muscle, run from one end of the cell to the other. Myofibrils are composed of sarcomeres, the fundamental contractile unit, connected in series. Each sarcomere is composed of interdigitating myosin containing thick filaments and actin containing thin filaments mirrored about the center of the sarcomere (the m-line). Myosin molecular motors that branch off of the thick filaments bind to nearby actin containing thin filaments and pull them towards the center of the sarcomere. Myosin motors act like a ratchet powered by the hydrolysis of adenosine triphosphate (ATP). Myosin's initial binding to actin is favorable when it holds ADP and P_i (the byproducts of the ATP hydrolysis that facilitated its last unbinding from actin). ADP and P_i take up a great deal of space, and the release of P_i results in the motor forcefully changing shape and tugging on the actin containing thin filament. Myosin motors are ubiquitous in cells, with roles in maintaining tension, mediating transport, and promoting cell division. Muscle cells are unique in that myosin motors are arranged in a highly structured elastic lattice, which promotes cell shortening along the myofibril's axis. This foundational mechanism of contraction is known as the sliding filament hypothesis. In chapter 1 we review the sliding filament hypothesis and how it laid the foundation for our understanding of muscle's multiscale function. Notably, however, the sliding filament hypothesis fails to account for many features of muscle contraction, for instance, radial kinematics, filament stretching, differing packing ratios and sarcomere geometries, and much,

much more.

Fascinatingly, the exact shape of the sarcomere has ramifications for muscle function. For instance, the spacing between thick and thin filaments is not fixed. Instead, the compliant lattice can stretch both radially (Cecchi et al. 1990) and axially (Wakabayashi et al. 1994, Huxley et al. 1994, Goldman & Huxley 1994). The spacing of the lattice affects molecular motor binding probability and the force a muscle can generate, and in turn, molecular motor binding exerts radial compressive force (Cecchi & Bagni 1994). In fact, nanometer changes in lattice spacing may result in entirely different functional roles of muscles at the organism scale (Tune et al. 2020), and muscle function can vary along a temperature gradient, along with lattice spacing, in naturally functioning organisms (George et al. 2012). Similarly, the stretching of the thick and thin filaments as forces are generated leads to a shift in the register of molecular motors and potential binding sites, which may tune their binding probabilities (Daniel et al. 1998). In addition to modulating binding probabilities, the radial (Williams et al. 2012) and axial (Wakabayashi et al. 1994) elasticity of muscle is an important component of its function.

In Chapter 2 we recorded the time course of the lattice's dilation and filament stretching during the *in vivo* function of the flight muscle of *Manduca sexta*. Uniquely, we were able to capture this x-ray diffraction simultaneously with the endogenous nervous activation of the muscles, which allowed us to probe the time course of lattice kinematics following activation. While *in vivo* x-ray diffraction had been done previously in two other systems (insects with asynchronous flight muscle) (Iwamoto & Yagi 2013, Irving & Maughan 2000, Irving 2006), these systems use a unique mechanism that decouples nervous activation from muscle contraction such that one contraction elicits multiple cycles of shortening. Although this is an incredible adaptation for the rapid contractions demanded by the flight mechanics of small insects, we wondered what the kinematics of muscle's contractile machinery would be like in a synchronously activated system. We used the flight muscle of the hawkmoth *Manduca sexta*, whose flight muscle contraction is synchronously coupled to nervous activation, as a model system The function of this flight muscle is similar in many respects to

human cardiac muscle (Tu & Daniel 2004), and yet *Manduca sexta* is uniquely amenable to *in vivo* x-ray diffraction. These results showed a remarkable breadth of lattice motions across individuals, and yet these motions occur within a mechanically coupled system. We used machine learning models to look for connections between them, but our results indicated that there could be latent parameters driving the diversity of lattice kinematic combinations we measured. These latent variables could range from the relative timing of the antagonistic muscle's contraction to the temperature of the muscle itself.

The dilation of the lattice measured by x-ray diffraction does not necessarily coincide with the sarcomere's shortening to maintain a constant lattice volume. Instead, as muscle contracts, individual sarcomeres may push fluid into the intracellular volume, as implied by the conservation of mass. The movement of fluid in muscle cells has received relatively little attention. Fluid flow may be an important mechanism for substrate delivery in muscle cells, similar to other cell systems. For instance, plant cells use cytoplasmic streaming to move cell components (Goldstein et al. 2008), slime molds use fluid flow to guide their growth (Alim et al. 2013), and rapidly crawling cells use fluid flow to deliver building blocks to their growing front edge (Keren et al. 2009). However, the energetic gains of a convective advantage in substrate delivery could be outweighed by the cost of viscous drag forces between the contractile machinery and the cytosol. We used a Finite Element Analysis (FEA) model to approximate the flow of fluid inside of sarcomeres and estimate its energetic cost. Contrasting this FEA model of flow in a system with filaments with existing analytic models of fluid flow allowed us to gain insight into how the filaments structure the flow field. Our results indicated that the energy lost to viscous drag on the sliding filaments is likely small compared to the cell's overall energy budget. However, these estimates are limited by unknowns. For instance, parameters like the viscosity of the cytosol and the depth of the bound water on the filaments' surfaces are difficult to measure. Nonetheless, paired with the recent finding that fluid flow provides a convective advantage to the sarcomere (Cass et al. 2019), it seems that fluid flow may be a low-cost mechanism that enables rapid substrate transport, which is especially important for muscles with a high contraction frequency.

Our results also revealed that fluid flow may have other impacts on function. For example, the shearing of fluid on molecular motors will spatially and temporally vary across in the interfilament gap, and it is as yet unknown what functional impact shearing forces on motors might have. Given that the stretching of filaments impacts force development by realigning motors and available binding sites, it is not unreasonable to wonder if the reorientation of unbound molecular motors in the inter-filament space by viscous shearing might alter their binding kinetics. Since the nanometer-scale molecular motors near a point that the continuum approximation may break down, Brownian motions and colloid scale effects become relevant. Yet, at the cell scale bulk fluid flow must also be considered. Coupling models across the many scales that are functionally important for muscle is an interesting challenge. Existing spatially explicit models rely on Monte Carlo simulations as a proxy for stochastic motor binding. However, this computationally expensive modeling method doesn't scale well to whole muscle and tissue simulations. Meanwhile, PDE based heuristic models of cell twitches used in FEA models of whole organs currently don't allow feedback from the tissue scale back to the subcellular scale, which could dynamically alter muscle function. While modeling muscle's multiscale mechanics will be a significant challenge, success in this arena will yield enormous practical gains for human health, computing, and basic science.

In this thesis, we review muscle's structure and function from the scale of individual molecular motors to the whole sarcomere, highlighting its multiscale properties (chapter 1). We document the motions of the contractile lattice in a normally functioning animal (chapter 2), and, finally, we estimate how fluid flows in the lattice of molecular machinery, and how it impacts muscle's function (chapter 3).

Chapter 1

THE SLIDING FILAMENT THEORY SINCE ANDREW HUXLEY: MULTISCALE AND MULTIDISCIPLINARY MUSCLE RESEARCH

Powers JD*, Malingen SA*, Regnier MR & Daniel TL. Annual Review of Biophysics. 2020.
**** Denotes co-first authors.***

1.1 Introduction and History

Two papers published simultaneously in 1954 (Huxley & Niedergerke 1954, Huxley & Hanson 1954) independently showed that striated muscle shortens as a result of the sliding between two sets of filaments containing the proteins myosin and actin. Thus was born the sliding filament hypothesis. There have been a series of impressive and informative reviews of the history and basis of the sliding filament theory of muscle contraction (e.g., (Cooke 2004, Huxley 2004, Sellers 2004, Squire 2016)). Rather than attempting an expansion on those superb perspectives, we focus here on the central idea that muscle contraction is the output of a dynamical system spanning spatial and temporal scales from nanometers and microseconds to meters and minutes, integrating biochemical and mechanical regulation across scales.

Striated muscle's highly structured, nearly crystalline organization sets it apart among biological systems (Figure 1). Single muscle cells are portioned into subcellular elements (myofibrils) that are formed of a series of axially arranged sarcomeres, each consisting of interdigitating systems of axial filaments – the thick and thin filaments. Thin filaments, extending from Z-disks, contain a double-helical strand of actin monomers along with troponin/tropomyosin complexes that are involved in the regulation of contraction. The myosin molecular motors constitute the bulk of the thick filaments and extend radially in the form of a three-start helix.

Supporting evidence for the sliding filament hypothesis was established in a series of papers that melded experimental and theoretical studies of muscle contraction. First, early polarized light (Huxley & Taylor 1958) and electron microscopy (Huxley & Hanson 1954) evidence pointed to the structural overlap of thick and thin filaments, suggesting the idea that the force generation increases with greater filament overlap, an hypothesis that was tested in the classic studies of length-tension relationships first established by Gordon, Huxley and Julian in 1966 (Gordon et al. 1966).

With the goal of understanding the fundamental molecular mechanisms underlying cross-bridge force generation, Huxley established the two- and three-state model of myosin motor mechanics. This model formed an hypothesis that was tested in another landmark paper by Huxley and Simmons in 1971 (Huxley & Simmons 1971). Their goal was to probe cross-bridge mechano-chemistry using exceedingly rapid length perturbations of activated muscle fibers. This so-called "quick release" experiment has the underlying concept that a very rapid release of the tension borne by cross-bridges would drive their dissociation from the thin filament, or at least a change in their conformation. Any mechanical transients that would follow from that quick release would therefore represent the temporal dynamics of the mechano-chemistry of the cross-bridge (Figure 2). Moreover, very quick releases would allow one to probe the most rapid events associated with the cross-bridge cycle. Thus, the dynamics of force generation are characterized with several phases of tension recovery (T1, T2, T3 and T4 phases).

Rapid release as well as rapid stretch experiments continue today, contributing significantly to the experimental methods carried out on muscle fibers. These approaches have been complemented by a host of other experimental efforts including force measurements in isometric and isotonic conditions for muscle fibers that are either intact (and electrically activated) or chemically "skinned" and activated by controlling the concentrations of calcium and ATP. In addition, the advent of powerful tools such as time-resolved X-ray diffractometry or optical tweezers for manipulating or measuring processes at the nanometer scale have yielded significant insight into the dynamics of force production of single molecules (Spudich

2001).

The current paradigm for muscle contraction built upon the sliding filament hypothesis and more than fifty years of research since has culminated in a generally accepted view of muscle contraction (for reviews see: (Gordon et al. 2000) and (Spudich 2001)). Briefly, the notion held by the field today is that cross-bridges use chemical energy derived from ATP hydrolysis to drive axial sliding motion between the thick and thin filaments. The sliding of the filaments is regulated by electrical, chemical, and structural components. Electrical activation of the cell leads to depolarization in the T-tubules, the opening of calcium channels, and the subsequent calcium-induced release of calcium from the sarcoplasmic reticulum into the myofibril (in an elegant process termed E-C coupling). While the muscle is relaxed, the troponin-tropomyosin complex blocks myosin-binding sites on the thin filament. But when calcium enters the system it binds with the troponin-tropomyosin complex, inducing a conformational change that reveals the binding sites and allows cross-bridges to form. Upon binding, cross-bridges release mechanical strain energy derived from ATP hydrolysis and generate force, which drives muscle contraction.

In the sections that follow, we review both current and past research efforts with an eye towards highlighting the multi-scale features of muscle, and the multidisciplinary approach investigators have used. Beginning with molecular levels of organization and culminating in cellular and tissue scales, we summarize selected experimental and theoretical approaches that have shaped our understanding of muscle function.

1.2 The molecular driver of filament sliding: Single myosin structure, kinetics, & mechanics

The linchpin theory of cross-bridges acting as independent force generators and the model developed by Huxley and Simmons in 1971 (Huxley & Simmons 1971) stands unique among the other theories of muscle contraction emerging at the time in that it accounts for the following characteristics of muscle contraction (Huxley 1974): 1) the dependence of tension on the extent of filament overlap, 2) the maximum speed of shortening is independent of filament

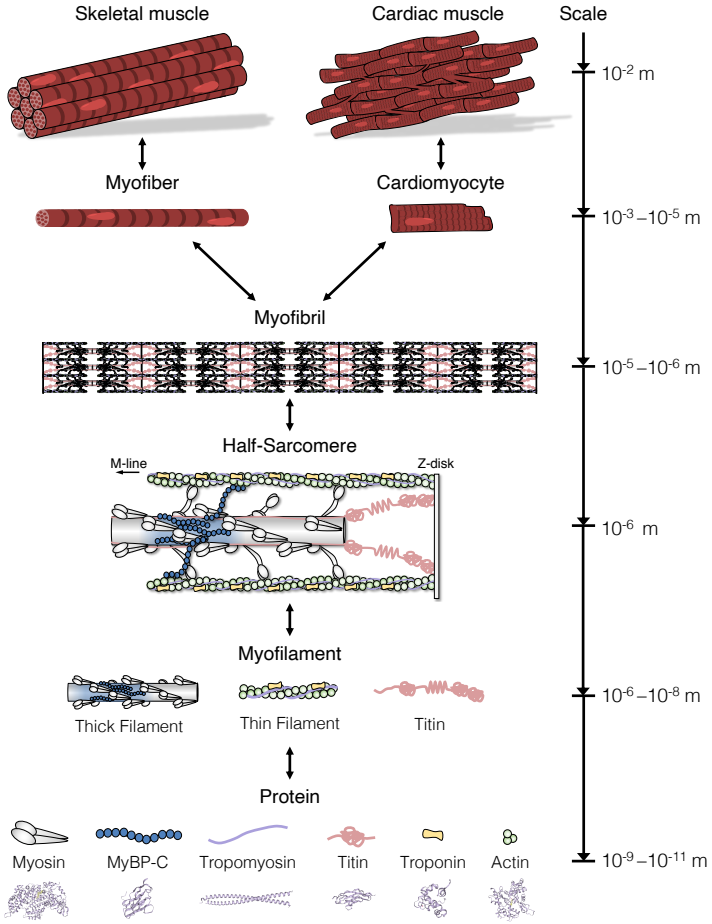

Figure 1.1: **An illustration of striated muscle across spatial scales.** Generally, skeletal and cardiac muscles are made up of myofibers and cardiomyocytes (respectively) that span tens of microns to tens of millimeters. The subcellular contractile organelle, the myofibril, is structurally similar in myofibers and cardiomyocytes, and is on the order of microns. The myofibril is composed of many serially linked sarcomeres (the half-sarcomere is shown for simplicity), each approximately 2–3 microns long. The three main myofilaments that comprise the sarcomere, the thick filament, the thin filament, and titin, are tens-to-thousands of nanometers in length. The main constituent proteins of the myofilaments are myosin (gray), myosin-binding protein C (MyBP-C; blue), tropomyosin (purple), titin (magenta), the troponin complex (yellow), and actin (green). The structural and functional properties of each spatial scale are highlighted throughout this review, from single protein to cellular level function. (The atomic representations of each protein or protein subunit are from the Protein Data Bank, as follows: Myosin: 4DB1; MyBP-C: 2K1M; Tropomyosin: 1IC2; Titin Ig domain: 1G1C; Troponin: 1MXL; Actin: 2ZWH.)

overlap, 3) the energetic cost of contraction per unit length decreases with increased speed of shortening, implying cyclic interactions which were proposed by Needham even before the sliding filament theory (Needham 1950), and finally 4) that muscle contraction does not depend strictly on lattice spacing. This theory also emerged while the collective behavior of myosin motors in other systems was discovered, lending credence to the idea that myosin molecular motors working in concert to produce muscle contraction. In the following section we describe the structure and mechanics of individual force-generating myosin motors and their regulation within the contractile lattice.

1.2.1 Single-myosin protein structure and the ATPase cycle

Each myosin within the thick filament is a hexameric protein comprised of two myosin heavy chains and four myosin light chains [for a review, see (Gordon et al. 2000)]. The C-terminal end of myosin is rod-shaped and a dimerization of the two heavy chains is structured as an alpha helical coil, known as the S2 fragment. The S2 segments of approximately 300 myosins bundle, forming the thick filament backbone. The two heavy chains of each myosin separate and branch, creating two independent globular regions, known as S1 heads. Each S1 head contains a nucleotide-binding pocket, where ATP is hydrolyzed to provide the energy for contraction. S1 heads also contain a region that interacts with actin during cross-bridge cycling. Each myosin heavy chain associates with two light chains: the essential light chain that is required for myosin function and a regulatory light chain that modulates the kinetics of cross-bridge cycling.

The cyclic myosin-actin interactions powering contraction are fueled by ATP in a process known as the chemo-mechanical cross-bridge cycle (Figure 2) (Cooke 1997, Gordon et al. 2000). In relaxed muscle, most myosin heads are not associated with actin, but are bound with ADP and inorganic phosphate (Pi) from preceding ATP hydrolysis. In this conformation the actin binding surface of myosin has polar and charged residues that can associate with actin when tropomyosin is not blocking the binding sites on actin. Myosin initially binds to actin via electrostatic interactions (weak binding), positioning the S1 head so that strong,

hydrophobic interactions develop. Force and strain develop when myosin isomerizes in a ratchet-like motion, releasing Pi and generating the power-stroke. Once ADP is released, there is a brief moment when myosin is in rigor. At that moment, ATP rapidly binds in the nucleotide binding pocket, and this Myosin-ATP state reduces the affinity of myosin for actin, allowing cross-bridge detachment and a recovery stroke of the S1 head. ATP hydrolysis is thought to occur mainly in this detached state of myosin, both in resting and contracting muscle, which re-primes myosin for subsequent cycles of cross-bridge formation.

1.2.2 Mechanics & dynamics of myosin motors during contraction

From their early work on tension transients following a quick-release of activated muscle fibers, Huxley and Simmons (Huxley & Simmons 1971) deduced that each motor molecule, when attached to actin, undergoes a small number of successive movements, each more energetically favorable than the last, thus providing a conceptual basis for the cross-bridge cycle (Huxley & Simmons 1971). Combining the quick-release protocol with time-resolved X-ray diffraction analyses in single intact skeletal muscle fibers, Piazzesi *et al.* (Piazzesi, Reconditi, Linari, Lucii, Sun, Narayanan, Boesecke, Lombardi & Irving 2002) provided some of the first in-situ measurements of the average axial motion of the center of mass of myosin motors relative to the thick filament. With 1 Å resolution, they found that the motion of myosin heads are best explained by 'working stroke' models rather than rapid attachment and detachment models of actomyosin, supporting the tilting lever arm hypothesis (Piazzesi, Reconditi, Linari, Lucii, Sun, Narayanan, Boesecke, Lombardi & Irving 2002). This was later confirmed by Hugh Huxley and colleagues who showed that the center of mass of myosin heads moves on average with a tilt of about 60 degrees during the working stroke (Huxley et al. 2006).

Understanding the forces that drive filament sliding and sarcomere shortening during contraction required a closer look at myosin motor mechanics and dynamics in intact muscle. Vincenzo Lombardi and Gabriella Piazzesi, both of whom trained under Andrew Huxley, provided novel insights into the in-situ motions and mechanics of the myosin motor during

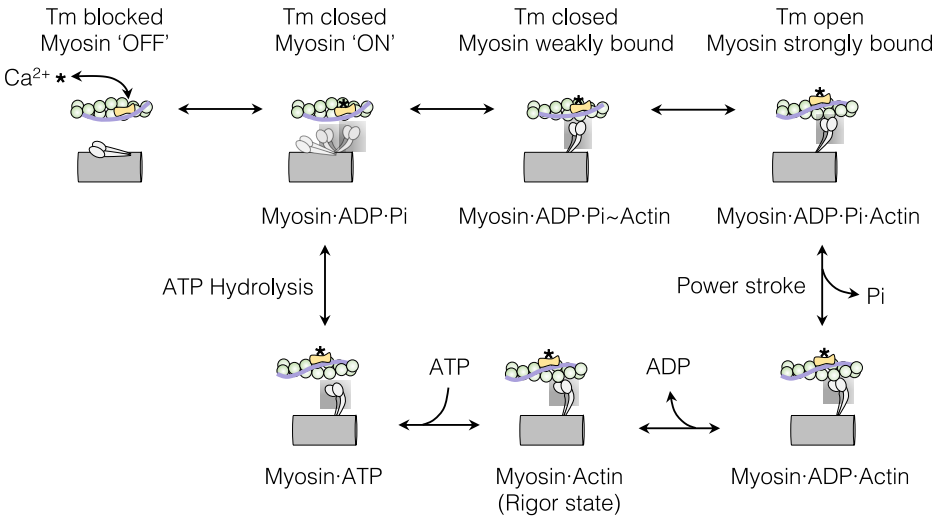

Figure 1.2: **The chemo-mechanical cycle of myosin motors in the sarcomere.** When Ca2+ is unbound from troponin (top left image) on the thin filament, tropomyosin (Tm) is in the 'blocked' state, sterically blocking myosin-binding sites on F-actin. Myosin is in a resting confirmation, folded onto the thick filament backbone. Upon Ca2+ binding to troponin, allosteric interactions within the troponin complex causes azimuthal displacement of Tm along F-actin, allowing Tm to reversibly occupy a 'closed' state. This 'closed' state partially exposes myosin-binding sites on F-actin, permitting weak actomyosin interaction. Myosin is loaded with its energy-bearing hydrolysis products, ADP and inorganic phosphate (Pi). Facilitated by multiple intra- and inter-filament cooperative activation mechanisms (e.g., nearest-neighbor thin filament activation via Tm, myosin-actin-tropomyosin interactions), Tm is further displaced to an 'open' state that permits strong myosin binding. The powerstroke (or working stroke) occurs when myosin undergoes a conformational change while maintaining its strong interaction with actin that results in force production along and between the thick and thin filaments. ADP is released post-powerstroke, producing a rigor state until ATP binds to the nucleotide-binding pocket of myosin. With ATP bound, the affinity of myosin for actin is reduced, and myosin dissociates from actin. ATP is then hydrolyzed again, priming myosin for another strong, force-producing interaction with actin.

muscle contraction. For example, in isometric contractions, there is an elastic distortion of the myosin motors of about 2–2.7 nm (contributing 40–50% of the sarcomere compliance), allowing for the development of force during contraction against high loads (Dobbie et al. 1998). Furthermore, by monitoring the axial motion of the myosin heads during the force response to a sudden decrease in fiber length, Piazzesi and colleagues demonstrated that the force-velocity relationship in skeletal muscle is determined by a modulation of the number of myosin motors (each with constant force and stroke size) rather than the force-generating capacity of individual motors (Piazzesi et al. 2007). In fact, it was later estimated by the same group that as few as 1–4 myosin motors per half-thick filament could provide maximum (unloaded) shortening in muscle (Fusi et al. 2017) with a working stroke size of 7 nm (Piazzesi, Lucii & Lombardi 2002). Huxley's original model attributed this relationship to a lower force exerted per myosin motor (Huxley 1957). Similarly, Caremani *et al.* (Caremani et al. 2016) recently demonstrated that the size and speed of the working stroke of cardiac myosin ranges from 3–8 nm and 1000–6000 s-1 depending on the load against which the muscle is contracting. Additionally, the force per myosin motor during an isometric twitch in cardiac muscle is similar to that of fast myosin in skeletal muscle [6 pN; (Brunello et al. 2014, Linari et al. 2007)], but has a stiffness that is 2–3-fold smaller than skeletal muscle myosin (Pinzauti et al. 2018).

1.2.3 Structure-function relationships of myosin from pathological and therapeutic perspectives

Our understanding of myosin structure and function in normal, healthy muscle paved the way for studies examining the functional consequences of altered myosin structure in disease. For example, a study focused on R403Q myosin mutation associated with hypertrophic cardiomyopathy (Tyska et al. 2000), showing that a heart disease associated with ventricular hypertrophy and diastolic dysfunction can have a single-molecule basis. The R403Q mutant myosin isolated from murine hearts has significantly increased actin-activated ATPase rates and higher average (ensemble) force production compared to normal (wild-type) myosin, but

no differences in single-myosin force production (Tyska et al. 2000). More recent studies using recombinant human cardiac myosin found that R403Q mutant myosin has a reduced affinity for actin, reduced ATPase rates, and produces less intrinsic force compared to wild-type myosin (Nag et al. n.d.). The range of functional properties for the R403Q myosin mutation has sparked debate about whether organ-level hypercontractility scales down to the single-protein level, and, more generally, the mechanisms by which mutated proteins drive organ-level remodeling and dysfunction.

With advancements in tools for investigating structural dynamics of myosin (e.g., small-angle X-ray diffraction, X-ray crystallography, time-resolved fluorescence microscopy, computational modeling), possible structural bases for cardiomyopathies linked to mutations in cardiac myosin have begun to emerge (Spudich 2014). A commonality among many mutations in myosin associated with hypertrophic cardiomyopathy appears to be an inability of myosin motors to sufficiently 'turn off,' or become unavailable for ATPase activity. This over-activity is likely due to the mutation-induced, allosteric restructuring of myosin that disrupts intra- and inter-molecular interactions that would otherwise stabilize the resting conformation. Motors that are unable to rest during diastole likely have an increased probability of forming force-generating cross-bridges during systole, therefore contributing to pathological hypercontractility (Nag et al. 2017, Spudich 2015, Yotti et al. 2019). The opposite case may also be true—mutations in myosin found in patients with dilated cardiomyopathy (a disease associated with hypo-contractility) have been found to inhibit the ability of myosin to fully activate during systole (Yotti et al. 2019).

The altered myosin motor structure caused by mutations associated with cardiac dysfunction raises the question of whether myosin structure can be targeted for therapeutic intervention. Some myosin-targeted small molecules (e.g., Omecamtiv Mecarbil (Winkelmann et al. 2015) and 2-deoxy-ATP (Powers et al. 2019)) have been shown to alter myosin structure, providing beneficial functional effects.

1.3 The filaments that slide, pull, & stretch: Myofilament structure, Mechanics, & Regulation

All of the dynamics discussed above play out in a lattice of compliant myofilaments. Thus, the forces generated by single molecules collectively interact at a higher level of organization. Here, we review the mechanical, geometric, and regulatory features of the key filaments that comprise the lattice.

1.3.1 Thin filament structure, mechanics, & regulation of contraction

Thin filaments are 1.1 µm long in vertebrate striated muscle and are composed of a double-helical coil of filamentous (F) actin, laced along its length with tropomyosin strands (Tobacman 1996). Each double-stranded tropomyosin covers seven globular (G) actins in each helical strand of F-actin and link with each other end-to-end. Troponin complexes contain a calcium-binding (TnC), an inhibitory (TnI) and a tropomyosin-linking (TnT) subunit on each strand of the thin filament, such that there is a ratio of seven actins to one tropomyosin and troponin complex (7:1:1), often called a structural regulatory unit. In the absence of calcium, inhibition of contraction occurs because tropomyosin strands lie in a position blocking the myosin binding sites on each G-actin of the thin filament, a position that is stabilized by troponin I interaction with two actins (one on each F-actin strand).

Following a cellular action potential, release of calcium from the sarcoplasmic reticulum leads to thin filament activation. Calcium binds to the N-terminal lobe of TnC, exposing hydrophobic residues, increasing the affinity of the N-lobe of TnC for TnI, which reduces the affinity of TnI for actin (da Silva & Reinach 1991). The reduced affinity of TnI for actin increases tropomyosin mobility on thin filaments, exposing myosin binding sites on actin (McKillop & Geeves 1993). Myosin binding to actin results in further displacement of tropomyosin and prevents it from moving back to a blocking position (Xu et al. 1999). When calcium dissociates from troponin, myosin motors detach from actin progressively, allowing tropomyosin to move back to an inhibitory position on the thin filament and sarcomere

relaxation to ensue.

To see how regulatory events in thin filaments influence larger scale function, it is helpful to examine the differences between cardiac and skeletal thin filament activation. In mammals, fast skeletal muscle TnC has two N-terminal calcium binding 'trigger' loops (Herzberg & James 1985, Houdusse et al. 1997) that ensure rapid thin filament activation and exposure of more than the 11 actin monomers of the structural regulatory unit, i.e. binding sites are thought to be exposed in neighboring regulatory units as well (Regnier et al. 2002). This has been suggested as a mechanism for cooperative activation in fast skeletal muscle, and computational models that account for cooperativity in thin filament activation support this general notion (Campbell et al. 2010). In contrast, cardiac TnC has only a single calcium binding loop, and calcium bound in this loop is insufficient to expose hydrophobic residues of TnI (Sia et al. 1997), reducing the ability of calcium binding alone to completely activate thin filaments (Wang & Fuchs 1994). Cardiomyocytes therefore rely on additional mechanisms of thin filament activation, such as cooperative activation between neighboring regulatory unites along the thin filament (Razumova et al. 2000) and cross-bridge binding (Campbell et al. 2010). Studies have shown that myosin binding to actin increases TnI affinity for TnC, though the size of the functional regulatory unit is thought to be 7 actin monomers or fewer (Gillis et al. 2007). Thus, a combination of cross-bridge binding plus calcium binding to neighboring troponins may be required for full activation of a regulatory unit in cardiac muscle. Furthermore, while skeletal muscle can modulate calcium-activated force based on firing frequency and/or recruitment of motor neurons innervating each cell, cardiac muscle activation is restricted to individual, cellular level mechanisms.

Because cardiac thin filaments are less sensitive to calcium than skeletal muscle thin filaments, modulation of myosin motors in cardiac muscle can also augment activation kinetics (and force) (Kreutziger et al. 2008). Moreover, with thin filament activation state being dependent on myosin, when calcium is released from troponin, as cross-bridges detach there can be a more rapid deactivation of the thin filament and return of the muscle to rest (Palmer et al. 2020). This is one mechanism of rapid deactivation that allows for rapid relaxation

as heart rate increases via adrenergic modulation during stress. Another mechanism that provides an increased rate of relaxation in cardiac muscle with adrenergic stimulation is phosphorylation of cardiac TnI (Kentish et al. 2001), a mechanism that is not available to skeletal muscle. This is accomplished with a cardiac-specific N-terminal extension on TnI (Solaro et al. 2008) that contains phosphorylation sites. When these sites are phosphorylated they interact with another region of TnI, the 'inhibitory peptide' to destabilize the interaction between TnI and TnC (Cheng et al. 2014, Warren et al. 2009), precipitating calcium release from TnC and deactivation of troponin and the thin filament.

1.3.2 Thick filament structure and composition

The thick filament of mammalian striated muscle is 1.8 µm long and consists mainly of myosin arranged as a helical, bipolar filament. The α-helical coiled-coils of the myosin tails form the backbone of the thick filament, and the myosin heads (two per molecule) extend outward radially from the surface of the backbone (Woodhead et al. 2005). The central portion of the thick filament (the M-line) is bare of myosin motors and contains unique titin protein domains and other proteins, such as myomesins, which physically link thick filaments together at the M-line ((Gautel 2011, Gautel & Djinović-Carugo 2016)). Myosin motors are arranged on the thick filament as 'crowns' of three heads, each head within the crown separated azimuthally by 120°. (Holmes et al. 2004, Reconditi 2006, Squire 2012). Subsequent crowns along the axis of the thick filament are separated by 14.3 nm (Figure 3) and rotated azimuthally by 40°such that the myosin head helical periodicity along the thick filament is 43 nm (Reconditi 2006, Squire 2012).

These structural details are supported with imaging data from high-intensity X-ray light. The bipolar arrangement of myosin heads along the thick filament axis produces unique X-ray diffraction patterns that, with today's advances in photon detectors enable high spatiotemporal-resolution measurements of the position and dynamics of motors during contraction. For example, one feature of the pattern (the meridional reflection, M3) corresponds to the axial distribution of myosin crowns along the thick filament (Figure 3). If the spacing

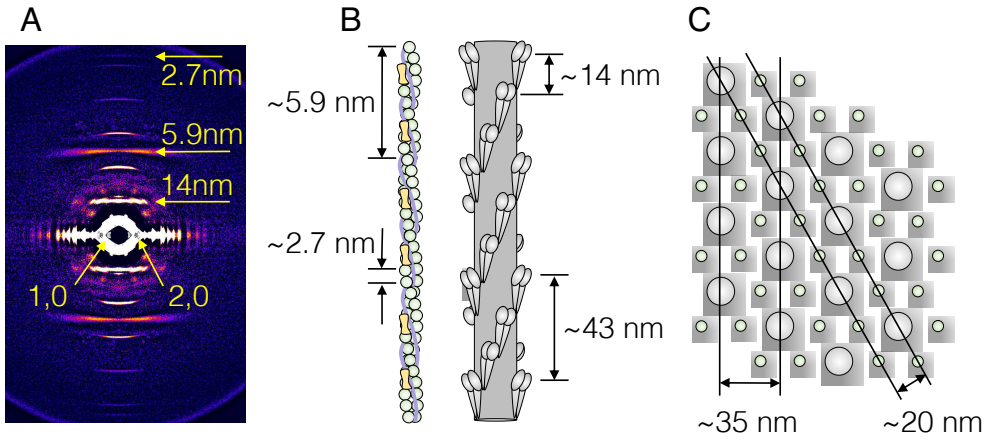

Figure 1.3: **The geometry of the myofilament lattice can be revealed by X-ray diffraction. (A)** An X-ray diffraction pattern of the synchronous flight muscle from Manduca sexta taken at the Advanced Photon Source at the Argonne Laboratory. The layer lines corresponding to the axial and radial reflections of the pseudo-crystalline structure of the sarcomeres. The vertical axis of reflections corresponds to axially periodic strictures along the filaments, while the horizontal axis corresponds to reflections caused by the filament lattice in the radial direction. **(B)** An axial view of a resting thin and thick filament. Actin monomers are 2.7 nm apart along the double-stranded filament, which has a helical periodicity of 5.9 nm. Myosin motors are arranged axially as 'crowns' of three motors every 14 nm. With an azimuthal rotation of 40°, the helical periodicity of the myosin crowns repeats every three crowns, or 43 nm. (C) The arrangement of the myofilament lattice produces two planes of symmetry: one that is produced by neighboring thick filaments separated by 35 nm, and a second that is produced by both thick and thin filaments, separated by 20 nm.

of the crowns were perfectly uniform along the thick filament, a single M3 intensity distribution would occur. However, mirrored myosin structures on each half of the thick filament produce intensity distributions at higher spatial frequencies (in reciprocal space) compared to the distribution from the crown repeats, and, with enough intensity, these higher order interference fringes can cause a splitting of the M3 peak into two narrower peaks ((Haselgrove 1975); see also Ref. (Reconditi 2006) for a review of the M3 split). Recent analyses of the split M3 reflection can inform on the in-situ axial motions of myosin heads during contraction (Huxley et al. 2006, Linari et al. 2000, Piazzesi, Reconditi, Linari, Lucii, Sun, Narayanan, Boesecke, Lombardi & Irving 2002, Reconditi et al. 2003, 2004) and quantify the fraction of myosin motors in resting, active, or force-generating states (Reconditi et al. 2017).

Recent studies have focused on myosin-binding protein-C (MyBP-C), another important thick filament-associated protein which localizes to the central third of the half-A-band (Previs et al. 2015), to determine its role in regulating contraction. In mammals, MyBP-C is expressed in three isoforms: slow-skeletal, fast-skeletal, and cardiac, and the functional role varies between each isoform (Lin et al. 2018), discussed briefly in Section 3.3 below. MyBP-C consists of multiple serially linked immunoglobulin and fibronectin domains and a unique 'linker' domain that serves as a phosphorylation site. As its name suggests, MyBP-C binds to myosin and the thick filament backbone via its C-terminal domains, while the first four N-terminal domains of MyBP-C (consisting primarily of Ig domains and phosphorylation sites) can interact with the thin filament (Razumova et al. 2008, 2006, Shaffer et al. 2009) and myosin S2 on the thick filament (Gruen & Gautel 1999).

1.3.3 Thick filament-based regulation of contraction

Recent evidence points to the thick filament as an additional component of the contractile regulatory system in striated muscle. This regulatory mechanism relies on, in part, feed-forward mechanosensation in the myosin filament: stress in the thick filament backbone (caused by force-generating motors or passive sarcomere stretch) is thought disrupt what are

likely electrostatic interactions that stabilize resting myosin heads in the 'interacting head motif' (Woodhead et al. 2005), thereby recruiting motors for force generation in a stress-dependent manner. Motors stabilized in this conformation [referred to as the 'OFF' state (Linari et al. 2015) or the 'super-relaxed' state (McNamara et al. 2015)], and are folded back onto the thick filament backbone with their heads pointing towards the M-line of the sarcomere (Reconditi et al. 2011), making ATP hydrolysis unfavorable. Support for this mechanism was recently advanced using time-resolved X-ray diffraction measurements of thick filament structure coupled with measurements of sarcomere-level mechanics. During isometric tetanus in skeletal muscle fibers, stress in the thick filament backbone develops after calcium-mediated thin filament activation, and progressively switches myosin motors "ON" during tetanus (Linari et al. 2015). Moreover, in the absence of calcium, passive stretch-induced thick filament strain releases resting motors, likely through similar mechanisms as during contraction (Fusi et al. 2016).

The thick filament mechanosensing hypothesis has also been tested in mammalian cardiac muscle ((Caremani et al. 2019, Marcucci et al. 2019, Piazzesi et al. 2018, Reconditi et al. 2017)). During a cardiac twitch, myosin motors are released from their resting state in proportion to systolic force (Reconditi et al. 2017). Thus, as venous return and metabolic demands vary beat to beat, cross-bridge recruitment is proportionately tuned to meet contractile demands, thereby optimizing the energetic efficiency of systole-diastole cycles. Moreover, the axial distribution of myosin recruitment along the thick filament backbone may be affected by MyBP-C. As force develops during a cardiac twitch, motors in the c-zone of the A-band are recruited first and support the majority of the force during the twitch (Brunello et al. 2020). The resting structure of the thick filament may be a promising therapeutic target to treat systolic heart failure ((Anderson et al. 2018, Powers et al. 2019)).

The function and regulatory role of MyBP-C in the sarcomere is an area of active investigation (Brunello et al. 2020, Harris et al. 2011, McNamara & Sadayappan 2018, McNamara et al. 2019, Moss et al. 2015). When myosin motors are in their resting conformation, MyBP-C may stabilize their conformation, releasing motors upon activation (McNamara

et al. 2019). Ablation of MyBP-C increases cross-bridge binding and cycling rates, likely by removing the physical constraints of MyBP-C on the myosin motors (Stelzer, Dunning & Moss 2006). This mechanism has also been explored as a potential treatment for diminished cardiac contractile function in dilated cardiomyopathy (Li et al. 2018). Additionally, although MyBP-C is mainly associated with the thick filament, recent evidence has emerged that it can also interact with actin, forming interfilament cross-links that may facilitate thin filament activation (Harris et al. 2016, Mun et al. 2014, Risi et al. 2018). Similarly, the protein myomesin bridges thick filaments together at the M-line, which likely regulates both axial and radial myofilament dynamics during contraction (Tskhovrebova & Trinick 2012).

1.3.4 Titin structure and mechanics

The early two-filament model of the sarcomere proposed by Huxley and colleagues could not explain all of the mechanical properties of resting muscle. An additional elastic element was needed to account for passive tension and stiffness in the sarcomere (independent of actin-myosin interactions), but such an elastic element was not discovered until many years after the initial Huxley models. Passive elements could for example, include contributions from the extracellular matrix, the Z-disks and various protein constituents, including the giant filamentous protein titin which spans the length of the entire half-sarcomere in muscle. It is the largest known protein (3–4 MDa) and is composed of many unique, serially linked domains that have specialized tasks in the sarcomere. Historically, titin was believed to be mainly a structural protein that connected the thick filament to the Z-disc, initially aptly named ‘connectin’ by Maruyama and colleagues (Maruyama et al. 1977, 1976). Today, titin has emerged as a highly dynamic and complex protein, involved in multiple mechanical and biochemical aspects of muscle function. As many features of titin have been comprehensively reviewed elsewhere (Fukuda et al. 2008, Granzier & Labeit 2004, 2005, Lindstedt & Nishikawa 2017, Linke & Hamdani 2014), we explore how recent information about the mechanical properties of titin has shaped our interpretation of the sliding filament theory in resting and contracting muscle.

While the structure and length of the I-band region of titin varies between muscle types and titin isoforms (Granzier & Labeit 2005), it generally consists of dozens of serially linked immunoglobulin (Ig) domains that flank a distinct region rich in proline (P), glutamate (E), valine (V), and lysine (K), termed the PEVK region, and a unique amino acid sequence that varies between isoforms and muscle types (the skeletal N2A region and the cardiac N2B or N2BA region). The A-band region of titin is less understood than the I-band region. It consists of Ig and fibronectin super-repeats that strongly interact with myosin and MyBP-C (Linke & Hamdani 2014), and it is likely much stiffer than that of the I-band region (Elhamine et al. 2014). Each super-repeat is approximately 43 nm in length, which coincides with the helical repeat distance of myosin crowns along the thick filament (Furst et al. 1989). It has therefore been hypothesized that the A-band region of titin facilitates myosin filament formation and structure (Tonino et al. 2017). Tonino *et al.* (Tonino et al. 2017) have recently shown that deleting two super-repeats in the A-band of murine cardiac and skeletal muscle causes a significant reduction in the length of the myosin filament. This change in thick filament length alters the sarcomere length-dependence of force and reduces contractility in both cardiac and skeletal muscle (Tonino et al. 2017).

The mechanical properties of the I-band region of titin contribute significantly to the total passive elasticity of muscle (Granzier & Irving 1995, Granzier & Wang 1993, Irving et al. 2011). Titin expressed in mammalian skeletal muscle is generally longer and therefore effectively more compliant than cardiac muscle titin. Using fluorescent probes positioned proximally and distally to the PEVK segment, Linke and colleagues showed that Ig domains extend first, while the length of the PEVK segment is preserved until much longer sarcomere lengths (Linke et al. 1998, 1996). Moreover, studies on whole titin molecules (Kellermayer et al. 1997, Mártonfalvi et al. 2014) and isolated titin fragments ((Marszalek et al. 1999, Rief et al. 1997) have shown that individual Ig domains dynamically unfold and refold under load, and that nearly all Ig domains are likely to be unfolded in random order at 10 pN (Bianco et al. 2015, Rivas-Pardo et al. 2016). Mártonfalvi *et al.* suggest that exposing ligand binding sites on titin may provide a mechano-regulated signaling motif to the I-band (Mártonfalvi

et al. 2014).

Load-dependent structural dynamics of the Ig domains in the I-band region of titin (Rivas-Pardo et al. 2016) together with the spring-like characteristics of the PEVK segment (Linke et al. 1998) provide the sarcomere with a length-dependent spring. A recent study used a mechanical model of the half-sarcomere ((Pertici et al. 2019); similar to that shown in Figure 4) to provide an in-situ quantitative description of the elasticity of the I-band region of titin during tetanic contraction (Powers et al. 2020). The stiffness of titin during contraction at long sarcomere lengths is 6 pN/nm, a value that is 100 times larger than the static stiffness responsible for the passive force-length relationship in resting muscle over the same range of sarcomere lengths (Powers et al. 2020). Similarly, changes in titin stiffness (e.g., due to phosphorylation or disease-causing mutations) may affect the force-generating capacity of myosin motors (Powers et al. 2018).

The apparent stiffness of the I-band region of titin in vivo depends on factors such as phosphorylation (Hamdani et al. 2017, Herwig et al. 2020, Koser et al. 2019), interactions with actin (Linke et al. 1998, Nishikawa et al. 2012), calcium-dependent stiffness upon muscle activation (Dutta et al. 2018), or isoform switches during development or disease progression (Granzier & Labeit 2004). Ongoing research efforts are aimed at elucidating the relationship between altered titin stiffness and muscle function, especially in disease contexts.

1.3.5 Titin-based regulation of contraction

The regulatory and structural roles of titin in contraction remains an active area of research. The I-band region of titin physically links the thick filament to the Z-disk and likely facilitates mechanical force transmission between the Z-disk and the myosin filament. Accordingly, during muscle contraction, titin may play a role in force equilibration, balancing axial forces within the sarcomere (Powers et al. 2018), or between serially linked sarcomeres during contraction (Maruyama et al. 1977, Wang et al. 1979).

Titin may also be involved in activating the other myofilaments in the sarcomere by transmitting forces between them during passive stretch. Recent work by Fusi *et al.* suggests

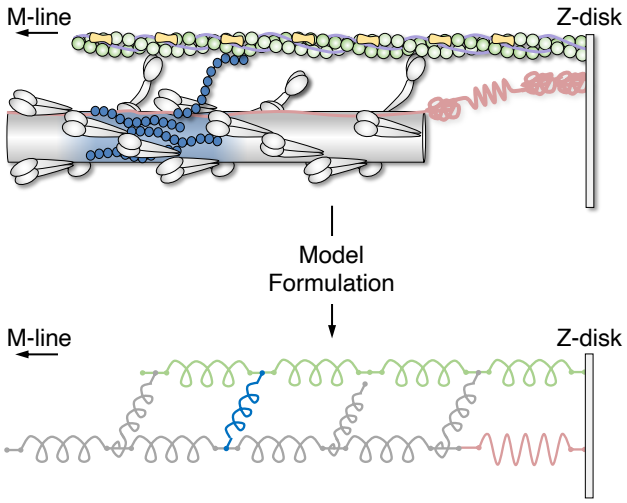

Figure 1.4: **An example of the half-sarcomere represented as a system of springs in computational and mathematical models.** Computational and mathematical models of muscle function often rely on dissecting complex sarcomere protein interactions into a system of Hookean springs. Models such as these provide approximations of mechanics, energetics, and kinetics of contraction/relaxation that can accurately recapitulate experimental observation and/or generate experimentally testable hypotheses. Myosin cross-bridges can be modeled as two-spring systems (gray) consisting of a linear spring plus a torsional spring at the thick filament backbone (Williams et al. 2010), and MyBP-C (blue) can be modeled as a spring in parallel with cross-bridges (Fusi et al. 2014). Titin can also be modeled as an additional spring in the I-band (pink) in parallel with the thin filaments and the array of cross-bridges (Powers et al. 2020, 2018)

titin may facilitate thick filament activation in skeletal muscle by imposing stretch-induced stress on the thick filament backbone, disrupting the resting conformation of myosin motors (Fusi et al. 2016). Moreover, the shorter sarcomere lengths at which cardiac muscle operates (compared to skeletal muscle) suggests the shorter titin molecule in cardiac muscle may be tuned to provide similar mechanical functions to cardiac muscle (Marcucci et al. 2017, 2019). The I-band region of titin in mammalian cardiac muscle was recently implicated in length-dependent activation of both thick and thin filaments, likely through a cooperative, strain-dependent mechanism upon stretch (Ait-Mou et al. 2016).

The A-band region of titin also plays a role in biochemical signaling. Indeed, titin binds to more than twenty-five other proteins (Linke & Hamdani 2014). Many titin-associated ligands interact with the M-band region of titin, such as calmodulin, filamin C, and obscurin (Linke & Hamdani 2014). Furthermore, the M-band region of titin interacts with muscle-specific RING-finger proteins-1/-2 (MURF1/2), which bind to microtubules and help maintain their stability (Granzier & Labeit 2004, Linke & Hamdani 2014). Lastly, myomesin interacts with the M-band region of titin, which provides links between thick filaments (Linke 2018).

Notably, the A-band region is also associated with cardiomyopathy-causing mutations. Approximately 25% of patients with end-stage dilated cardiomyopathy have titin-associated truncating mutations (Herman et al. 2012), many of which are located in the A-band region of titin. In cardiomyocytes lacking full-length titin, myofibrils are more susceptible to damage during mechanical loading compared to cardiomyocytes with full-length titin (Shih et al. 2016). However, depending on the location of truncation-causing mutation, a recently discovered shorter isoform of titin (called Cronos titin (Zaunbrecher et al. 2019, Zou et al. 2015)) can facilitate myofibrillar organization in the absence of full-length titin, which can partially preserve cardiac contractility in human cardiac myocytes (Zaunbrecher et al. 2019).

1.4 A Microscale Machine of Sliding Filaments: Sarcomere Structure, Organization, and Mechanics & Dynamics of the Sarcomere

Just as individual motor proteins generate forces and interact within a lattice of compliant, regulated, myofilaments, the scaffolding of filaments within the whole sarcomere connects function across scales. Among the earliest experimental approaches connecting these spatial scales was the classic length-tension relationship established by Gordon, Huxley and Julian (Gordon et al. 1966). It was instrumental in supporting the sliding filament hypothesis and theory of independent force generators, and highlighted the notion that muscle force depends on its geometric state (Evans & Hill 1914). In the sections that follow, we explore recent experimental and theoretical advances that have revealed additional geometric and dynamic features of force generation at the sarcomere scale. These follow from emerging techniques for time-resolved data and computational methods that were not feasible at the onset of the sliding filament hypothesis.

1.4.1 Structure & organization of the lattice

A host of imaging technologies have been brought to bear in our understanding of the structure and organization of the myofilament lattice and sarcomeres of striated muscle. These include electron microscopy (EM), X-ray diffraction, laser diffraction, and fluorescence confocal microscopy. EM was among the earliest imaging technologies used to reveal sarcomere structure (Hanson & Huxley 1953). While it directly reveals the layout of electron-dense structures with extremely high spatial resolution (recent microscopes approaching sub-angstrom resolution (Rose 2008)), tissue fixation can alter the sizes, spacing, and organization of subcellular structures. In contrast, X-ray diffraction patterns of muscle can reveal the myofilament lattice geometry without the need for fixation (or any modification of the muscle tissue, (Squire 2012)). Indeed, muscle X-ray diffraction can be done on intact whole animals and muscles (George et al. 2013, Malingen et al. 2020). Early X-ray diffraction experiments beginning in the 1940s (Astbury 1947) required long exposure times, precluding detailed measurements

of the temporal dynamics of active muscle until the 1960s (Elliott et al. 1965, Huxley et al. 1965). With the advent of powerful synchrotron radiation and high-speed digital detectors in the 1980s time-resolved experiments exceeding 100 Hz have now become possible (Huxley et al. 1980, Iwamoto 2019), enabling measurements of axial and radial structural changes of the sarcomere in active muscle.

In mammalian skeletal muscle, the interdigitating myofilaments in the overlap region of the sarcomere are arranged in a three-dimensional lattice with a double-hexagonal symmetry that enables cross-bridges from multiple thick filaments to interact with a single actin filament (Figure 3). In the I-band region, the thin filaments form a rectangular lattice as they insert into the Z-disk (Squire & Knupp 2005). However, variations in the myofilament packing ratio and lattice geometry varies considerably across different animal taxa (Hoyle 1967), suggesting structural adaptations in the lattice enable functional specialization (Shimomura et al. 2016). For example, packing ratios can vary from 6:1 thick to thin filaments in cockroach leg muscles (Hagopian 1966), 5:1 in Lethocerus (Tregear & Squire 1973), and 12:1 in the common garden snail (Royuela et al. 2000). Interestingly, variation in features like packing ratios not only impact the number of available binding sites, but may also affect other aspects of structural mechanics, such as electrostatics, filament lattice spacing, and cross-bridge kinetics. This is a ripe area for future research.

Extending from the theory of independent force generators, muscles with many short sarcomeres connected in series will be well adapted to rapid contraction, while muscles with longer sarcomeres (and myofilaments) are better suited to slower, high force contractions ((Hagopian 1966, Huxley & Niedergerke 1954). This theoretical hypothesis is born out in structure-function relationships seen across taxa (Osborne 1967) and even across muscle groups within a single organism, where both the packing ratios of thick to thin filaments and filament lengths is correlated with either large forces or rapid contractions (Shimomura et al. 2016).

In the 1970s an alternative hypothesis to the theory of independent force generators suggested electrostatic forces drove muscle contraction (Elliott et al. 1970, Huxley 1974, Morel

et al. 1976, Shear 1970). However, the sliding filament theory by independent force generators took precedence over that alternative hypothesis (Huxley 1980), diminishing interest in electrostatic interactions. We know today, however, that such interactions help stabilize the lattice (Rome 1968, Smith 2014). The repulsive forces between negatively charged filaments and constricting forces (likely arising from elastic structural components such as the Z-disks, M-line proteins like myomesins, and proteins like titin and myosin binding protein C, which are interwoven in the myofilament lattice) yield a stable equilibrium (Moisescu 1973). Independent of steric interactions with cross-bridges, the thin filaments are more subject to collapse at low pH than the thick filaments (Matsuda & Podolsky 1986), although at normal pH the lattice does not collapse, indicating the importance of mechanical forces. While either electrostatic forces alone (Millman et al. 1983) or mechanical forces alone (Smith 2014) can roughly account for lattice spacing, the data are best fit by models that take both electrostatic and mechanical forces into account (Smith 2014).

In addition to stabilizing the lattice, the charges of lattice proteins also attract polar water molecules, resulting in a layer around filaments. In total, 30% of the lattice volume is osmotically inactive, with 20-25% taken up by protein (Millman 1998). The remaining fluid in the lattice is free to flow and could mediate substrate transport, which is discussed further in section 4.2 below.

1.4.2 Radial sarcomere dynamics and interfilament regulatory mechanisms

In addition to taxonomic variation in the thick-to-thin filament packing ratio, the radial spacing of filaments can also vary between species, and temporally during contraction. By its name, the sliding filament hypothesis gives the impression that the radial spacing of the myofilaments does not vary during contraction. However, as muscle contracts and relaxes, the spacing between myofilaments in the lattice changes, which has important implications for myosin motor binding kinetics, fluid flows, and radial elastic energy storage. Decreased lattice spacing can bring myosin molecular motors closer to the thin filament, thus increasing the probability of cross-bridge binding (Adhikari et al. 2004, Cecchi & Bagni 1994). Additionally,

changes in lattice spacing alter the strain in bound cross-bridges, and the direction of the forces they apply (Schoenberg 1980). Spatially explicit modeling of the system corroborates experiments, highlighting that lattice spacing is an important regulator of axial muscle force (Tanner et al. 2007, 2008, Williams et al. 2010, 2013). Given its importance for muscle function, what are the rules that govern lattice spacing?

Early X-ray diffraction experiments showed that resting muscles maintained a constant volume with the lattice dilating as sarcomeres shortened and constricting upon sarcomere lengthening (Elliott et al. 1965, Rome 1968). The lattice also maintains a constant volume during length changes in resting fibers of the crayfish leg, where 12 thin filaments surround each thick filament ((April et al. 1971)). However, because cross-bridges produce axial and radial forces, the isovolumetric hypothesis cannot be fully tested in resting fibers. In the 1990s time-resolved X-ray diffraction patterns of active muscles revealed that cross-bridges exert radial forces that compress the filament lattice, demonstrating that the lattice is not isovolumetric ((Cecchi & Bagni 1994), (Cecchi et al. 1990)). Further, in one of the first in-vivo X-ray diffraction experiments, the lattice spacing of Drosophila's cyclically contracting flight muscle was shown to be constant during natural function (Irving & Maughan 2000). In contrast, X-ray diffraction patterns from the cyclically contracting flight muscle of Manduca sexta reveal that the lattice dilates and compresses, but there is considerable variation between individual animals in both the magnitude and temporal patterns of lattice kinematics (Malingen et al. 2020). Additionally, the dynamics of lattice spacing are also correlated with naturally occurring temperature gradients within the thorax (George et al. 2013). Moreover, differences in lattice spacing as small as 1 nm have been correlated with the distinct functional roles (e.g. mechanical work) played by adjacent cockroach leg muscles which are otherwise identical (George et al. 2013, Tune et al. 2020). Thus, feedback between active cross-bridges and the radial lattice spacing can control the temporal dynamics of work and force in contracting muscle.

The dense packing of filaments has been shown to slow the diffusion of substrates to their target sites by computational (Aliev & Tikhonov 2004, Shorten & Sneyd 2009), and

experimental studies (de Graaf et al. 2000, Maughan & Godt 1999, Papadopoulos et al. 2001) with decreases in lattice spacing decreasing the rate of diffusion (Kekenes-Huskey et al. 2013). Diffusion rates depend on the size of substrates, and the anisotropic structure of the lattice results in more rapid axial diffusion than radial diffusion for some substrate sizes (Arrio-Dupont et al. 2000, Hochachka 1999). Additionally, diffusion rates may be a driver of organelle positioning within muscle cells. For example, mitochondria are subject to mirrored constraints, including the diffusion of the oxygen necessary for ATP production, and the diffusion of ATP into the dense contractile lattice (Kinsey et al. 2011). The time constraint imposed by slow diffusion may be especially problematic for cells contracting at high frequencies, where substrate exchange (e.g. calcium, ATP, etc.) with organelles sitting exterior to the lattice must occur over rapid timescales.

Diffusion is not the only mechanism that could drive substrate exchange between the lattice and surrounding intracellular environment. Dynamic changes in the volume of the lattice, modulated by cross-bridges, necessitates fluid flow that could have important implications for substrate exchange. Interestingly, using a simplified model of viscous shear stresses for flow between filaments, A. Huxley came to the conclusion that such stresses are not important (Huxley 1980). That said, the implications of fluid flow for muscle function is still a relatively open area for muscle research.

The relationship between cross-bridges and lattice spacing is one example of interfilament regulation of the sarcomere that differs from many of the mechanisms we discussed above in Section 3 that focused on individual filament-associated proteins. Thus, muscle employs multiple regulatory mechanisms, spanning the scale of single molecules to the dynamic motions of ensembles of myofilaments.

1.4.3 Axial sarcomere dynamics and interfilament regulatory mechanisms

The importance of lattice geometry is highlighted in the classic study by Gordon, Huxley and Julian (1966) highlighting the dependence of active force on sarcomere length (Gordon et al. 1966). Three main features emerged from their paper. First, at long sarcomere length

(3.5 µm), where thick and thin filaments barely overlap, few cross-bridges can contribute to force. Force rises linearly during contraction as sarcomere length decreases to 2.2 µm where filament overlap allows the maximal number of cross-bridges to form with the thin filaments. This region is called the 'descending' portion of the length-tension relationship (even though it ascends during contraction). From 2.0 and 2.2 µm force peaks and remains constant. From 2.0 to 1.3 µm, force declines linearly as a consequence of steric hindrance between actin filaments, titin, the thick filament, and the Z-disk. This is called the 'ascending' portion of the length-tension relationship. Thus, the power of muscle depends on the SL at which it is contracting. This length dependence of active force adds to passive tension, which rises exponentially with sarcomere length, which is primarily due to titin (see Section 3.5 above). It should be noted that as the lattice expands during contraction, the increased distance between myosin and actin reduces the likelihood of cross-bridge formation, thus also contributing to the decrease in force with decreases in length. Additionally, experiments that involved osmotic compression of the lattice suggest that at long sarcomere lengths, lattice compression may also inhibit axial force generation by constraining the angle at which cross-bridges can generate axial forces (Williams et al. 2013). Thus, the force length relationship may follow from more complex lattice kinematics than were initially suggested in the pioneering work of Gordon *et al.*

The dependence of force on sarcomere length is also a key determinant of cardiac muscle function. Over a century ago, Otto Frank and Earnest Starling observed in independent studies that the systolic pressure is modulated by diastolic filling, thus providing beat-to-beat regulation of cardiac output. While the subcellular origins of this feature of cardiac muscle, now referred to as the Frank-Starling law of the heart, are still under active investigation (Ait-Mou et al. 2016, Farman et al. 2011, Smith et al. 2009, de Tombe et al. 2010), the length-dependence of tension and calcium sensitivity in cardiac myocytes is generally believed to be an integral component. In particular, cardiac muscle differs from skeletal muscle in that it operates mainly on an ascending limb of the length-tension relationship (Caremani et al. 2016). Consequently, during diastolic filling when ventricles are stretched, the sarcomere

length of resting cardiomyocytes increases leading to larger forces. A variety of mechanisms may contribute to the sarcomere length dependence of force in cardiac muscle, many of which are under active investigation, such as length-dependent calcium sensitivity of force (Konhilas et al. 2002, de Tombe et al. 2010), recruitment of myosin motors (Campbell et al. 2018, Mann et al. 2020, Reconditi et al. 2017), and titin strain (Ait-Mou et al. 2016).

In addition to the functional consequences of lattice spacing and length-dependent force generation, filament compliance may play a significant role in regulating muscle function. The idea of compliance as a factor gained attention with a series of papers in 1994 (Goldman & Huxley 1994, Huxley et al. 1994, Wakabayashi et al. 1994) that introduced experimental data pointing to periodicity changes in the thick and thin filaments in relation to the tension they bore. Those papers lead to spatially explicit computational models that suggested, as tension develops in myofilaments, axial strain can realign myosin-binding sites on actin filaments, augmenting cross-bridge recruitment (Daniel et al. 1998). Spatially explicit models with filament compliance (Campbell 2006, Daniel et al. 1998, Mijailovich et al. 2016) allowed Tanner *et al.* to explore the influence of the degree of cooperativity between neighboring regulatory units along myofilaments on force output (Tanner et al. 2012). Additionally, while the focus of attention on sarcomere elasticity tends to be dominated by the myofilaments, the functional roles of Z-disk compliance is also an active area of research (Gautel 2011, Luther 2009).

1.4.4 The ends of the sarcomere: Z-disks and myotendinous junctions

The vast majority of muscle research has centered on myofilament structure, regulation and organization. Far less attention has focused on the Z-disk (Z-line, Z-band) which joins sarcomeres end-to-end, transmitting forces between sequential sarcomeres. Thin filaments anchor into the Z-disk via α-actinin and nebulin (Luther 2009) Similarly, titin interacts with actin and α-actinin to mechanically connect thick filaments to the Z-disk (Young et al. 1998). Additionally proteins such as myozenin and γ-filamin (Takada et al. 2001) and LIM-domain proteins play important roles in the structural integrity of the sarcomere, signaling,

and mechanosensing (Hoshijima 2006, Pyle & Solaro 2004). Myriad other Z-disk proteins have been linked to various muscular dystrophies (Davies & Nowak 2006) in which crucial structural connections between the sarcomere and the sarcolemmal surface are compromised.

For vertebrate muscle, the thin filament lattice arrangement shifts from hexagonal packing to rectangular packing as it attaches to the Z-disk. The thickness of the Z-disk varies considerably from 30 nm in fast skeletal muscle fibers to 100 nm in cardiac fibers (Luther et al. 2003). Interestingly, a recent study shows that the rapidly contracting sonic muscles of the midshipman fish have exceptionally wide Z-disks (1200 nm), about the same width as the A-band in these specialized sound producing muscles (Burgoyne et al. 2019). The greater thickness in cyclically loaded muscles such as cardiac and sound production muscles raises the interesting question whether the Z-disk serves a role elastic energy storage in addition to a role in force transmission.

In transverse view, the network of α-actinin proteins form one of two possible geometries: a square lattice or a basketweave. Early experiments suggested that the shift in geometry depended on the state of active tension—in relaxed fibers, the proteins form a square lattice, whereas in the active state the structure resembles a basketweave geometry (Goldstein et al. 1990). However, a recent study suggests that tropomyosin movement may influence the shift from square lattice to basketweave independent of the level of the force generation (Perz-Edwards & Reedy 2011). In the end, the roles in elastic energy storage and force transmission for Z-disks and myotendinous junctions remain an open area for future investigations.

Axial force transmission along the train of sarcomeres continues across Z-disks to the myotendinous junction (MTJ) where the cell is folded extensively as it connects to the extracellular matrix—the degree of folding depends upon the fiber type (Tidball & Daniel 1986). At the MTJ, connections between the lattice and the sarcolemma are mediated by various structure proteins, including dystrophin. Defects in dystrophin proteins compromise the associations of thin filaments with the membrane at the MTJ. Thus, similar to the Z-disk, the MTJ remains an open area for future research in muscle physiology and pathophysiology.

1.4.5 Efficiency is an emergent property of multiscale interactions

How efficiently do myosin motors convert chemical energy into mechanical energy? Muscle efficiency was first investigated through the lens of heat (Evans & Hill 1914). Long before the sliding filament hypothesis Fenn showed that muscle which performs work emits more heat than an isometrically contracting muscle (Fenn 1923). Huxley noted that any model of muscle contractility must account for the Fenn effect (Huxley 1980). The modulation of the rates of cross-bridge cycling ultimately provides a mechanistic link between muscle mechanics and chemical kinetics (Huxley & Simmons 1971, Kushmerick & Davies 1969), allowing for an explanation of the Fenn effect. In 1987, Homsher provided an excellent review of the relationship between muscle enthalpy production and actomyosin ATPase (Homsher 1987).

For a linearly elastic spring, the mechanical energy is the product of the spring stiffness and the square of its distortion. Thus, the energy derived from ATP hydrolysis must be greater than the mechanical work associated with distortion of the cross-bridge (Piazzesi et al. 2007). However, a challenge in estimating efficiency is decoupling energy-consuming processes in the cell, like ion pumping, from the work performed by cross-bridges themselves. Measurements of efficiency in skinned fibers shows that there is considerable diversity across organisms, fast and slow muscle types, and operating conditions (e.g., temperature, load, and velocity) (Kushmerick & Davies 1969, Smith et al. 2005). Of specific interest, the efficiency of human skeletal muscle is estimated to be about 20% (He et al. 2000). Documenting the efficiency of individual myosin motors in the lattice is challenging since, by operating asynchronously, they perform work on negatively strained neighbors (Kaya & Higuchi 2010). To estimate myosin motor efficiency Sugi *et al.* (Sugi et al. 2003) recorded the power generated by glycerinated fibers where cross-bridge power strokes were synchronized by limiting the amount of ATP in the system to approximately one per myosin motor and using the laser-induced release of caged calcium for activation. Their study showed that the efficiency of individual myosin motors within the filament lattice is, conservatively, 70% (Sugi et al. 2003), which was much greater than previous estimates in vertebrate muscle.

1.5 Ideas for the future

We are acutely aware of the vast amount of exciting muscle history and research that we have not reviewed here, such as the challenging open questions about the evolutionary diversity of muscles and their function, to the diverse of functions that muscles must accomplish, to questions about sarcomerogenesis and the underlying developmental processes in which mechanical and genetic regulatory pathways conspire to create nearly paracrystalline structures, to myriad other open questions in the field. We chose instead to set the stage for questions that we have found interesting, those largely related to the challenges for understanding multiscale dynamics of muscle and melding models and experiments.

1.5.1 The multiscale problem

The muscle in a mouse that weighs only a few grams is not all that different from that in whales weighing many thousands of kilograms: muscle scales from mice to whales and does so with a structure that is stunningly conserved. However, as discussed in the introduction, the fundamental concepts of muscle contraction (launched with the pair of 1954 Nature papers introducing the sliding filament hypothesis) included evidence of the vast spatial and temporal scales across which mechanisms of muscle function must span. Since then, a common interest has emerged in the field of muscle research: to develop a deep mechanistic understanding of the multiscale processes—from atom to organ—that govern muscle function. While such multiscale problems are not unique to muscle, understanding the function of muscle on multiple spatiotemporal scales is central to many areas of active research, from interpreting functional and structural diversity across animal taxa, to engineering new technologies, to developing therapies for muscular pathologies.

To a considerable extent, the extreme spatial organization of muscle with repeated modules lends itself well to multiscale studies. For example, time-resolved X-ray diffraction provides data that reflects geometric changes at the scale of Angstroms and nanometers. When coupled with other imaging methods (such as laser diffractometry that can provide

micrometer (sarcomere) scale information) along with force and length measurements at the centimeter scale, simultaneous mechanical and structural data can be acquired across nearly eight orders of magnitude ($10^{10} to 10^{2}$). Few biological systems lend themselves to such a broad range of immediate spatiotemporal information.

Creating predictive models that span such scales is a challenge. For example, molecular dynamics models now provide deep insight into functional dynamics of single myosin molecules, including interactions with various nucleotides (Regnier & Homsher 1998, Regnier et al. 1998). But such modeling approaches are computationally intensive and cannot be scaled to the millions of interacting molecules that constitute a single sarcomere.

As we described above, spatially explicit sarcomere scale models (micrometer) that incorporate lattice geometry (Tanner et al. 2007, Williams et al. 2010, 2012, 2013), filament compliance (Campbell 2006, Daniel et al. 1998, Mijailovich et al. 2016), cross-bridge and titin mechanics (Powers et al. 2018), cooperative binding (Tanner et al. 2007), and thin filament regulation (Tanner et al. 2012) provide insight into the interaction between chemical kinetic and structural features, also do not scale well. As with molecular dynamics simulations, the computational demands of these Monte-Carlo based approaches preclude predictions of contractile dynamics at the scale of centimeters (thousands of sarcomeres).

Similarly, more heuristic models of muscle force generation such as Hill relationships, force-length relationships, and activation dynamics (force-time relationships) allow predictive models of tissue, limb and organ scale dynamics. But these approaches give little insight into vastly smaller spatial and temporal scales. A core challenge of understanding muscle function across physical scales is the inherent influence of processes at each scale on processes at other scales. That is, mechanisms from one spatiotemporal scale cannot be easily untangled from mechanisms at adjacent scales. Consequently, models at the molecular level of organization are often quite difficult to apply to larger spatial scales and vice versa. Indeed, the two-way coupling between macroscopic and microscopic scales is a fundamental challenge we face today. This is particularly true of molecular models driven by Monte-Carlo simulations. This challenge of multiscale dynamics will require methods to extract reduced order behaviors

from detailed high-dimensional simulations.

In addition to coupling across spatial and temporal scales, there remain additional open areas that reflect coupled processes. For example, the coupling between force and activation is inherent in stretch activation, cooperative binding, and mechanosensing (Linari et al. 2015) in the lattice. Additionally, recent work points to an interesting, and poorly explored, coupling between volume changes of the lattice, fluid flow, and substrate delivery. Thus, contractions may result in fluid exchange between the lattice and surrounding cell volume, where organelles like the sarcoplasmic reticulum and mitochondria are located. Ultimately, coupling between experimental, theoretical, and computational efforts will enable us to develop models that may be used as tools for understanding disease and for designing novel therapeutics.

1.5.2 Acknowledgements

The authors are grateful for scientific discussions with Tom Irving at BioCAT at the Advanced Photon Source at the Argonne National Laboratory. This work was supported by: Army Research Office W911NF-14-1-0396 and the Joan and Richard Komen Endowed Chair to TLD, the Bioengineering Cardiac Training Grant from the National Institute of Biomedical Imaging and Bioengineering (T32EB1650) and a fellowship from the ARCS Foundation to SAM, the National Institute of Arthritis and Musculoskeletal and Skin Diseases P30 AR074990 to MR and TLD, and the National Heart, Lung, and Blood Institute F32 HL152573 to JDP.

Chapter 2

IN VIVO X-RAY DIFFRACTION AND SIMULTANEOUS EMG REVEAL THE TIME COURSE OF MYOFILAMENT LATTICE DILATION AND FILAMENT STRETCH

Malingen SA, Asencio AM, Cass JA, Ma W, Irving TC & Daniel TL. Journal of Experimental Biology. 2020.

Abstract

Muscle's function within an organism depends on the feedback between molecular to meter-scale processes. While the motions of muscle's contractile machinery are well described in isolated preparations, only a handful of experiments have documented the kinematics of the lattice occurring when multi-scale interactions are fully intact. We used time-resolved x-ray diffraction to record the kinematics of the myofilament lattice within a normal operating context: the tethered flight of *Manduca sexta*. Since the primary flight muscles of *Manduca sexta* are synchronous, we used these results to reveal the timing of *in vivo* cross-bridge recruitment, which occurred 24 (s.d. 26) ms following activation. In addition, the thick filaments stretched an average of 0.75 (s.d. 0.32)% and thin filaments stretched 1.11 (s.d. 0.65)%. In contrast to other *in vivo* preparations, lattice spacing changed an average of 2.72 (s.d. 1.47)%. Lattice dilation of this magnitude significantly impacts shortening velocity and force generation, and filament stretching tunes force generation. While kinematics were consistent within individual trials, there was extensive variation between trials. Using a mechanism-free machine learning model we searched for patterns within and across trials. While lattice kinematics were predictable within trials, the model could not create predictions across trials. This indicates that the variability we see across trials may be explained by latent variables occurring in this naturally functioning system. The diverse kinematic combinations we documented mirror muscle's adaptability and may facilitate its robust function

in unpredictable conditions.

Introduction

Using ubiquitous molecular machinery, muscle performs diverse functions within an organism; at turns functioning as a motor, structural support, a repository for elastic energy, or as a shock absorber (Dickinson et al. 2000). A muscle's functional output – the force it creates and its length change – depends upon multi-scale interactions. Arrays of molecular motors interact (generating piconewton-scale forces) in a feedback loop with interacting muscle groups (generating newton-scale forces) within the animal's body. The highly organized lattice of contractile machinery which powers contraction also changes shape as a result of internal forces, temperature, and externally applied forces. In turn, the shape of the lattice tunes force production.

For instance, increasing the spacing between molecular motors and the thin filaments to which they bind decreases binding probability, and therefore decreases force output (Williams et al. 2013). The spacing of the lattice co-varies with naturally occurring temperature gradients, and has the potential to shift the function of otherwise identical muscle sub-units from motors to springs and dampers (George et al. 2013, 2012). Additionally, the thick and thin filaments which house myosin molecular motors and actin binding sites are far from a rigid system; instead they stretch in conjunction with internal axial forces and muscle activation. Filament stretching has important mechanical implications, accounting for about 70% of muscle's total compliance (Wakabayashi et al. 1994), and resulting in increased binding probability due to changes in the axial register of molecular motors and prospective binding sites (Daniel et al. 1998). While lattice dilation (Williams et al. 2013, Fukuda et al. 2005, Metzger & Moss 1987) and filament stretch (Squire 1997) have noteworthy mechanical implications, the relationship of their magnitude and timing within a naturally functioning organism has remained enigmatic. To address this, we documented molecular motor recruitment following nervous activation, filament stretching and changes in lattice spacing in a novel *in vivo* experimental system: the synchronous flight muscles of the hawkmoth

Manduca sexta.

The advent of high-speed digital detectors in the early 2000's made *in vivo*, time-resolved x-ray diffraction possible. Landmark studies of lattice kinematics in naturally functioning systems have largely focused on asynchronous insect flight muscles (fruitfly: *Drosophila* and bumblebee: *Bombus*) (Dickinson et al. 2005, Irving & Maughan 2000, Iwamoto & Yagi 2013). Irving & Maughan, for example, were the first to document the molecular kinematics of a mutant fly *in vivo*, connecting molecular mutations with their functional outcomes across the scales of animal flight behavior (Irving & Maughan 2000). However one limitation of these systems is that in asynchronous muscle neural activation is decoupled from cycles of muscle shortening and lengthening; instead activation serves to keep the muscle in a contractile state by continuously suffusing myofibrils with calcium ions. Asynchronous muscle is uniquely specialized to power high-frequency wing flapping (Syme & Josephson 2002). Iwamoto and Yagi leveraged this to record the mechanism of stretch activation independent of calcium release and re-uptake (Iwamoto & Yagi 2013).

In contrast to asynchronous muscle, many mammalian skeletal muscles are activated in partial tetany, with multiple neural impulses stimulating larger contractile forces. Vertebrate cardiac muscle, on the other hand, has a one-to-one relationship between activation and contraction. In a manner analogous to cardiac muscle, the dominant flight muscles of *Manduca sexta* are synchronous with, generally, a one-to-one correspondence between neural activation and muscle contraction. Additionally, they mirror cardiac muscle in their function, contracting against fluid loads and acting predominantly on the ascending portion of their length-tension curve (Tu & Daniel 2004).

By pairing simultaneous recording of muscle activation with x-ray diffraction data, we were able to phase average lattice kinematics using the organism's natural activation. These results uniquely show the timing of molecular motor recruitment and the resulting lattice kinematics (stretching and dilation) following activation. Using phase averaged data we found that the molecular kinematics are consistent within individuals, often showing large excursions: the lattice can dilate by as much as 2.5 nm (5.4%), thick filaments can stretch

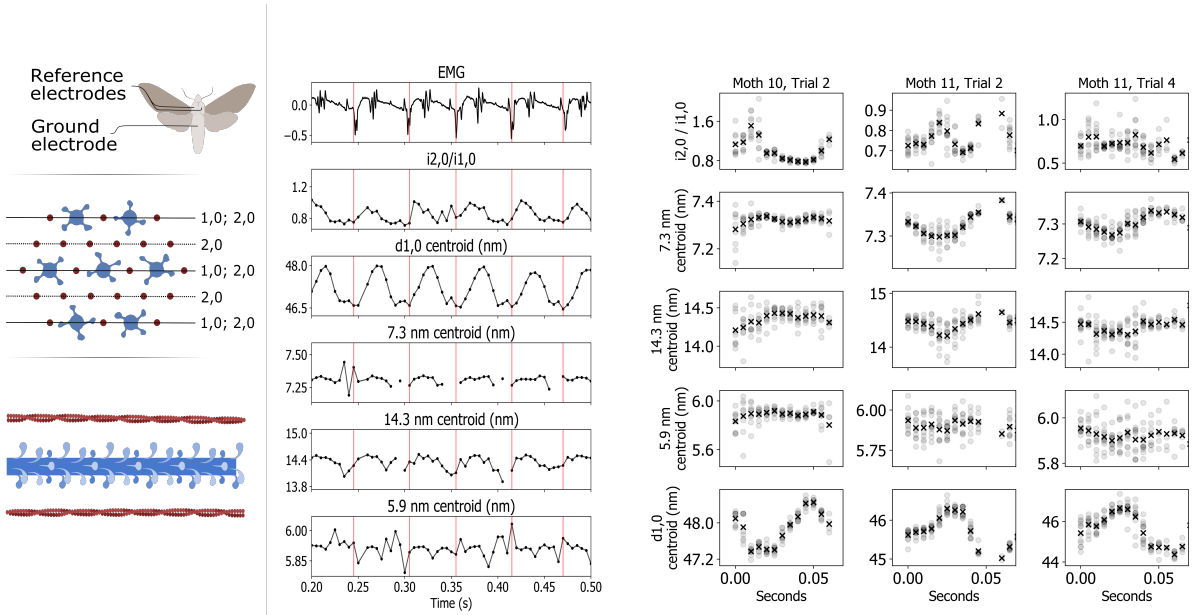

Figure A

Figure B

Figure 2.1

Time resolved lattice kinematics are consistent within a trial but vary between trials. (A) The muscle's activation recorded in the EMG signal is indicated by a vertical red line. The time of the EMG peak was rounded to the nearest $\frac{1}{200}$th of a second to match the frame rate of the detector, leading to a slight mismatch with the EMG recording which had a resolution of 25,000 Hz (Methods: Electromyogram). In the EMG trace shown, the large amplitude peaks are from the activation of the DLMs, while the EMG also picked up the activation of the neighboring antagonistic muscle group, the Dorsal Ventral Muscles. These are seen in smaller amplitude spikes. Cross-bridge recruitment was inferred by the radial shift of mass between the 1,0 and 2,0 planes as cross-bridges move towards the thin filaments following activation. Lattice spacing was measured using the 1,0 reflection. Thick filament stretching was inferred from changes in the spacing of the 7.3 nm meridional reflection and thin filament stretching from changes in the axial spacing of the 5.9 nm off-meridional reflection. (B) Data was phase averaged using the muscle's endogenous depolarization. The mean of each time point following activation is marked with an X. All of the data we collected is shown in the supplement (Fig: S4).

by as much as 1.2%, and thin filaments by as much as 2.1%. In light of experimental and computational studies, the magnitude of these results support the notion that lattice kinematics significantly modulate muscle function (Daniel et al. 1998, Williams et al. 2013, Metzger & Moss 1987). As is expected in a fully intact, normally functioning animal, there was considerable variation in both the timing and extent of lattice motions across individuals. These results highlight that while individuals may manifest the same functional outcome at the organism scale (flight), the mechanics of the lattice underneath can vary. Considering this, lattice kinematic data need to be considered within the context of individuals without supposing that latent variables are equal across individuals (Gomez-Marin & Ghazanfar 2019).

Materials and Methods

2.0.1 Animal preparation

To record cross-bridge recruitment and lattice kinematics as a function of electrical activation we used an insect synchronous muscle. The dorsal longitudinal muscles (DLMs) of *Manduca sexta* are synchronously activated, and are an excellent system for x-ray diffraction experiments since the thorax is composed of about a cubic centimeter of highly ordered muscle and the exoskeleton produces negligible scattering. The clear diffraction patterns produced by this muscle made it possible to collect time resolved data without frame averaging. We used a random mix of male and female moths 1-2 weeks post eclosion. We did not record sex and our limited sample size precludes analysis of sex differences.

We cold anesthetized a moth, tethered it and placed it in the beam line (Fig. 2.2). Moths were unencumbered except by Electromyography (EMG) electrodes inserted into the thorax and the ventral tether. The tether was a flattened stainless steel needle coated in cyanoacrylate glue inserted between the second and third coxae and crystalized with sodium bicarbonate. The moth was positioned on the tether with a pitch angle of approximately 30° to the horizon, similar to natural flight orientation. The moth was placed on the beamline

with its body axis, and hence the axis of the dorsal longitudinal muscles, at a right angle to the beam's incidence. The beam passed through the anterior, dorsal quadrant of the thorax, intersecting at approximately the d-c DLM subgroup based on external morphology (Eaton et al. 1988). It was aimed consistently in a small section where the wings would not obstruct the beam path. A hot air soldering iron set to its lowest heat setting was placed approximately 1m in front of the moth while a fan with a filter attached was placed behind the moth to collect dislodged scales. The warmth of the soldering iron and the wind current created by it and the fan stimulated natural flight behavior and kept the moth warmer than the room's cool ambient temperature.

Electromyogram (EMG)

EMG electrodes with hooked tips were inserted into the posterior of the thorax after puncturing the exoskeleton with a needle. The ground electrode was inserted into the abdomen

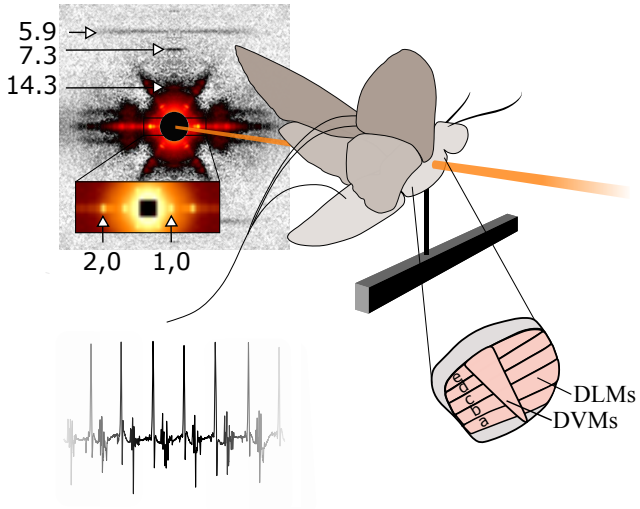

Figure 2.2: **The moth was tethered within the beamline such that the beam passed through the dorsal-anterior portion of the thorax where the DLM's comprise the bulk of the tissue volume.** Simultaneous EMG data was collected to measure membrane depolarization. The x-ray diffraction image shown is after convex hull background subtraction, which leaves the reflections due to periodic structures intact, but removes the decaying intensity around the backstop due to the beam's dispersion. This diffraction image is shown in isolation in the Supplement (Fig: S2).

(Fig. 2.2). In order to record the rapid electrical transient of muscle activation the EMG must be recorded at high temporal resolution. Therefore we recorded this data at 25,000 Hz. Since the purpose of recording muscle activation was to correlate it with the kinematics measured using x-ray diffraction we rounded the timing of muscle activation to the nearest $\frac{1}{200}$th of a second in order to correspond with the time base we used to record lattice kinematics. Because of this it may appear that there is jitter in the peak detection. The data (both x-ray diffraction and EMG) from animals that did not have periodic EMG signals with identifiable peaks for the full one second recording was excluded.

X-ray diffraction

Beamline setup

The experiment was performed at the Biophysics Collaborative Access Team (BioCAT), beamline 18ID at the Advanced Photon Source, Argonne National Laboratory, Lemont, IL, USA (Fischetti et al. 2004). The beam energy was 12.0 keV with an incident flux of 10^{13} photons/s and attenuated as needed to 10^{12} photons$\cdot$s^{-1}. It was focused to 250x250 μm at the animal's thorax, and 60x150 μm at the detector with a sample to detector distance of 2 m. The sample was oscillated over a 1 mm excursion in the beam at $20 - 30$ mm$\cdot$s^{-1} in order to mitigate radiation damage. This method of oscillating the tissue relies upon the supposition that all sarcomeres in a local region are behaving in the same manner, so moving the sample will not alter the x-ray periodicities observed. We used a photon counting Pilatus 3 1M (Dectris Inc.) with 981x1043, 172x172 μm, pixels with a 20-bit dynamic range.

Raw image data was collected at 200 Hz with 1 ms of dead time per frame, and with the X-ray shutter open continuously.

Data reduction from x-ray diffraction images

The 32-bit tagged image file format (TIFF) image stacks returned by the x-ray detector were annotated using the Musclex software suite developed by the Biophysics Collaborative

Access Team (BioCAT) (Jiratrakanvong et al. 2018). Images were annotated by two different individuals and cross-validated to ensure that there was not a substantial difference between them (Fig: S3). Trials where data was not traceable were excluded. Each image was quadrant folded to center and average intensities across axes of symmetry and annotated for meridional and equatorial intensity peaks. We used versions of Musclex prior to version 1.14.12. These have an error in the image centering algorithm that results in the image center being rounded to the nearest pixel. This means there is a center placement error of ¡0.5 pixels that could result in a maximum radial compression of the image of 0.5 pixels. An improvement in centering is being implemented in future versions which reduces the error inherent in interpreting physically continuous data recorded in a pixel framework by remapping intensity based on the calculated image center.

Cross-bridge recruitment

Cross-bridge recruitment can be inferred by the shifting of mass away from the thick filaments and towards the thin filaments. Since the flight muscle of *Manduca sexta* has a packing ratio of 1:3 thick to thin filaments, the intensity of the 1,0 peak contains thick and thin filament mass, while the 2,0 peak is the sum of the second-order harmonic of the 1,0 and the intensity due to layers containing only thin filaments (Fig: 2.1). As cross-bridges move towards the thin filaments, there is a decrease of the 1,0 intensity due to the shifting of mass towards the layers of thin filaments. In contrast, the 2,0 stays relatively constant since there is little change in the total mass on these planes. Therefore the ratio of 2,0 to 1,0 intensity is expected to be highest during peak cross-bridge binding. This differs from vertebrate muscle, where the ratio of the 1,1 reflection and 1,0 reflection is a surrogate for cross-bridge binding. The intensities of the 1,0 and 2,0 reflections were computed using Musclex's "Equator" function, which first sets a box around the equator, uses convex hull background subtraction, and finally calculates peak intensity.

Lattice spacing

Lattice spacing was measured by tracking the 1,0 reflection's centroid motion using Musclex's Equatorial function and a Voigt model fitted to three peaks: 1,0; 1,1 and 2,0. This data was gathered simultaneously with cross-bridge recruitment. Notably, the Voigt model we used within the Equator function's framework is over-determined with only two peaks, so we tracked the 1,1 reflection intensity in the fit model as well. The distance of the centroid of the 1,0 equatorial reflection from the backstop correlates by Bragg's law to the distance between layers of the filament lattice containing the thick filament.

Filament strain

Thick and thin filament strain were calculated using axial filament spacing changes recorded along the meridian and in layer lines of the diffraction pattern. We used Musclex's Diffraction Centroids function to estimate the axial spacing of the following intensity peaks: the 14.3 nm meridional, an indicator of spacing changes between layers of myosin crowns; the 7.3 nm meridional, an indicator of spacing changes in the myosin containing thick filament backbone; and the 5.9 and 5.1 nm off meridional actin layer lines, which correspond to the pitches of the left and right genetic helices. At the exposure times we used, the actin layer lines were relatively weak. The 5.9 nm layer line intermittently yielded reliable data, while the 5.1 nm layer line was not measurable for most trials. The data presented for the 5.9 nm layer line should be interpreted with due caution since without 5.1 nm data filament twisting and stretching cannot be differentiated.

Data handling

All of the code we used can be found in the GitHub repository: In_vivo_Myofilament_Lattice_Kinematics. All of the data that we used in preparing this manuscript can be found on Dryad at the link: https://doi.org/10.5061/dryad.s1rn8pk51 under the same name as this manuscript.

Permutation bootstrap

To assess if a signal contained significant cyclic changes at the same frequency as the muscle's activation we used a permutation bootstrap. We took the Fourier transform of a time series signal, which returned the power of the signal across frequency space. We then compared the power of the raw signal at wing beat frequency to the power obtained for a signal composed of the original signal, but randomly shuffled. If out of 1,000 permutations, fewer than 5% had a power greater than or equal to the original signal's power at wing beat frequency the signal was used to compute average periodic excursions. If more than 5% had a power greater than or equal to the original signal's, we cannot evaluate what component of the data is noise, so the signal was excluded from computing excursions. Out of the 11 trials we recorded, 11 showed significant periodic changes in lattice spacing, 9 showed significant periodic changes in cross-bridge recruitment, 7 showed significant periodic thick filament stretch, 6 showed significant periodic changes in the 14.3 nm centroid spacing and 6 showed significant periodic thin filament stretch. These results correspond to the annotator's observations that data encoded on the equator is typically much stronger, while at the exposures lengths we used data encoded along the meridian was more challenging to track.

Spike triggered average (STA)

The STA is created by phase averaging time course x-ray diffraction data using the muscle's depolarization as the start point. One phase is defined to be the period of time between sequential membrane depolarizations (the interspike interval). Interspike intervals were denoted using Python scripts which identify EMG peaks and down sample their time resolution to that of the x-ray data, indicating the frame during which depolarization occurred.

Correlation

The correlation of signals as a function of proportion of interspike interval lag was used to determine if there was a consistent phase offset of cross-bridge recruitment and thick

filament stretch, and of cross-bridge recruitment and lattice spacing change across trials. We also calculated the correlation of two signals as a function of absolute time lag (Fig: S5) and found no consistent pattern. Correlation was calculated using Numpy's built in correlation function.

Gradient boosted decision tree mechanism-free model (xGBoost)

xGBoost is a library to create gradient boosted decision trees that can be used for regression, classification and prediction (Chen & Guestrin 2016). Gradient boosting iteratively combines weak hypotheses (in the case of xGBoost a weak hypothesis is a decision tree that has an imperfect prediction) that follow the gradient descent of an error loss function. At each iteration, a new tree is added with the goal of fixing the error left in the model prediction from the previous iterations. The loss function can be generalized as any differentiable function. xGBoost is a particularly fast and effective implementation of the machine learning algorithm 'gradient boosted decision trees' that has been used to win many Kaggle competitions (Cook 2020). We used it to create a mechanism-free prediction of lattice dilation from filament stretching and cross-bridge recruitment data. Specifically, the model used the 14.3 nm reflection's intensity (often used as an indicator of cross-bridge recruitment in vertebrate systems), the ratio of the reflections of the 2,0 and 1,0 planes, the 7.3 nm reflection's centroid and the 5.9 nm off meridional's centroid. Since the change of the lattice's shape from one timestep to the next depends not only on the state of these parameters, but also their time history, we extended the information available to the model by including the time history of cross-bridge recruitment and filament stretching up to 11 time steps (0.055 s) prior to the time point to be predicted.

To create the xGBoost model, factors like the number of decision trees it uses and how many decision points each tree can encompass must be specified. These characteristic features of the model are called hyperparameters. Optimizing the choice of hyperparameters can be accomplished by methods like grid search, coordinated descent, or a genetic algorithm. We chose to use a genetic algorithm. In essence, a small set of models (10 in our case) are

constructed with randomly selected hyperparameters; these are a first generation. The next generation is created by combining the hyperparameters of the most successful models in the parent generation, along with random "mutation" to one of the hyperparameters. We used a total of 7 generations and allowed the crossing of 4 of the parameter models. We adapted code for an implementation of the genetic algorithm for selecting hyperparameters for xGBoost that can be found on the GitHub repo "Hyperparameter-tuning-in-XGBoost-using-genetic-algorithm" (Jain 2018*a*,*b*) In the interest of reproducibility, the model's hyperparameters can be found in the supplement (Table S1,2).

Results

We recorded cross-bridge recruitment, axial filament strains, and radial lattice dilation as a function of endogenous muscle activation during *in vivo* tethered flight. These were indicated respectively by the ratio of the intensities of the 2,0 to the 1,0 equatorial reflections; axial shifts of the centroid of the 7.3 nm meridional reflection and axial shifts of the 5.9 nm actin off meridional reflection, and finally radial shifts in the position of the equatorial reflections (Fig: 2.1A). We also recorded the axial shifting of the 14.3 nm meridional reflection. With a detector frame rate of 200 Hz and wing beat frequencies ranging between 13-19 Hz (mean 16 (s.d. 2), we obtained 11-15 x-ray diffraction images from each cycle of shortening and lengthening. Each trial lasted one second, and we created spike triggered averages (STAs) by phase averaging the data based on the peaks of each individual's electromyogram (EMG). Most individuals had consistent STAs, however there was variability between individuals in the time course and excursions of their STAs for a given data type (Figs: 2.1, S4). We calculated the excursion of a signal as the difference between the maximum and minimum of the STA for each trial.

2.0.2 The timing and extent of cross-bridge recruitment, filament stretching, and lattice dilation are revealed in spike triggered averages (STAs)

By using a synchronous muscle group, we were able to correlate muscle activation and the resulting recruitment of myosin molecular motors to the thin filaments. The peak cross-bridge recruitment occurred an average of 0.024 (s.d. 0.026) seconds following activation, with a resolution of 0.005 seconds. We measured the extent of filament stretching by calculating the excursion (maximum minus minimum) of the 7.3 nm reflection's STA. This revealed that thick filaments stretch by an average 0.75 (s.d. 0.32)% across 7 trials. By first calculating the excursion of each trial and subsequently computing the mean across trials we avoid the blunting of the signal that can occur if the excursion is calculated from the amalgamation of all trial's normalized STAs. Likewise, we calculated the lattice's dilation as the maximum minus the minimum of the STA for each trial, with a mean taken across all 11 trials. The lattice dilated by 2.72 (s.d. 1.47)%, which corresponds to 1.24 (s.d. 0.66) nm.

For each of these data types, the pattern of the STA was relatively consistent across many cycles of shortening and lengthening within an individual trial. This is especially apparent in the case of the d1,0, which, as the clearest diffraction signal, is least subject to error

Summary of data					
Data type	# of trials	Baseline	Excursion	Percent excursion	Peak time
i2,0/i1,0	9	0.708 (s.d. 0.076)	0.250 (s.d. 0.204)	35.35 (s.d. 26.92)%	0.024 (s.d. 0.026) s
7.3 nm centroid	7	7.29 (s.d. 0.02) nm	0.06 (s.d. 0.02) nm	0.75 (s.d. 0.32)%	0.058 (s.d. 0.024) s
5.9 nm centroid	6	5.87 (s.d. 0.04) nm	0.07 (s.d. 0.04) nm	1.11 (s.d. 0.65)%	0.044 (s.d. 0.025) s
d1,0	11	45.84 (s.d. 0.88) nm	1.24 (s.d. 0.66) nm	2.72 (s.d. 1.47)%	0.032 (s.d. 0.018) s
14.3 centroid	6	14.26 (s.d. 0.08) nm	0.30 (s.d. 0.13) nm	2.08 (s.d. 0.91)%	0.039 (s.d. 0.026) s

Table 2.1: For each of the 11 total trials, and each data type we ran a permutation test to see if there was a significant frequency component at wing beat frequency. If the chance of a random permutation yielding a power as high or higher than the raw data at wing beat frequency was less than 5% we factored it into this summary. If it was greater than 5% we can only conclude that if there are periodic changes occurring, they are of lower amplitude than the noise envelope. The number of trials that passed the permutation test is recorded in the column "Number of trials". For each trial and datatype, its baseline value was the minimum point in the STA. The average baseline as the mean of across all trials. The excursion of each datatype was calculated as the average across all trials of the STA maximum minus the STA minimum. The percent excursion was the absolute excursion divided by the baseline for each trial – these were averaged across all trials. Finally the peak time was the time elapsed from the beginning of the STA to its maximum, which was averaged across all trials.

during annotation. However the STAs reveal extensive variation across individuals, which means that there is a large standard deviation in the timing and extent of myofilament lattice kinematics.

2.0.3 Interrelationship of lattice kinematics: inter- and intra-indiviudal patterns

Our kinematic data capture filament motions within a mechanically coupled system. Here we explore whether there are consistent relationships between the various lattice kinematics within individuals and, additionally, whether there are patterns common to all individuals. Since thick filament strain results from active tension development, passive tension development and filament activation (Wakabayashi et al. 1994, Ma et al. 2018, Irving et al. 2011, Piazzesi et al. 2018), we hypothesized that the stretching of the thick filament indicated by movement of the 7.3 nm meridional reflection would be maximally correlated with increased cross-bridge binding at a relatively fixed phase offset. However the maximum cross-correlation between cross-bridge recruitment and thick filament stretch shows variable timing offsets across individual trials, demonstrating a complicated relationship between these variables. This may be partially explained by recent work which demonstrates that there is a non-linear relationship between tension and thick filament extension (Ma et al. 2018). Proteins similar to titin may also contribute to sarcomere elasticity in *Manduca sexta* (Yuan et al. 2015) with significant non-linear behavior (Powers et al. 2018, Trinick 1996, Tskhovrebova et al. 1997) and temperature dependence (Bullard et al. 2006). Finally, while stretching of the filaments indicates internal axial force, cross-bridges also exert force radially. This means that the magnitude of the component of cross-bridge force applied axially changes as a function of the angle between motors and binding sites (Schoenberg 1980, Williams et al. 2010). In light of these considerations, it would be remarkable if the movement of mass towards the thin filaments alone explained the periodic stretching of the thick filaments, or the periodic dilation of the lattice. But taken together, can we use these data to fully model the system?

If the data are sufficient to explain one another mechanistically, even though the link-

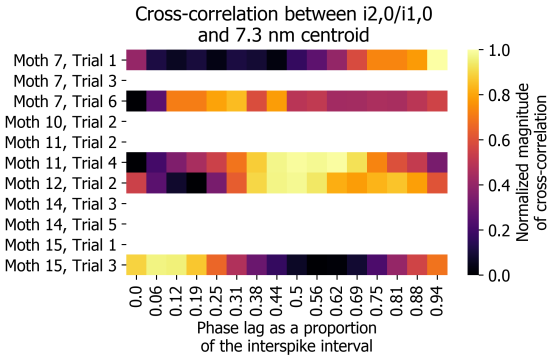

(a) Cross-correlation of cross-bridge recruitment and thick filament stretch

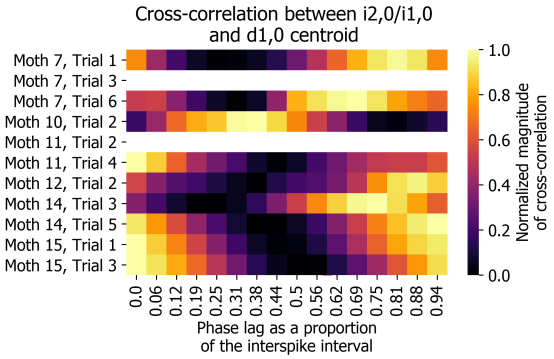

(b) Cross-correlation of cross-bridge recruitment and lattice dilation

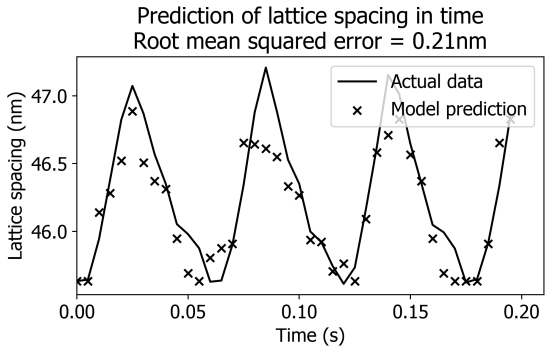

(c) A mechanism-free model creates a good prediction of lattice spacing change on untrained lattice spacing data when it is trained and tested using data from the same trial, but different time points.

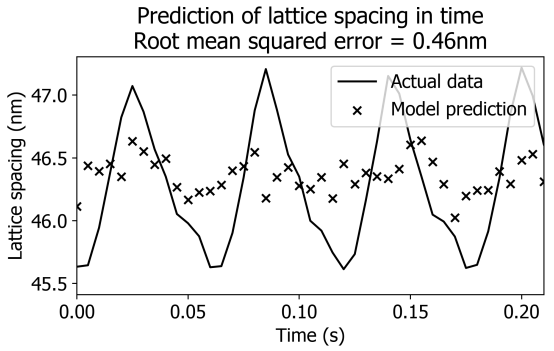

(d) The same mechanism-free model framework fails to create an adequate prediction of lattice spacing change when the model is trained on all trials but one and tested on the with-held trial.

Figure 2.3: **The relationship between lattice kinematics is not consistent across trials.** Panel A) shows that there is not a consistent phase offset of cross-bridge recruitment and filament extension. The magnitude of the cross-correlation is normalized, and phase offset is measured in proportion of the interspike interval (the period of time between subsequent muscle activation). Some trials do not contain adequate data for all data pairings – a permutation bootstrap was used to determine for each datatype within a trial if it contained a significant periodic component at wingbeat frequency, and those that did were included. Correlation as a function of time lag in seconds can be found in the Supplement (Fig: S5). Panel B) shows the correlation between cross-bridge recruitment and lattice spacing. Panels C) and D) show a mechanism-free model's prediction of lattice spacing from filament strains and cross-bridge recruitment in time. Panel C) shows a prediction for the case where the model is trained on 75% of a trial's data, and tested on the other 25%. The average Root Mean Squared Error (RMSE) was 0.27 nm. Panel D) shows a representative image from the case where the model was trained on the data from all trials, except for one that was with-held as a test set. The average RMSE across all trials trained in this manner was 0.79 nm. The disparity between the model's performance under these paradigms suggests that while this model is capable of making good predictions from these types of data sets (panel C), the predictions made by the model cannot extrapolate effectively across individuals for this data set (panel D).

age is non-obvious, they should be sufficient to train a mechanism-free, data-based model. (Though by creating a mechanism-free model we cannot exclude the possibility that the data are insufficient to explain one another mechanistically, but contain enough correlative information to successfully predict one-another.) We used a gradient boosting decision tree algorithm housed in the xGBoost library (Chen & Guestrin 2016) to train a mechanism-free model. First we trained the model with 75% of a trial's data, using the other 25% as a test set to evaluate model performance. We set up the model to predict lattice spacing from filament stretching and cross-bridge recruitment since lattice spacing is typically the cleanest of the signals tracked in x-ray diffraction due to its intensity. In addition to using the current state of filament stretch and cross-bridge recruitment to predict the current lattice spacing, we also provided the model with the time history of the predictor variables up to 11 time-steps (0.055 s) previous to the current state. For these within-trial predictions the random forest-based model performed well, with a Root Mean Square Error (RMSE) of 0.27 nm, demonstrating that it is possible to predict lattice spacing change from filament stretching and cross-bridge recruitment within a trial.

We then addressed our larger question – can we create a prediction of lattice spacing change from cross-bridge recruitment and filament stretching data that holds across individuals? We iteratively withheld the data from one individual as a test case and trained the model with the data from all other individuals. The average RMSE across all trials was 0.78 nm. This shows that the themes the model uses to create intra-individual predictions do not generalize well across individuals.

Discussion

Combining high-speed, time-resolved x-ray diffraction with simultaneous recording of the electrical activation of the synchronous flight muscles of the hawkmoth *Manduca sexta* we resolved myofilament lattice kinematics during fully intact tethered flight. Taken together, our data reveal intra-individual patterns of axial myofilament stretching, radial spacing changes, and cross-bridge recruitment that follow the endogenous activation of muscles. This method

gives us a window into the molecular motions that underlie muscle force production.

2.0.4 Cross-bridge recruitment

While x-ray evidence for the timing of the excitation-contraction pathway has been used in isolated fibers (Reconditi et al. 2011), the time course of cross-bridge recruitment following activation for fully intact and *in vivo* preparations has not previously been reported. Muscle contraction is triggered by motor neuron activation, leading to depolarization of the muscle cell membrane and the subsequent release of calcium from the sarcoplasmic reticulum into the cytoplasm surrounding the filament lattice. Calcium binding initiates the shifting of the troponin - tropomyosin complex away from actin binding sites and the dissociation of molecular motors from the thick filament, allowing the formation of cross-bridges between the filaments (Gordon et al. 2000, Squire & Morris 1998, Stelzer, Fitzsimons & Moss 2006). Our data show that peak cross-bridge recruitment occurs an average of 0.024 (s.d. 0.026) seconds following activation, to a resolution of 0.005 seconds. While the time course of cross-bridge recruitment was generally consistent in an individual trial over many cycles of sequential shortening and lengthening, there was variation between individuals, resulting in the large standard deviation.

The variation in lattice kinematics that we recorded in a fully intact system could arise from several latent variables. For example, temperature varies both spatially and temporally in *Manduca sexta*. Temperature gradients correlate with variation in lattice kinematics at the molecular-scale, and molecular-scale variation corresponds to functional gradients across the muscle group at the organism scale (George et al. 2013). In addition to gradients across a muscle group, the mean temperature of the muscle group increases with increasing wing beat frequency in *Manduca sexta* (Heinrich & Bartholomew 1971). Temperature may contribute to the observed variation in our system since the diffusion of substrates like calcium ions and molecular motors is slower in cool muscle. However the experimental constraints of simultaneous EMG recordings and high speed, time-resolved x-ray diffraction in a naturally functioning animal limit our ability to resolve spatio-temporal patterns of temperature in

the muscle. In favor of an intact preparation, we did not control temperature and all of the moths were flapping their wings at different frequencies of their own volition. While temperature likely contributes to the variation we observe in our data, diversity in the timing of maximum cross-bridge recruitment could also arise from other mechanisms, such as other steps in the excitation-contraction pathway, or co-occurring lattice spacing changes and filament stretching.

Although the ratio of the intensities of the 2,0 and 1,0 reflections is often used to quantify the shifting of mass between them (Irving 2006), peak intensities could in theory be affected by changes in lattice ordering (Bershitsky et al. 2009) over a cycle of shortening and lengthening. Additionally, shifting of mass from the thick to the thin filaments does not necessarily imply binding. However, despite these caveats, the shifting of mass is well correlated with strong motor binding in vertebrate muscle (Squire 1997, Harford & Squire 1992). This ratio is an accessible surrogate for cross-bridge recruitment during time-resolved x-ray diffraction.

2.0.5 Filament stretching

Filament stretching modulates muscle's function. Axial filament stretching accounts for a large component of the sarcomere's total compliance (about 70% (Wakabayashi et al. 1994)), enabling the return of stored elastic strain energy. The stretching of filaments also means that cross-bridges do not act independently of one another. Instead, as the relative separation between binding sites and cross-bridges changes, binding probability is also altered. Spatially explicit modeling demonstrates that these changes in axial register may mediate force output (Daniel et al. 1998). In addition to changes in axial register, strain in the thick filament may alter its twist. In *Lethocerus* asynchronous flight muscle thick filament strain is accompanied by a change in twist of about 12° that would help move heads closer to actin target zones as thick and thin filaments are strained (Perz-Edwards et al. 2011). Unfortunately X-ray patterns from *Manduca sexta*'s flight muscle lack the rich layer lines that *Lethocerus* muscle displays, so we could not identify changes in helical twist of the thick filament. The extent to which filament twist occurs in *Manduca sexta* as a function of filament extension remains

conjectural until other experiments are devised to detect such changes.

Despite its functional significance, the extent of filament stretch occurring during natural muscle function was unknown until recent evidence from time-resolved x-ray diffraction revealed subtle (0.2 %) thick filament stretching in the dominant flight muscles of *Drosophila* (Dickinson et al. 2005). Our measurements show that the thick filament stretches by an average 0.75 (s.d. 0.32)% across 7 trials as indicated by changes in the 7.3 nm meridional intensity peak (Fig: 2.2). While the symmetry of *Manduca sexta*'s thick filament is not yet known it may be different from vertebrate filaments, possibly akin to *Lethocerus*, which has four-fold rotational symmetry (Hu et al. 2016, Reedy et al. 2000). Thus the 7.3 nm reflection may not be exactly equivalent to the M6 reflection in vertebrate muscle, nor the 14.3 nm reflection to the M3. With this caveat, in analogy with vertebrate muscle, the 7.3 nm reflection likely includes contributions from the second-order of the 14.3 nm myosin head repeat with additional contributions from the thick filament backbone (Brunello et al. 2006). The imperfect correlation of the spacing and intensity changes of the 7.3 nm reflection and the 14.3 nm reflection in vertebrate muscle, however, indicates that the 7.3 nm reflection is dominated by structures in the backbone; meanwhile, the 14.3 nm reflection is dominated by the periodicity of the myosin heads so that spacing changes in the 7.3 nm reflection may be used as a measure of thick filament extensibility (Brunello et al. 2006, Huxley et al. 1998, Linari et al. 2000, Ma et al. 2018). We have shown the cross-correlation of the 7.3 nm and 14.3 nm repeats from these data in the Supplement (Fig: S1). We conjecture that the same pattern seen in vertebrate muscle holds for the flight muscle of *Manduca sexta*. Though larger than those observed in *Drosophila*, the values we report are near those observed in isolated vertebrate fibers under isometric contraction (Wakabayashi et al. 1994, Brunello et al. 2006, Huxley et al. 1994). This result confirms the relevance of these parameters to *in vivo* function in a synchronous muscle group during natural function. Additionally, by measuring the extension of filaments within individuals rather than averaging across trials, the blunting of the signal that occurs when averaging phase offset data is avoided.

2.0.6 Lattice dilation

Muscle function is also impacted by the spacing of the myofilament lattice, which is thought to play a role in the Frank-Starling mechanism in the mammalian heart (Moss & Fitzsimons 2002). cross-bridge binding alters lattice spacing, and in turn their binding probability and the direction of the forces they generate are regulated by lattice spacing (Schoenberg 1980). Radial cross-bridge extension has also been proposed as a site of elastic energy storage that could be returned to power cyclic contraction (Williams et al. 2012, George et al. 2013). Through mechanisms such as these, lattice spacing change results in a steeper length-tension curve than would be produced if only filament overlap changed during contraction (Williams et al. 2010). Since these muscles act on the steep ascending portion of their length-tension curve they generate larger forces in response to perturbations that stretch them, without a need to modify nervous control. Therefore in the case of cardiac muscle when blood pressure suddenly rises and increases ventricular filling, or in the case of flight muscle when a gust of wind buffets against the wing, the muscle autonomously contracts more forcefully (Tu & Daniel 2004). This is an example of a cell-scale set point that yields a reflexive response to environmental perturbations at the organism scale, lending robustness to rapidly changing external demands (Moss & Fitzsimons 2002).

Isolated muscle preparations have yielded mixed interpretations of how lattice spacing changes over the course of a contraction, although it is clear that lattice spacing is influenced by both mechanical and electrostatic interactions (Smith 2014). Often the lattice is assumed to have either a constant spacing during contraction, or to be isovolumetric. But these assumptions don't capture the extent of lattice spacing change observed experimentally. For instance, in skinned fiber preparations it was shown that during force generation lattice spacing tended toward a spacing near that observed when the membrane was intact (Millman 1998). Meanwhile it was shown in relaxed, intact vertebrate muscle fibers that the sarcomere can be approximated as being isovolumetric, but when cross-bridges are active both axial tension and sarcomere length are determinants of lattice spacing (Bagni et al. 1994). Are

lattice spacing changes occurring during *in vivo* muscle function?

The average lattice spacing excursion we measured across 11 trials was 2.72 (s.d. 1.47)%, corresponding to 1.24 (s.d. 0.66) nm. These data stand in contrast to the results of Irving *et al* (Irving & Maughan 2000), which showed no measurable lattice spacing change in the flight muscles of *Drosophila* to a resolution of 0.05 nm; the equivalent of ±0.1% lattice spacing change in their system. While these are significant changes in spacing, they are smaller than the approximately 4% change in spacing needed to maintain a constant volume based upon the strains of this muscle group (about 9% (Tu & Daniel 2004)). The average lattice spacing change we measured corresponds to an alteration in the force generated in osmotically compressed demembranated myofibrils of nearly 20% (Williams et al. 2013). Therefore we expect that lattice spacing change may be an important determinant of the force produced by this muscle group. Moreover, the maximum lattice spacing excursion we recorded was nearly twice the mean (2.5 nm). Akin to cross-bridge recruitment and filament stretching, lattice spacing change followed a stereotyped time course within individual trials, but the time course of lattice dilation demonstrated great breadth across trials. Similar parameters to those noted for cross-bridge recruitment and filament stretch may also give rise to the variation we observed in lattice spacing.

2.0.7 Interrelationship of lattice kinematics: inter- and intra-indiviudal patterns

Ultimately, the myofilament lattice is a mechanically coupled system, but we cannot intuit how each of the pieces relate to one another across the widely variable STAs that we documented. Moreover, cross-correlation did not reveal thematic phase relationships between kinematics across trials, but rather highlighted the variation in the timing of kinematics relative to each other.

In response to these limitations, we built a mechanism-free machine-learning model to predict lattice dilation using the other kinematics we recorded. While the model performed well within trials, it was not able to forecast across trials effectively. The model cannot find relationships in the training set that explain the test set data, and instead of interpolating

the model must extrapolate to forecast across trials, reflecting the visibly variable STAs. This may indicate that there are mechanisms that we did not record which account for the inter-trial variation. Latent variables like temperature, externally applied forces, the timing of activation, and antagonistic muscle activation are components that may be necessary to mechanistically explain myofilament lattice dynamics. These results demonstrate that the myofilament lattice uses a panoply of kinematic combinations, the breadth and significance of which we have yet to grapple with during natural function.

Conclusion

At the organism scale muscle exhibits diverse functionality, at turns powering motion, stabilizing the body, storing energy, and dissipating energy (Dickinson et al. 2000). Molecular to organism scale feedback enables muscle to meet these demands. We recorded myofilament lattice kinematics during natural behavior at all scales, revealing that thick filaments stretch by 0.75 (SD: 0.32)% and that the lattice dilates by 2.72 (SD 1.47)%. By using the synchronous flight muscles of *Manduca sexta*, we were able to record that peak cross-bridge recruitment occurs 24 ms (SD: 26 ms) after activation *in vivo*. Despite the inherent uncertainty in interpreting x-ray diffraction data from a muscle group with unresolved ultrastructure, this system holds promise for understanding the *in vivo* dynamics of a muscle group with striking similarities to human cardiac muscle. We recorded extensive inter-individual variation in the timing and extent of lattice kinematics that could not be predicted by a powerful, mechanism-free model. The machine learning model we used capitalizes on weak patterns in data to make predictions, regardless of whether those patterns are mechanistic or correlative relationships. The inability of this model to forecast across trials indicates that latent variables (such as variation in the timing of muscle activation and the interaction of many muscles in the animal's body) may give rise to the behavior we documented. While we cannot pinpoint the source of the variation we observed, it points to the need to explore how muscle uses a broad palette of kinematics to produce functional movement in a constantly changing environment.

Acknowledgements

The authors gratefully acknowledge the thoughtful feedback of Joseph Powers, Abigail von Hagel and Michael Regnier on muscle biophysics; and the feedback of Valentina Staneva, Callin Switzer, Satpreet Singh and Bingni Brunton on data analysis.

Chapter 3

FLUID FLOW IN THE SARCOMERE

Malingen SA, Hood K, Lauga E, Hosoi A & Daniel TL.

Abstract

The highly organized, densely packed molecular machinery of the sarcomeres of muscle cells facilitate rapid cell contractions. While many of the principle proteins that accomplish contraction have been well studied, the mechanical impact of fluid shearing between the sliding filaments of the sarcomere has received minimal attention. Recently, it has been proposed that fluid flow augments the substrate transport while imposing minimal energetic costs, however this analysis used analytic models of fluid flow in the molecular machinery that couldn't capture its full complexity. By building a finite element model of the sarcomere we estimated the explicit flow field. This model reveals that fluid flow likely results in minimal energetic costs through viscous shearing on sliding filaments. The model also highlights that between shearing filaments there is a steep velocity gradient, and demonstrates that the maximal radial fluid velocity occurs near the tips of the sliding filaments. These insights point towards many open questions: how might fluid forces impact molecular motor binding probabilities? How does the efflux of fluid from a sarcomere impact neighboring organelles and potentially facilitate substrate exchange?

Introduction

Muscle contraction is enacted by nanometer-scale molecular machinery housed in highly organized sarcomeres (the fundamental contractile units of the muscle cell) which are connected in a series running from one end of the cell to the other. Each sarcomere is composed of arrays of interdigitating thick and thin filaments centered on the M-line (Fig: 3.2)(Craig &

Padrón 2004). Thick filaments anchor the myosin molecular motors that power contraction when they bind to adjacent actin containing thin filaments. Myosin binding is triggered by activation of the muscle cell, and a series of regulatory steps that includes calcium regulation of thin filament binding sites (Gordon et al. 2000). Powered by the hydrolysis of adenosine triphosphate (ATP) (Oster 2002), myosin molecular motors pull the thin filaments past the thick filaments, resulting in a net shortening of the sarcomere (Squire 1997). Sarcomere function relies on a panoply of proteins beyond the actin and myosin (see, for instance (Lange et al. 2006)), and sarcomeric proteins turnover as damaged components are removed and new protein incorporated (Willis et al. 2009). These tightly packed proteins are percolated by fluid, and since muscle cells are fluid filled, contraction necessitates movement of that fluid relative to the matrix of proteins. Although the mechanics of the proteins themselves have been studied extensively (Millman 1998, Squire 1997), it is largely unknown how the flow of cytoplasm within the contractile lattice and incumbent fluid forces impact function.

Two fundamental issues arise when one considers the fluid environment surrounding the lattice of contractile filaments. First, the sliding motions of filaments relative to one another will necessarily yield fluid dynamic forces. Second, as the sarcomere shortens it is possible that there are changes in lattice volume within the cell, with fluid moving out of the lattice as the sarcomere shortens. Compounding these issues, the contractile machinery is constituted of a complex geometry of tightly packed proteins; with tiny gap distances, drag forces may be large. Intracellular fluid mechanics are increasingly seen as drivers of general cell function (Mogilner & Manhart 2018), and fluid flow has been cited as a limitation for the rate of cellular deformation (Moeendarbary et al. 2013), however these issues have yet to be comprehensively explored in muscle, a tissue capable of 1,000 Hz contraction frequencies (Sotavalta 1953).

The viscous drag force on sliding filaments in the lattice was first estimated by Huxley (Huxley 1980) (Fig: 3.1) to be on the order of tens of femtoNewtons using a hydrodynamic estimate of a slender cylinder sliding axially within a larger diameter cylinder using the

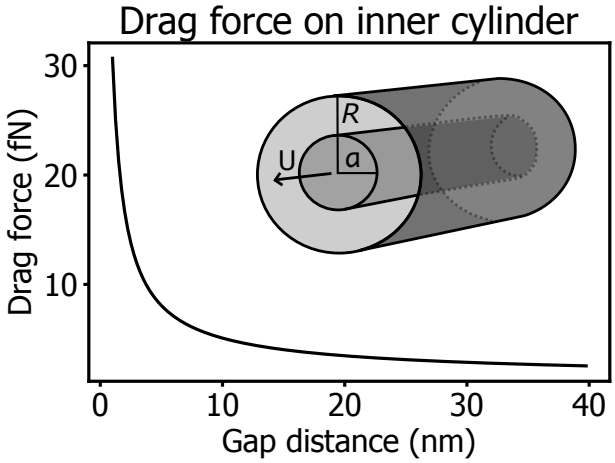

Figure 3.1: The drag force on a $1,000$ nm cylinder sliding at $1,000$ nm/s through a larger diameter cylinder depends on the gap distance between the cylinders. Here we assumed that the fluid between the cylinders had the viscosity of water (8.9E-4 Pa $\cdot$ s).

equation:

$$\text{Viscous drag} = \frac{2\pi\mu U l}{\ln(a/R)} \tag{3.1}$$

where μ is the viscosity of the fluid, U is the relative velocity of the cylinders, l is the length of overlap between the cylinders, a is the radius of the smaller cylinder and R is the radius of the larger cylinder. This estimate of drag is derived from the Stokes equation, continuity and an assumption that there is no radial or azimuthal flow in the system. Notably, there is a typo in the original equation for viscous drag in reference (Huxley 1980).

Although the drag forces on individual filaments are estimated to be small, increasing the viscosity of the fluid results in decreased shortening velocity. Instead of the drag on filaments slowing sarcomere shortening, increased fluid viscosity hampers the diffusion of molecular motors to prospective binding sites (Chase et al. 2000, 1998). The transport of calcium and ATP from the sarcoplasmic reticulum and mitochondria, respectively, to the interior of the myofilament lattice is mediated by the cytoplasm. Despite its importance, the viscosity of the cytoplasm and relevant occlusion of the space remains unknown. Experimentally, fluorescence recovery after photobleaching (FRAP) experiments have demonstrated that diffusion is limited in muscle cells as a function of particle size due to crowding and screening (Arrio-Dupont et al. 2000, 1996). The constraint of diffusion time may be especially important for muscles that contract at high frequencies where substrate demands may be particularly high.

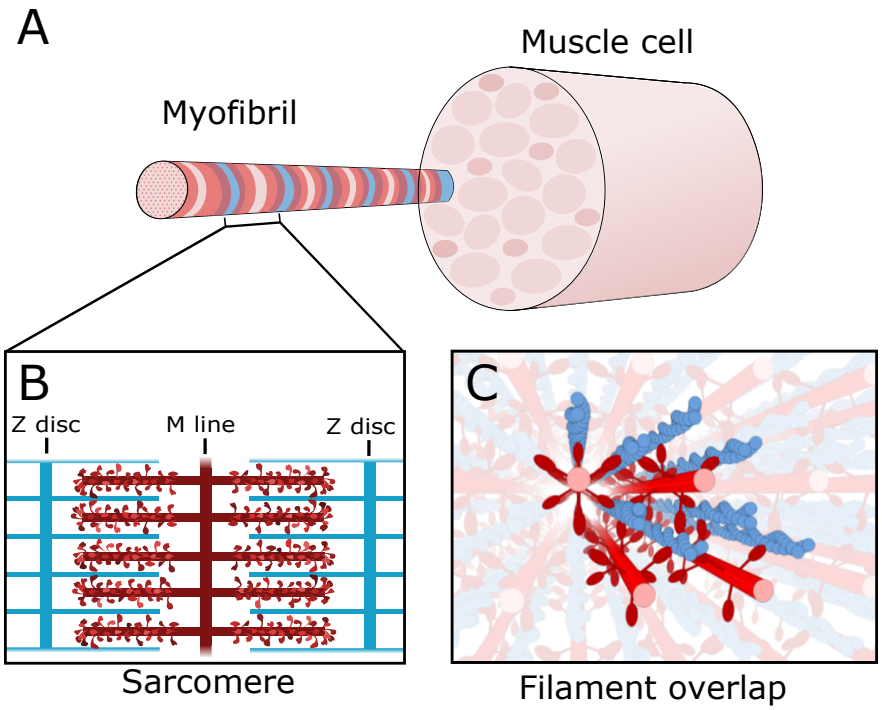

Figure 3.2: A) Individual muscle cells contain many bundles of contractile machinery, the myofibrils. While not membrane bound the myofibrils contain densely packed contractile machinery, excluding larger organelles like the sarcoplasmic reticulum and mitochondria, which occupy the space between them. B) Each myofibril is composed of sarcomeres connected in series which, in the case of skeletal muscle, run the length of the muscle cell. The sarcomere is composed of interdigitating thick and thin filament arrays which are mirrored about the m-line. Molecular motors branching off of the thick filament bind to the thin filaments and pull them towards the m-line, resulting in net muscle shortening. The z-disks structurally anchor the thin filaments, and since they have a tightly woven structure we modeled them as impermeable boundaries. C) The thick and thin filaments form a hexagonally packed lattice. The relative ratio of thick to thin filaments varies across species and muscle types.

However diffusion is not the only process mediating substrate transport. Since the lattice of contractile machinery is not constrained to a constant volume (Bagni et al. 1994, Irving & Maughan 2000, Cecchi et al. 1990), bulk fluid flow in addition to the flow driven by filament shearing must be coupled to diffusion. Using the diffusion, reaction, and advection equation for flows in model sarcomeres Cass *et al.* demonstrated that, during cyclic contraction, bulk fluid movement augments substrate transport (Cass et al. 2019) over diffusion alone. We have expanded on and contrasted our analysis of fluid flow with the analytic models they derived.

In this paper we used computational fluid dynamics to explore the flows in more complex geometries than could be done with our prior analyses. To do so, we have created a finite element model of a sarcomere-like geometry to estimate the fluid flows and forces. Our results corroborate the observation that fluid flow may impose minimal energetic consequences, while potentially augmenting substrate transport.

Results

We have contrasted a finite element model of fluid flow in the sarcomere with two analytic models: the first is derived from kinematic constraints and the boundary conditions, and the second follows from Darcy's law in which local flows are proportional to the pressure gradient. Both analytic models were developed fully by Cass *et al* in an exploration of flow-mediated substrate transport in sarcomeres (Cass et al. 2019). By creating a computational model which explicitly captures fluid flow around filaments we have explored the effect of varying the sarcomere length (i.e. the filament overlap) and the drag forces on filaments as a function of their diameter. Our results uniquely reveal how filaments impact flow structure.

Key assumptions

Due to the small spatial scales of the system, inertial forces are assumed to be negligible and the system is approximated by the Stokes equation. Despite the small length scale, we have assumed that the fluid is continuous and incompressible in each model (see Methods:

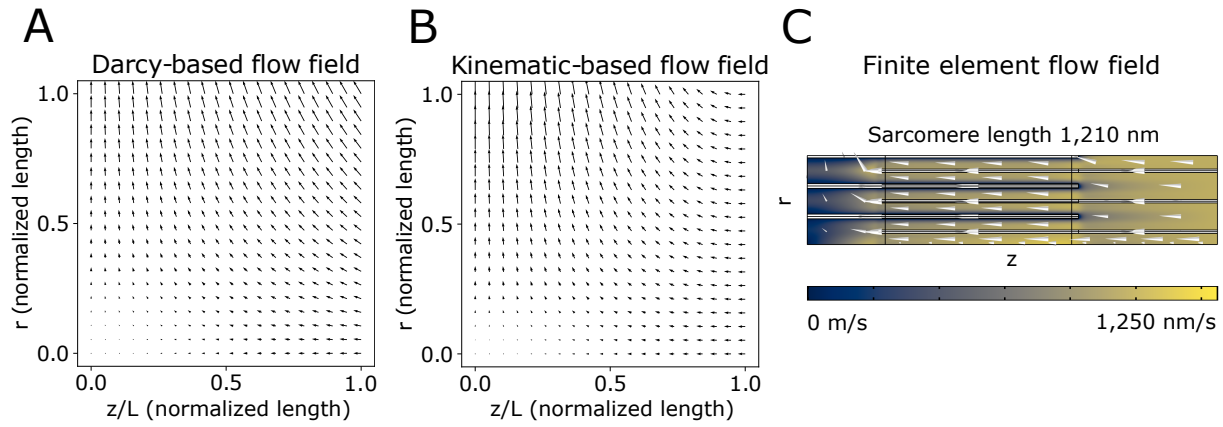

Figure 3.3: In each plot arrows denote velocity magnitude and direction. In the finite element model, these arrows overlay a heat map which indicates velocity magnitude. The Darcy-based analytic fluid flow model shows that the peak radial flow occurs at the m-line, although there is significant radial flow across the sarcomere's edge, violating the no slip condition at the z-disc. In contrast, the analytic flow field derived from the kinematic boundary conditions of the sarcomere meets the necessary boundary conditions. It also shows a peak radial outflow at the m-line and a region of stagnation at the center of the sarcomere (r = 0 and z = 0). The finite element solution to the kinematic boundary conditions allows the explicit inclusion of filaments in the system, which stream the flow. The peak radial flow occurs at the tips of the thick and thin filament arrays, and there is fluid shearing between the filaments. In contrast to the analytic solutions, the fluid largely stagnates at the m-line unless the thin filaments are nearly pushed up against it (Fig 3).

Conceptual underpinnings).

Kinematic model

Using the boundary and symmetry conditions inferred from the sarcomere's kinematics and geometry, this model provides an admissable solution to flow in the half-sarcomere. While uniqueness is not guaranteed, these solutions for radial and axial fluid velocity (u_r and u_z respectively) satisfy the equation of continuity:

$$u_r(r,z) = -U\frac{3}{4}\frac{r}{L}\left[1-\left(\frac{z}{L}\right)^2\right] \tag{3.2a}$$

$$u_z(z) = -U\frac{3}{2}\frac{z}{L}\left[1-\frac{1}{3}\left(\frac{z}{L}\right)^2\right] \tag{3.2b}$$

where r is the radial coordinate, z is the axial coordinate, U is the instantaneous shortening velocity of the sarcomere, and L is the axial length of the sarcomere. In contrast to the Darcy based model below, this kinematic model captures the physical constraint of the no slip condition on the z-disc. However this model does not account for the internal structure of the myofilament lattice, which can be roughly characterized by axial and radial permeabilities, which are typically used in solutions based on Darcy law.

Darcy based analytic solution

Since the sarcomere is a densely packed space, fluid flow may be better approximated using Darcy's law and considering the anisotropic permeability of the lattice. Although the sarcomere can be considerd to have three regions (a region with only thick filaments, a region of filament overlap and a region of thin filaments only), here we have prescribed axially uniform permeability. However in this model we can use an axial permeability different from the radial permeability, which is relevant since fluid may flow more readily through the channels between filaments than across them.

Axial flow can be described as plug flow combined with pressure-dependent Darcy flow:

$$u_z(z) = -\frac{U}{2} - \frac{k_l}{\mu}\frac{\mathrm{d}p}{\mathrm{d}z} \tag{3.3}$$

where k_l is the coefficient of axial permeability, μ denotes the fluid's viscosity and p denotes pressure. The radial component of velocity also depends on the axially varying pressure and the lattice's radial permeability, k_r. The radial velocity is found by applying the conservation of mass, which balances radial and axial flow rates with boundary conditions:

$$u_r(r, z) = \frac{rk_r}{R^2\mu}p(z) \tag{3.4}$$

where k_r is the coefficient of radial permeability and R is the sarcomere's radius. Pressure for the system is derived as:

$$p(z) = \frac{\mu U R}{2k_l\alpha \sinh(\alpha L/2R)} \cosh\left(\alpha\frac{z - L/2}{R}\right), \quad \alpha^2 = \frac{2k_r}{k_l}. \tag{3.5}$$

One advantage of this model is that the influence of radial and axial permeability can be investigated numerically by varying α. These parameters are not known experimentally, and may vary across muscles (for instance, many invertebrates have different lattice packing ratios than vertebrates (Shimomura et al. 2016)), or could be impacted by protein mutation. A limitation of this model is that it does not obey the no-slip condition on the z disc.

We numerically solved for the fluid flow in a simplified sarcomere-like geometry using COMSOL multiphysics' Creeping Flow interface. In order to reduce the computational load, which is perhaps the largest drawback of this method, we used radial symmetry and solved the flow in an axial wedge (Fig 2) of the sarcomere. We modelled the thick and thin filaments as rods and applied the no-slip boundary condition (fluid velocity at the surface is the same as the velocity of the rods). The axial velocity at the m-line was zero (by symmetry) and the velocity at the z-disc was set to $-U$ in the axial component and 0 in the radial component (no-slip condition). Fluid was allowed to leave the model at the boundary by a zero pressure

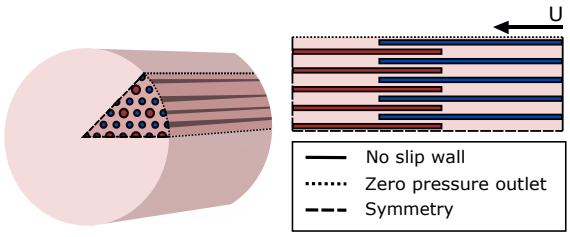

Figure 3.4: The finite element model uses symmetry to first reduce the system to a half sarcomere, and further consider a 1/8th wedge of the sarcomere. The sides of the wedge were prescribed a mirroring boundary condition while the outer edge was prescribed as a zero pressure outlet. Due to symmetry, the boundary condition at the M-line is mirroring, while the boundary condition at the z-disc is a no-slip moving wall sliding towards the M-line at velocity U = 1,000 nm/s. The surfaces of the thick and thin filaments also have a no-slip boundary condition, however the thick filaments are stationary, while the thin filaments move along with the z-disc at a velocity of U = 1,000 nm/s.

outlet.

Comparison of models

Each model has its advantages. The analytic models are computationally efficient and can be effectively incorporated in more complex analytic models, such as the diffusion, reaction and advection processes that occur in cells, however they neglect important structural details. The kinematic model accurately captures boundary conditions, but is unable to account for the internal structure of the lattice that may effect the patterns of flow. The Darcy based model accounts for the axial and radial permeability of the lattice, but it fails to meet the no-slip condition on the z-disc. Qualitatively these analytic models still provide similar flow fields: the fluid is ejected at the M-line and axial and radial flow velocities are zero at the very center of the sarcomere due to symmetry. These qualitative results differ from the finite element model, in which the maximum radial outflow occurs at the ends of the thin filaments. In fact, the flow is largely stationary near the M-line until the sliding thin filaments generate shearing. Nonetheless the analytic models may still be reasonable approximations of fluid flow in the sarcomere since many muscles operate on the ascending and plateau portions of their length tension curves (Ahn et al. 2018, Tu & Daniel 2004, Burkholder & Lieber 2001), although some muscles do at times operate on their descending limb (Gidmark et al. 2013,

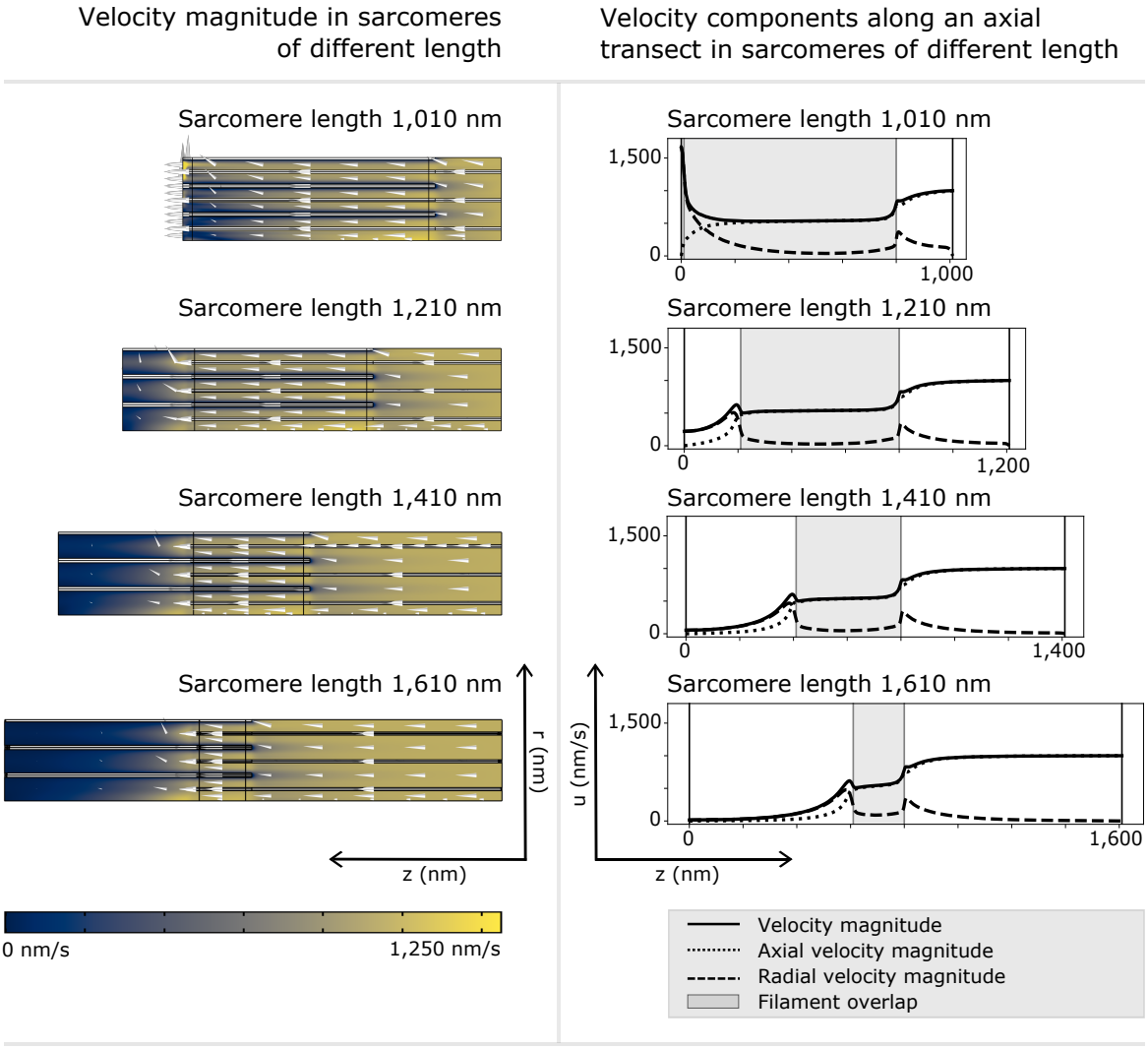

Figure 3.5: The velocity magnitude is shown as a heat map. Values over 1,250 nm/s only occurred in a small region near the M-line of the 1,010 nm geometry, and these were cut off and forced to appear as 1,250 nm/s so that the finer structure of the flow fields could be compared across simulations. The velocity along an axial transect near the border of the geometry is shown. The velocity is largest at the tips of filaments.

Azizi & Roberts 2010).

There is also a region of fluid shearing between individual thick and thin filaments. How fluid shearing in this region impacts myosin molecular motor binding probability is unknown.

While fluid flow generally augments substrate transport to the interior of the myofibril (Cass et al. 2019), the explicit nature of the flow field and its ramifications for substrate transport have not been investigated. Given that the spatial arrangements of organelles like the sarcoplasmic reticulum, mitochondria and t-tubules are highly organized, and that in addition to the myofilaments these organelles obstruct diffusion (Shorten & Sneyd 2009) while serving as sources of key substrates, the explicit structure of fluid flow may be important for transport in muscle cells, similar to other cell types (Mogre et al. 2020). For instance, mitochondrial locations are constrained by both the need to acquire oxygen, and to supply the myofibril with ATP (Kinsey et al. 2011). Developing a model of transport that accounts for the spatial distribution of organelles and structurally relevant flows is an exciting avenue to better determine the structural constraints of muscle cells.

Drag forces: do they matter?

Our model of fluid flow is limited by a number of unknowns, such as the viscosity of the fluid and the extent to which water is bound to filaments. In other cell types cytoplasm's viscosity can be approximated as that of water, and yet in the packed intra-cellular space, features like macromolecular crowding and bound water may have significant implications for drag forces and processes mediated by diffusion (Luby-Phelps 1994). The sarcoplasm is filled with an unknown panorama of proteins that could result in molecular crowding, and the depth of the bound water layers around thick and thin filaments is not certain, although osmotic compression indicates that 30% of the myofilament lattice is osmotically inactive, with a protein volume of $20 - 25\%$, indicating that $5 - 10\%$ of the volume is composed of bound cytoplasm (**?**). We assumed that the cytoplasm has the material properties of water and performed a sweep of different filament diameter values to investigate the effect of a bound water layer. These results confirm an early hydrodynamic estimate that drag forces

are small (Huxley 1980). Although drag force increases with filament diameter, even when filaments were nearly touching one another viscous drag was still small when contrasted with the picoNewton scale forces generated by individual cross bridges (Piazzesi et al. 2007, Molloy et al. 1995). Since drag force linearly depends on cytoplasmic viscosity, using the viscosity of water is likely a lower bound for the drag forces that myofilaments actually experience. Even scaling the viscosity up to $1,000\times$ that of water, however, the drag forces are still on the same order of magnitude as the forces generated by single myosin molecular motors (Linari et al. 2007). These results support earlier results that demonstrated increasing fluid viscosity reduced contraction velocity by slowing cross-bridge kinetics, rather than by imposing drag forces that hampered contraction (Chase et al. 1998).

While the forces themselves do not prohibit filament sliding, it is interesting to ask if the total energetic cost of overcoming viscous shearing is similarly negligible. To address this issue, we used our computed drag forces for thin and thick filaments at the center of the sarcomere along with their velocity to compute the rate of energy expenditure by viscous shearing. Then, for an idealized sarcomere that contains 500 thick filaments and 3,000 thin filaments and that shortens at 1,000 nm/s, we computed the lower-bound total rate of viscous energy dissipation to be 0.004 fW. Since this is not the most intuitive number, we put this number in a more biological context we used an estimate of the energy released by ATP hydrolysis of 69 kJ/mole (Wackerhage et al. 1998) to convert W to ATP molecules dissipated per second. We estimate at the lower bound that approximately 35 ATP molecules per second are dissipated by viscous drag forces given the minimum filament diameters given by electron microscopy, the viscosity of water, a 1:3 thick to thin filament packing ratio and D10 of 45 (nm) (corresponding to a surface to surface gap distance of 20 nm).

Although the 1:3 packing ratio we used is common among invertebrate muscles, there is diversity in packing ratio across taxa (**?**). In vertebrates, a 1:2 packing ratio is standard. However across invertebrates there are multiple examples of muscles with many more thin filaments than either the 1:2 or 1:3 packing ratios. To investigate how drag forces depend on packing ratio, we computed the fluid flow for a sarcomere with a packing ratio of 1:5 (which

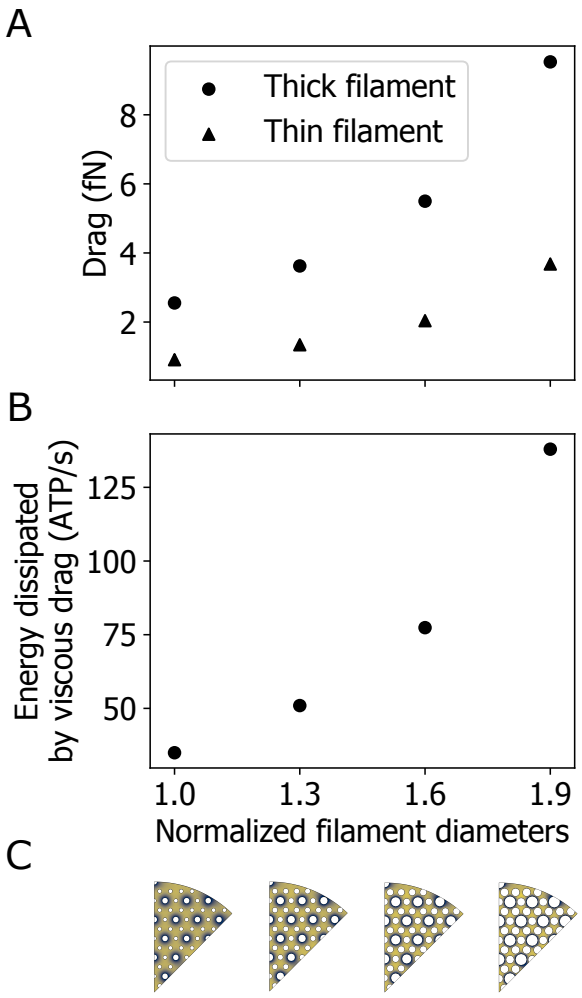

Figure 3.6: A) Drag force increases with increasing filament diameters. Drag forces were measured using a surface integration on a thin and a thick filament near the center of the sarcomere. We multiplied the filament diameters by a scaling factor (normalized filament diameter) till their surfaces nearly touched since their effective *in vivo* diameters are unknown. B) The energy dissipated by viscous drag forces on the sliding filaments was estimated by assuming that the sarcomere is composed of 500 thick filaments and 3,000 thin filaments and shortens at 1,000 nm/s. Although more energy is dissipated by viscous drag as filament diameter is increased, the overall energetic expense is relatively small compared to the cell's overall energy demands. C) The diameter of the filaments was increased by multiplying their base diameter by a scaling factor: the normalized filament diameter. To illustrate how the geometry changes as filament diameter is increased we have shown a cross-sectional heatmap of velocity magnitude for each of the simulations.

is approximately the packing ratio of cockroach femoral muscle (Hagopian 1966), although it has also been estimated at a 1:6 packing ratio (Jahromi & Atwood 1969)). With a smaller thick to thin filament ratio, the thick filament drag force magnitude was slightly larger than that of the corresponding model with a 1:3 packing ratio (3.2 fN to 2.6 fN respectively), and a slightly smaller thin filament drag force (0.6 fN to 0.9 fN respectively).

Although these estimates are small in contrast to the forces generated by individual molecular motors (on the order of picoNewtons), viscous drag forces could have broader ramifications, such as pushing molecular motors into a different position and altering their binding probability. Since contraction of the micron-scale sarcomere is enabled by the cyclic action of nanometer-scale molecular motors working in concert, small reorientations could have a large effect. Additionally, the effective diameter of the filaments given bound water and the presence of molecular motors projecting from the backbone has received minimal attention.

Future horizons

In this analysis we simplified the myofilament lattice to a continuum system to model fluid flow, revealing that the fluid flow depends on the degree of filament overlap. We estimated fluid flow in the sarcomere with analytic models and a finite element based approach using COMSOL. Each stems from finding an approximate solution to the Navier-Stokes equation for a geometry and motion similar to those observed in sarcomeres. We have also posited that the system is continuous and individual molecular interactions can be neglected since the Knudsen number is

$$\mathrm{Kn} = \frac{\lambda}{L} \approx \frac{0.3\mathrm{nm}}{20\mathrm{nm}} = 0.015 \tag{3.6}$$

given a mean free path (λ) of liquid water of approximately 0.3 nm (Padding & Louis 2006) and a representative length scale of the system (L) of 20 nm. However, this system is close to the scale at which the continuum hypothesis breaks down ($\mathrm{Kn} \approx 0.1$), and we note that in the future bulk hydrodynamic modeling may need to be coupled with methods that account

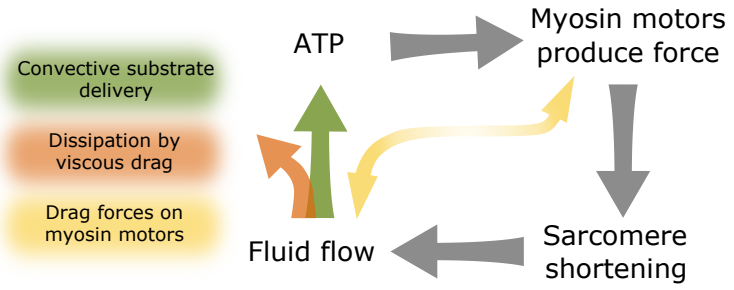

Figure 3.7: ATP powers the shape change of the myosin molecular motors which ultimately results in sarcomere shortening. Due to the shortening of the sarcomere, there is a flow of fluid, potentially in and out of the lattice. The movement of fluid could impact function by augmenting substrate delivery to the interior of the densely packed lattice. The shearing of filaments with the fluid will also result in the dissipation of energy by viscous drag. The drag force of the fluid on molecular motors could bias there positions and alter their binding probabilities. Whether this would have a positive or negative impact on contractility is unknown, and would likely depend on the dynamic character of the flow field.

for non-continuum effects. This may be especially true for investigating the ramifications of fluid flow around molecular motors. Methods that may be effective are Direct Simulation Monte Carlo (DSMC, which takes a probabilistic view of particle location based on the Boltzmann equation) (Alexander & Garcia 1997), fluctuating hydrodynamics (which blends stochasticity with the deterministic Navier-Stokes equation to approximate particle effects at a bulk scale (Chaudhri et al. 2014)) or molecular dynamics (MD, which, although computationally expensive, explicitly accounts for particle collisions) (Nie et al. 2004). Due to the range of time and size scales represented, estimating the dynamics of the cytoplasm during muscle contraction will likely require techniques that "coarse-grain" individual particle motions, coupling large scale hydrodynamics with Brownian motion (Padding & Louis 2006).

Although fluid flow within the sarcomere is of interest, fluid flow into and out of the sarcomere will interact with exterior organelles (e.g. mitochondria, sarcoplasmic reticulum and surrounding myofibrils), which may have functional implications that depend explicitly on cell geometry. Thus the scales over which models must couple may range from nanometers (as drag forces bias cross bridge motions) to millimeters (as fluid mediates transport in whole cells). Integrating from molecular to cell scales is an exciting horizon for cell biologists necessitating an understanding Brownian dynamics, colloidal dynamics and continuum mechanics

(Maheshwari et al. 2019). Striated muscle boasts a uniquely organized and well-studied system to build models integrating across these scales.

Conclusion

We contrasted two analytic models of fluid flow in the sarcomere with a finite element model created with COMSOL to characterize fluid flow in a sarcomere-like geometry. The method of regularized Stokeslets is another viable numerical method to estimate low Reynolds number fluid flow problems (Cortez 2001, Cortez et al. 2005). The fluid flow field is significantly impacted by the presence of filaments occluding the space, with the regions of largest velocity magnitude near the z disc, and maximum radial outflow at the tips of the filaments.

Drag forces and diffusion are impacted by a number of hard-to-characterize parameters: the viscosity of the cytoplasm, the degree of molecular crowding (and the size of the molecules crowding the space), layers of bound water and electrostatic interactions. Despite these uncertainties, we estimate that the energetic cost due to viscous dissipation is small compared to the cell's overall energy use. However it is important to note that we assumed we assumed a steady sliding velocity, rather than sliding induced by impulsive forces, which could lend more importance to viscous drag on filament sliding (Elliott & Worthington 2001). Therefore, advective flow may be an energetically inexpensive mechanism that augments substrate transport, and fluid flow could bias cross bridge binding with as yet unknown effects.

Methods

Conceptual underpinnings

We estimated fluid flow in the sarcomere with analytic models and a finite element based approach using COMSOL. Each ultimately derives from finding an approximate solution for the Navier-Stokes equation for a geometry and motion similar to those observed experimentally. Assuming continuity, the Navier-Stokes equations (equation 3.7) along with the

equation of continuity (equation 3.8) fully describe the movement of a fluid (Bird 2002):

$$\rho\left(\frac{\partial \boldsymbol{u}}{\partial t} + \boldsymbol{u}\cdot\nabla\boldsymbol{u}\right) = -\nabla p + \mu\nabla^2\boldsymbol{u} + \rho\boldsymbol{f} \tag{3.7}$$

where ρ is the density of the fluid, t denotes time, $\mathbf{u}$ is a vector describing the fluid's velocity, p is a scalar accounting for pressure, μ is the fluid's viscosity and $\mathbf{f}$ captures external body forces (such as gravity).

Positing that the sarcoplasm is incompressible and that the flow is steady, the continuity equation expressed in cylindrical coordinates is:

$$\frac{1}{r}\frac{\partial}{\partial r}(ru_r) + \frac{1}{r}\frac{\partial u_\theta}{\partial \theta} + \frac{\partial u_z}{\partial z} = 0. \tag{3.8}$$

Considering axisymmetric flow, the coninuity equation reduces to:

$$\frac{1}{r}\frac{\partial}{\partial r}(ru_r) + \frac{\partial u_z}{\partial z} = 0. \tag{3.9}$$

Next we consider the Reynolds number, which is the ratio of inertial to viscous stresses in the system. Given a characteristic length scale of 3 μm $= 3\times10^{-6}$ m (which is a common sarcomere length), velocity of 1 μm/s $= 1\times10^{-6}$ m/s, viscosity of $8.9\times10^{-}4$ Pa $\cdot$ s and density of 997 kg/m^3 the Reynolds number is:

$$\begin{aligned} Re &= \frac{DU\rho}{\mu} \\ &= \frac{1\times10^{-6}\cdot 1\times10^{-6}\cdot 997}{8.9\times10^{-4}} \\ &\approx 3\times10^{-6} << 1 \end{aligned} \tag{3.10}$$

A Reynolds number much less than one means that viscous forces predominately determine the behavior of the system, and so inertial forces can be taken as zero. Therefore we can simplify the system of governing equations, yielding the linear Stokes equation:

$$\nabla p = \mu \nabla^2 \boldsymbol{u} + \boldsymbol{f} \tag{3.11}$$

These governing equations undergird the modeling methods we used. Ultimately, each of the modeling methods we used searches for a possible solution to these equations using the boundary conditions posed by the geometry and motion of the sarcomere. Here we provide a brief explanation of the Darcy-based and kinematic-based fluid flow models which are fully developed in (Cass et al. 2019).

Development of Darcy based model

This model combines plug flow and Darcy based flow, which allows the variation of permeability. The half sarcomere can be considered to have three regions (thick filaments only, filament overlap and thin filaments only) that change in proportion with shortening. This model simplifies the problem by considering only a single region of overlapping filaments and approximating flow as a combination of plug flow and Darcy flow due to the motion of the z-disc and the presence of filaments occluding the space. Plug flow varies only as a function of axial location and decreases as a function of the change in pressure and the resistance of the lattice to fluid flow:

$$u_z(\mathrm{z}) = -\frac{U}{2} - \frac{k_l}{\mu}\frac{\mathrm{d}p}{\mathrm{d}z} \tag{3.12}$$

where k_l is the longitudinal permeability of the fibers and is proportional to the inter-fiber distance squared ($k_l \sim \delta^2$). In our case, the inter-fiber distance $\delta = \frac{D10}{\sqrt{3}}$.

Pairing the observation that there is no net change in volume through radial or axial volume flow with a Darcy relationship for the edge of the fibers ($r = R$) where k_r denotes the radial permeability of the fiber bundle:

$$u_r(R, z) = \frac{k_r}{R\mu} p(z) \tag{3.13}$$

we come to an equation describing the pressure (the steps of this derivation are in the

Supplement):

$$\frac{\mathrm{d}^2 p}{\mathrm{d}z^2} = \frac{\alpha^2}{R^2} p(z), \quad \alpha^2 = \frac{2k_r}{k_l}. \tag{3.14}$$

Since this is a second order linear homogeneous differential equation, the solution takes the form of an exponential, which can be expressed as the sum of a hyperbolic sine and hyperbolic cosine. While there are two roots of the equation, but since k_l, k_r and R are all positive the system can be simplified. Hence the general solution for pressure is:

$$p(z) = p_1 \cosh\left(\alpha \frac{z}{R}\right) + p_1 \sinh\left(\alpha \frac{z}{R}\right). \tag{3.15}$$

Given the boundary conditions for pressure:

$$\left.\frac{\mathrm{d}p}{\mathrm{d}z}\right|_{\mathrm{L}} = \frac{\mu U}{2k_l}, \left.\frac{\mathrm{d}p}{\mathrm{d}z}\right|_{0} = -\frac{\mu U}{2k_l} \tag{3.16}$$

and the fact that the solution for pressure is even with respect to the mid-point $z = L/2$, where L is the half-sarcomere's length, the solution can be simplified to:

$$p(z) = p_1 \cosh\left(\alpha \frac{z - L/2}{R}\right). \tag{3.17}$$

where:

$$p_1 = \frac{\mu U R}{2k_l \alpha \sinh(\alpha L/2R)} \tag{3.18}$$

. Then the radial velocity at the sarcomere's edge (R) is:

$$u_r(R, z) = \frac{U\alpha}{4} \frac{\cosh\left(\alpha \frac{z - L/2}{R}\right)}{\sinh\left(\alpha L/2R\right)}. \tag{3.19}$$

The radial flow within the sarcomere can be obtained from the conservation of mass. By taking a local average, and assuming flow is axisymmetric, we obtain:

$$\frac{\partial r u_r}{\partial r} = -r \frac{\mathrm{d}u_z}{\mathrm{d}z}. \tag{3.20}$$

Assuming that this expression is regular about r = 0, integrating by r yields:

$$u_r(r,z) = -\frac{r}{2}\frac{\mathrm{d}u_z}{\mathrm{d}z}. \tag{3.21}$$

Then since

$$\frac{\mathrm{d}u_z}{\mathrm{d}z} = -\frac{k_l}{\mu}\frac{\mathrm{d}^2 p}{\mathrm{dz}^2} = -\frac{k_l\alpha^2}{\mu R^2}p(z) = -\frac{2k_r}{\mu R^2}p(z), \tag{3.22}$$

we obtain

$$u_r(r,z) = \frac{rk_r}{R^2\mu}p(z) = \frac{r}{R}u_r(R,z). \tag{3.23}$$

Kinematics based model

The kinematic based model was inferred from the system's boundary conditions. While uniqueness is not shown, this solution is continuous and meets the available kinematic conditions, so it is an admissible solution. First, by the no slip condition, fluid at the z-disc has zero radial velocity:

$$u_r(r,L) = 0. \tag{3.24}$$

The m-line and the radial center of the sarcomere also define two planes of symmetry. At the m-line there can be zero net axial shear, while along the axial center there can be no net radial shearing:

$$\frac{\partial}{\partial z}u_z(r,0) = 0, \tag{3.25}$$

$$\frac{\partial}{\partial z}u_r(0,z) = 0. \tag{3.26}$$

In addition to the equation of continuity these conditions constrain the solution space, and

Table 3.1: The base values used for the model geometries are provided. The filament radii were later increased by a scaling factor ranging from 1 - 1.9.

Structure	Size (nm)
Thin filament radius	5
Thin filament length	1000
Thick filament radius	7
Thick filament length	800
Lattice spacing (D10)	45

they are met by the model:

$$u_r(r,z) = -U\frac{3}{4}\frac{r}{L}\left[1-\left(\frac{z}{L}\right)^2\right], \tag{3.27a}$$

$$u_z(z) = -U\frac{3}{2}\frac{z}{L}\left[1-\frac{1}{3}\left(\frac{z}{L}\right)^2\right]. \tag{3.27b}$$

Finite element model

The geometry of the model was based on structural data from electron microscopy (Squire 1997, AL-Khayat 2013, Hayes et al. 1971). Since there is variation in measured filament diameters from transmission electron microscopy (TEM), and the effective *in vivo* diameter may not be represented well by TEM images (since there may be layers of bound water, and since electron microscopy requires fixation), we varied filament diameters using scaling factors. We used a model with a 1:3 thick-to-thin filament packing ratio for the base simulations. We also used a model with a 1:5 thick-to-thin filament packing ratio since there is natural variation in packing ratios across taxa. We used symmetry to reduce the computational cost of the simulation, first reducing the simulation to a half sarcomere from the m-line to z-disc, and then further constraining it to a one-eighth wedge, resulting in a one-sixteenth of a sarcomere. In order to reduce the computational load we limited the model's radius to be six times the lattice's spacing (the D10).

Simulation details

Creeping flow simulations

We used a free tetrahedral mesh paired with COMSOL's option for a normal mesh element size calibrated for fluid dynamics. The maximum element size was 1.49E-8 and the minimum element size was 4.44E-9 with a maximum element growth rate of 1.15 and curvature factor of 0.6 and 0.7 resolution of narrow regions.

3.0.1 Acknowledgement

The authors are grateful to Jim Riley and G.M. "Bud" Homsy for helpful discussions about low Reynolds number fluid mechanics, and to Julie Theriot for discussing viscosity and transport in living cells. Dave Williams graciously provided the 3D rendering of the thick and thin filaments used in figure 2. The Army Research Office (W911NF-14-1-0396 to TLD) and the Joan and Richard Komen Endowed Chair to TLD provided support to this project. SAM was funded by a Bioengineering Cardiac Training Grant from the National Institute of Biomedical Imaging and Bioengineering (T32EB1650) and a fellowship from the ARCS Foundation. This project also received funding from the European Research Council (ERC) under the European Union's Horizon 2020 research and innovation programme (grant agreement 682754 to EL). Peko's funding. KTH was supported by National Science Foundation Grant DMS-1606487

CONCLUSION & DISCUSSION

In this thesis we explored kinematics and mechanics in the myofilament lattice. Our results highlight muscle's multiscale function, and point to further unanswered questions.

In the first paper reviewing the sliding filament theory and years of work that built upon it we highlight muscle's multiscale properties. Muscle function at the organism scale emerges from the combined actions of millions of independently acting molecular motors. Intricate regulation at the molecular scale is accomplished both through chemical signalling, and through the geometry of the lattice itself. However it is difficult to say how complete our picture of muscle function is since we are as yet unable to create predictive models that integrate across scales.

Modeling of muscle function from cell to tissue scale is an exciting avenue of discovery, with stakeholders in medicine, basic science, and industry partners that leverage massive computing resources. Current state-of-the-art models occupy different scales; spatially explicit models capture molecular phenomena but do not translate to the tissue scale, while heuristic models of cell contractility paired with finite element models of whole organs are unable to couple tissue scale mechanics to the subcellular architecture. Meanwhile, machine learning tools ranging from fundamental techniques like the Singular Value Decompostion to highly capable neural nets are revolutionizing the analysis of data gathered from both biological systems and from models of biological systems. Creating predictive models of muscle function that bridge across scales may be closer than ever with tools like these.

In chapter two I share the results of a study where we recorded the kinematics of a muscle's molecular machinery during *in vivo* function. This study uniquely captured the motion of the molecular machinery in a muscle where activation is synchronously tied to muscle contraction. However due to the constraints of x-ray diffraction in a naturally func-

tioning animal it is difficult to capture large amounts of data. We were limited in how many moths we were able to record from, and we were unable to simultaneously capture other variables in the system, for instance thorax temperature, antagonistic muscle activation, etc. Our relatively small dataset highlighted that the motions of the molecular machinery are immensely variable between animals. This lead us to wonder if the variation we observed resulted from unmeasured system features, like the functioning of antagonistic muscles. And the limited size of our dataset made it challenging to find broad brushstrokes describing lattice kinematics during natural function.

Currently, Daniel lab members are collecting a large data set linking endogenous muscle activation of the dorsal longitudinal muscles (DLMs) (from which we gathered x-ray diffraction data) and their antagonistic muscle pair, the dorsal ventral muscles (DVMs) with the resulting anterior-posterior strain in the thorax (an indicator of the strain in the DLMs which are attached to the thorax by small apodemes which strain minimally). This richer dataset could provide 1) valuable insight into the diversity of dynamic muscle strain in naturally functioning moths 2) the features of muscle activation that drive the emergent muscle strain 3) the data needed to build a machine learning model that could use muscle activation to predict the organism scale muscle strain. By coupling a model that predicts strain from a muscle activation signal with x-ray diffraction experiments where muscle activation is simultaneously recorded, nanometer scale structural changes could be correlated to organism scale muscle strain. Ultimately, studies like these could culminate in creating a mechanistic model that links lattice kinematics with organism scale function.

In chapter three we reported on the results of a computational model of fluid flow in the sarcomere. By using a finite element model we were able to come to a fuller picture of how fluid moves in the lattice of molecular machinery. We observed that radial flows were largest at the tips of filaments, which in most sarcomeres results in a large outflow at the m-line. Interestingly, this may be functionally important for the location of exterior organelles. This observation highlights another question: how does the flow out of individual sarcomeres couple to that of neighboring sarcomeres, and how does this moving fluid interact with the

sarcoplasmic reticulum, the mitochondria, and the organelles responsible for the integration of new proteins into the lattice, and the disposal of degraded proteins?

Our model also demonstrated that there is a region of fluid shearing between the filaments, which means that molecular motors may experience different shears depending upon their proximity to a thick or thin filament. We are as yet unable to answer how viscous drag forces impact individual molecular motor binding kinetics. If viscous drag has a significant impact on the binding kinetics of single motors, then this factor may need to be implemented in spatially explicit models of sarcomere contraction. However, a compatible heuristic describing the effect of drag forces on motor kinetics remains enigmatic. Further compounding the challenge, fluid interactions with molecular motors lie at the interface of continuum and non-continuum scales, where colloidal and Brownian effects are likely imperative. While these challenges are daunting, current research in low Reynolds number fluid mechanics in other cell types could lay the groundwork for answering them in muscle.

Despite intense study, muscle function still elicits a sense of wonder. It performs extreme functions across the animal kingdom with largely conserved machinery, integrating the actions of molecular motors with organism scale cues. In writing this thesis I have been struck by how many questions remain unanswered, such as those highlighted in this conclusion section. These questions have broad ramifications. Although muscle is often studied in the context of human disease, the principles we are learning in this tissue may be applicable to many other cell systems, for instance, the importance of fluid flow for cell function. The demand to create comprehensive predictive models for this multiscale tissue has driven forward scientific computing, and the unique features of muscle inspire engineering. Further, muscle physiology at times constrains the movement of organisms and is also one of the tissues enabling extreme behaviors (like high-frequency flight). All told, this fascinating cell type epitomizes the concept of "gestalt"; that the whole is greater than the sum of its parts.

BIBLIOGRAPHY

Adhikari, B. B., Regnier, M., Rivera, A. J., Kreutziger, K. L. & Martyn, D. A. (2004), 'Cardiac length dependence of force and force redevelopment kinetics with altered cross-bridge cycling', *Biophysical journal* **87**(3), 1784–1794.

Ahn, A., Konow, N., Tijs, C. & Biewener, A. (2018), 'Different segments within vertebrate muscles can operate on different regions of their force–length relationships', *Integrative and comparative biology* **58**(2), 219–231.

Ait-Mou, Y., Hsu, K., Farman, G. P., Kumar, M., Greaser, M. L., Irving, T. C. & de Tombe, P. P. (2016), 'Titin strain contributes to the frank–starling law of the heart by structural rearrangements of both thin-and thick-filament proteins', *Proceedings of the National Academy of Sciences* **113**(8), 2306–2311.

AL-Khayat, H. A. (2013), 'Three-dimensional structure of the human myosin thick filament: clinical implications', *Global Cardiology Science and Practice* **2013**(3), 36.

Alexander, F. J. & Garcia, A. L. (1997), 'The direct simulation monte carlo method', *Computers in Physics* **11**(6), 588–593.

Aliev, M. K. & Tikhonov, A. N. (2004), 'Random walk analysis of restricted metabolite diffusion in skeletal myofibril systems', *Molecular and cellular biochemistry* **256**(1-2), 257–266.

Alim, K., Amselem, G., Peaudecerf, F., Brenner, M. P. & Pringle, A. (2013), 'Random network peristalsis in physarum polycephalum organizes fluid flows across an individual', *Proceedings of the National Academy of Sciences* **110**(33), 13306–13311.

Anderson, R. L., Trivedi, D. V., Sarkar, S. S., Henze, M., Ma, W., Gong, H., Rogers, C. S., Gorham, J. M., Wong, F. L., Morck, M. M. et al. (2018), 'Deciphering the super relaxed state of human β-cardiac myosin and the mode of action of mavacamten from myosin molecules to muscle fibers', *Proceedings of the National Academy of Sciences* **115**(35), E8143–E8152.

Andruchov, O., Andruchova, O. & Galler, S. (2006), 'The catch state of mollusc catch muscle is established during activation: experiments on skinned fibre preparations of the anterior byssus retractor muscle of mytilus edulis l. using the myosin inhibitors orthovanadate and blebbistatin', *Journal of experimental biology* **209**(21), 4319–4328.

April, E. W., Brandt, P. W. & Elliott, G. F. (1971), 'The myofilament lattice: Studies on isolated fibers: I. the constancy of the unit-cell volume with variation in sarcomere length in a lattice in which the thin-to-thick myofilament ratio is 6: 1', *The Journal of Cell Biology* **51**(1), 72–82.

Arrio-Dupont, M., Cribier, S., Foucault, G., Devaux, P. F. & d'Albis, A. (1996), 'Diffusion of fluorescently labeled macromolecules in cultured muscle cells', *Biophysical journal* **70**(5), 2327–2332.

Arrio-Dupont, M., Foucault, G., Vacher, M., Devaux, P. F. & Cribier, S. (2000), 'Translational diffusion of globular proteins in the cytoplasm of cultured muscle cells', *Biophysical journal* **78**(2), 901–907.

Astbury, W. T. (1947), 'Croonian lecture-on the structure of biological fibres and the problem of muscle', *Proceedings of the Royal Society of London. Series B-Biological Sciences* **134**(876), 303–328.

Azizi, E. & Roberts, T. J. (2010), 'Muscle performance during frog jumping: influence of elasticity on muscle operating lengths', *Proceedings of the Royal Society B: Biological Sciences* **277**(1687), 1523–1530.

Bagni, M., Cecchi, G., Griffiths, P., Maéda, Y., Rapp, G. & Ashley, C. (1994), 'Lattice spacing changes accompanying isometric tension development in intact single muscle fibers', *Biophysical Journal* **67**(5), 1965 – 1975.

Bershitsky, S. Y., Ferenczi, M. A., Koubassova, N. A. & Tsaturyan, A. K. (2009), 'Insight into the actin-myosin motor from x-ray diffraction on muscle', *Frontiers in Bioscience* **14**(8), 3188–3213.

Bianco, P., Mártonfalvi, Z., Naftz, K., Kőszegi, D. & Kellermayer, M. (2015), 'Titin domains progressively unfolded by force are homogenously distributed along the molecule', *Biophysical journal* **109**(2), 340–345.

Bird, R. B. (2002), 'Transport phenomena', *Appl. Mech. Rev.* **55**(1), R1–R4.

Brunello, E., Bianco, P., Piazzesi, G., Linari, M., Reconditi, M., Panine, P., Narayanan, T., Helsby, W., Irving, M. & Lombardi, V. (2006), 'Structural changes in the myosin filament and cross-bridges during active force development in single intact frog muscle fibres: stiffness and x-ray diffraction measurements', *The Journal of physiology* **577**(3), 971–984.

Brunello, E., Caremani, M., Melli, L., Linari, M., Fernandez-Martinez, M., Narayanan, T., Irving, M., Piazzesi, G., Lombardi, V. & Reconditi, M. (2014), 'The contributions of filaments and cross-bridges to sarcomere compliance in skeletal muscle', *The Journal of physiology* **592**(17), 3881–3899.

Brunello, E., Fusi, L., Ghisleni, A., Park-Holohan, S.-J., Ovejero, J. G., Narayanan, T. & Irving, M. (2020), 'Myosin filament-based regulation of the dynamics of contraction in heart muscle', *Proceedings of the National Academy of Sciences* **117**(14), 8177–8186.

Bullard, B., Garcia, T., Benes, V., Leake, M. C., Linke, W. A. & Oberhauser, A. F. (2006), 'The molecular elasticity of the insect flight muscle proteins projectin and kettin', *Proceedings of the National Academy of Sciences* **103**(12), 4451–4456.

Burgoyne, T., Heumann, J. M., Morris, E. P., Knupp, C., Liu, J., Reedy, M. K., Taylor, K. A., Wang, K. & Luther, P. K. (2019), 'Three-dimensional structure of the basketweave z-band in midshipman fish sonic muscle', *Proceedings of the National Academy of Sciences* **116**(31), 15534–15539.

Burkholder, T. J. & Lieber, R. L. (2001), 'Sarcomere length operating range of vertebrate muscles during movement', *Journal of Experimental Biology* **204**(9), 1529–1536.

Campbell, K. S. (2006), 'Filament compliance effects can explain tension overshoots during force development', *Biophysical journal* **91**(11), 4102–4109.

Campbell, K. S., Janssen, P. M. & Campbell, S. G. (2018), 'Force-dependent recruitment from the myosin off state contributes to length-dependent activation', *Biophysical journal* **115**(3), 543–553.

Campbell, S. G., Lionetti, F. V., Campbell, K. S. & McCulloch, A. D. (2010), 'Coupling of adjacent tropomyosins enhances cross-bridge-mediated cooperative activation in a markov model of the cardiac thin filament', *Biophysical journal* **98**(10), 2254–2264.

Caremani, M., Pinzauti, F., Powers, J. D., Governali, S., Narayanan, T., Stienen, G. J., Reconditi, M., Linari, M., Lombardi, V. & Piazzesi, G. (2019), 'Inotropic interventions do not change the resting state of myosin motors during cardiac diastole', *Journal of General Physiology* **151**(1), 53–65.

Caremani, M., Pinzauti, F., Reconditi, M., Piazzesi, G., Stienen, G. J., Lombardi, V. & Linari, M. (2016), 'Size and speed of the working stroke of cardiac myosin in situ', *Proceedings of the National Academy of Sciences* **113**(13), 3675–3680.

Cass, J. A., Williams, C. D., Irving, T. C., Daniel, T. L. & Sponberg, S. N. (2019), 'A mechanism for sarcomere breathing: volume changes and advective flow within the myofilament lattice', *arXiv preprint arXiv:1904.12420* .

Cecchi, G. & Bagni, M. A. (1994), 'Myofilament lattice spacing affects tension in striated muscle', *Physiology* **9**(1), 3–7.

Cecchi, G., Bagni, M., Griffiths, P., Ashley, C. & Maeda, Y. (1990), 'Detection of radial crossbridge force by lattice spacing changes in intact single muscle fibers', *Science* **250**(4986), 1409–1411.

Chase, P. B., Chen, Y., Kulin, K. L. & Daniel, T. L. (2000), 'Viscosity and solute dependence of f-actin translocation by rabbit skeletal heavy meromyosin', *American Journal of Physiology-Cell Physiology* **278**(6), C1088–C1098.

Chase, P. B., Denkinger, T. M. & Kushmerick, M. J. (1998), 'Effect of viscosity on mechanics of single, skinned fibers from rabbit psoas muscle', *Biophysical journal* **74**(3), 1428–1438.

Chaudhri, A., Bell, J. B., Garcia, A. L. & Donev, A. (2014), 'Modeling multiphase flow using fluctuating hydrodynamics', *Physical Review E* **90**(3), 033014.

Chen, T. & Guestrin, C. (2016), Xgboost: A scalable tree boosting system, *in* 'Proceedings of the 22nd ACM SIGKDD international conference on knowledge discovery and data mining', ACM, pp. 785–794.

Cheng, Y., Lindert, S., Kekenes-Huskey, P., Rao, V. S., Solaro, R. J., Rosevear, P. R., Amaro, R., McCulloch, A. D., McCammon, J. A. & Regnier, M. (2014), 'Computational studies of the effect of the s23d/s24d troponin i mutation on cardiac troponin structural dynamics', *Biophysical journal* **107**(7), 1675–1685.

Cook, A. (2020), 'Intermediate machine learning'.
URL: *https://www.kaggle.com/alexisbcook/xgboost*

Cooke, R. (1997), 'Actomyosin interaction in striated muscle', *Physiological reviews* **77**(3), 671–697.

Cooke, R. (2004), 'The sliding filament model: 1972–2004', *The Journal of general physiology* **123**(6), 643–656.

Cortez, R. (2001), 'The method of regularized stokeslets', *SIAM Journal on Scientific Computing* **23**(4), 1204–1225.

Cortez, R., Fauci, L. & Medovikov, A. (2005), 'The method of regularized stokeslets in three dimensions: analysis, validation, and application to helical swimming', *Physics of Fluids* **17**(3), 031504.

Craig, R. & Padrón, R. (2004), 'Molecular structure of the sarcomere', *Myology* **3**, 129–144.

da Silva, A. C. R. & Reinach, F. C. (1991), 'Calcium binding induces conformational changes in muscle regulatory proteins', *Trends in biochemical sciences* **16**, 53–57.

Daniel, T. L., Trimble, A. C. & Chase, P. B. (1998), 'Compliant realignment of binding sites in muscle: transient behavior and mechanical tuning', *Biophysical journal* **74**(4), 1611–1621.

Davies, K. E. & Nowak, K. J. (2006), 'Molecular mechanisms of muscular dystrophies: old and new players', *Nature reviews Molecular cell biology* **7**(10), 762–773.

de Graaf, R. A., van Kranenburg, A. & Nicolay, K. (2000), 'In vivo 31p-nmr diffusion spectroscopy of atp and phosphocreatine in rat skeletal muscle', *Biophysical journal* **78**(4), 1657–1664.

de Tombe, P. P., Mateja, R. D., Tachampa, K., Mou, Y. A., Farman, G. P. & Irving, T. C. (2010), 'Myofilament length dependent activation', *Journal of molecular and cellular cardiology* **48**(5), 851–858.

Dickinson, M., Farman, G., Frye, M., Bekyarova, T., Gore, D., Maughan, D. & Irving, T. (2005), 'Molecular dynamics of cyclically contracting insect flight muscle in vivo', *Nature* **433**(7023), 330.

Dickinson, M. H., Farley, C. T., Full, R. J., Koehl, M., Kram, R. & Lehman, S. (2000), 'How animals move: an integrative view', *science* **288**(5463), 100–106.

Dobbie, I., Linari, M., Piazzesi, G., Reconditi, M., Koubassova, N., Ferenczi, M. A., Lombardi, V. & Irving, M. (1998), 'Elastic bending and active tilting of myosin heads during muscle contraction', *Nature* **396**(6709), 383–387.

Dutta, S., Tsiros, C., Sundar, S. L., Athar, H., Moore, J., Nelson, B., Gage, M. J. & Nishikawa, K. (2018), 'Calcium increases titin n2a binding to f-actin and regulated thin filaments', *Scientific reports* **8**(1), 1–11.

Eaton, J. L. et al. (1988), *Lepidopteran anatomy.*, John Wiley & Sons Limited.

Elemans, C. P., Mead, A. F., Jakobsen, L. & Ratcliffe, J. M. (2011), 'Superfast muscles set maximum call rate in echolocating bats', *Science* **333**(6051), 1885–1888.

Elhamine, F., Radke, M. H., Pfitzer, G., Granzier, H., Gotthardt, M. & Stehle, R. (2014), 'Deletion of the titin n2b region accelerates myofibrillar force development but does not alter relaxation kinetics', *Journal of cell science* **127**(17), 3666–3674.

Elliott, G., Lowy, J. & Millman, B. (1965), 'X-ray diffraction from living striated muscle during contraction', *Nature* **206**(4991), 1357–1358.

Elliott, G., Rome, E. & Spencer, M. (1970), 'A type of contraction hypothesis applicable to all muscles', *Nature* **226**(5244), 417–420.

Elliott, G. & Worthington, C. (2001), 'Muscle contraction: viscous-like frictional forces and the impulsive model', *International journal of biological macromolecules* **29**(3), 213–218.

Evans, C. & Hill, A. V. (1914), 'The relation of length to tension development and heat production on contraction in muscle', *The Journal of physiology* **49**(1-2), 10.

Farman, G. P., Gore, D., Allen, E., Schoenfelt, K., Irving, T. C. & de Tombe, P. P. (2011), 'Myosin head orientation: a structural determinant for the frank-starling relationship', *American Journal of Physiology-Heart and Circulatory Physiology* **300**(6), H2155–H2160.

Fenn, W. O. (1923), 'A quantitative comparison between the energy liberated and the work performed by the isolated sartorius muscle of the frog', *The Journal of physiology* **58**(2-3), 175.

Fischetti, R., Stepanov, S., Rosenbaum, G., Barrea, R., Black, E., Gore, D., Heurich, R., Kondrashkina, E., Kropf, A., Wang, S. et al. (2004), 'The biocat undulator beamline 18id: a facility for biological non-crystalline diffraction and x-ray absorption spectroscopy at the advanced photon source', *Journal of synchrotron radiation* **11**(5), 399–405.

Fukuda, N., Granzier, H. L., Ishiwata, S. & Kurihara, S. (2008), 'Physiological functions of the giant elastic protein titin in mammalian striated muscle', *The Journal of Physiological Sciences* **58**(3), 151–159.

Fukuda, N., Wu, Y., Farman, G., Irving, T. C. & Granzier, H. (2005), 'Titin-based modulation of active tension and interfilament lattice spacing in skinned rat cardiac muscle', *Pflügers Archiv* **449**(5), 449–457.

Furst, D. O., Nave, R., Osborn, M. & Weber, K. (1989), 'Repetitive titin epitopes with a 42 nm spacing coincide in relative position with known a band striations also identified by major myosin-associated proteins. an immunoelectron-microscopical study on myofibrils', *Journal of cell science* **94**(1), 119–125.

Fusi, L., Brunello, E., Reconditi, M., Piazzesi, G. & Lombardi, V. (2014), 'The non-linear elasticity of the muscle sarcomere and the compliance of myosin motors', *The Journal of physiology* **592**(5), 1109–1118.

Fusi, L., Brunello, E., Yan, Z. & Irving, M. (2016), 'Thick filament mechano-sensing is a calcium-independent regulatory mechanism in skeletal muscle', *Nature communications* **7**(1), 1–9.

Fusi, L., Percario, V., Brunello, E., Caremani, M., Bianco, P., Powers, J. D., Reconditi, M., Lombardi, V. & Piazzesi, G. (2017), 'Minimum number of myosin motors accounting for shortening velocity under zero load in skeletal muscle', *The Journal of Physiology* **595**(4), 1127–1142.

Gautel, M. (2011), 'The sarcomeric cytoskeleton: who picks up the strain?', *Current opinion in cell biology* **23**(1), 39–46.

Gautel, M. & Djinović-Carugo, K. (2016), 'The sarcomeric cytoskeleton: from molecules to motion', *Journal of Experimental Biology* **219**(2), 135–145.

George, N., Irving, T., Williams, C. & Daniel, T. (2013), 'The cross-bridge spring: can cool muscles store elastic energy?', *Science* **340**(6137), 1217–1220.

George, N., Sponberg, S. & Daniel, T. (2012), 'Temperature gradients drive mechanical energy gradients in the flight muscle of manduca sexta', *Journal of Experimental Biology* **215**(3), 471–479.

Gidmark, N. J., Konow, N., LoPresti, E. & Brainerd, E. L. (2013), 'Bite force is limited by the force–length relationship of skeletal muscle in black carp, mylopharyngodon piceus', *Biology letters* **9**(2), 20121181.

Gillis, T. E., Martyn, D. A., Rivera, A. J. & Regnier, M. (2007), 'Investigation of thin filament near-neighbour regulatory unit interactions during force development in skinned cardiac and skeletal muscle', *The Journal of physiology* **580**(2), 561–576.

Goldman, Y. E. & Huxley, A. F. (1994), 'Actin compliance: are you pulling my chain?', *Biophysical Journal* **67**(6), 2131.

Goldstein, M., Schoeter, J. & Sass, R. (1990), 'Two structural states of the vertebrate z band', *Electron microscopy reviews* **3**(2), 227–248.

Goldstein, R. E., Tuval, I. & van de Meent, J.-W. (2008), 'Microfluidics of cytoplasmic streaming and its implications for intracellular transport', *Proceedings of the National Academy of Sciences* **105**(10), 3663–3667.

Gomez-Marin, A. & Ghazanfar, A. A. (2019), 'The life of behavior', *Neuron* **104**(1), 25–36.

Gordon, A., Homsher, E. & Regnier, M. (2000), 'Regulation of contraction in striated muscle', *Physiological reviews* **80**(2), 853–924.

Gordon, A., Huxley, A. F. & Julian, F. (1966), 'The variation in isometric tension with sarcomere length in vertebrate muscle fibres', *The Journal of physiology* **184**(1), 170–192.

Granzier, H. L. & Irving, T. C. (1995), 'Passive tension in cardiac muscle: contribution of collagen, titin, microtubules, and intermediate filaments', *Biophysical journal* **68**(3), 1027–1044.

Granzier, H. L. & Labeit, S. (2004), 'The giant protein titin: a major player in myocardial mechanics, signaling, and disease', *Circulation research* **94**(3), 284–295.

Granzier, H. L. & Labeit, S. (2005), 'Titin and its associated proteins: the third myofilament system of the sarcomere', *Advances in protein chemistry* **71**, 89–119.

Granzier, H. & Wang, K. (1993), 'Passive tension and stiffness of vertebrate skeletal and insect flight muscles: the contribution of weak cross-bridges and elastic filaments', *Biophysical journal* **65**(5), 2141–2159.

Gruen, M. & Gautel, M. (1999), 'Mutations in β-myosin s2 that cause familial hypertrophic cardiomyopathy (fhc) abolish the interaction with the regulatory domain of myosin-binding protein-c', *Journal of molecular biology* **286**(3), 933–949.

Hagopian, M. (1966), 'The myofilament arrangement in the femoral muscle of the cockroach, leucophaea maderae fabricius', *The Journal of Cell Biology* **28**(3), 545–562.

Hamdani, N., Herwig, M. & Linke, W. A. (2017), 'Tampering with springs: phosphorylation of titin affecting the mechanical function of cardiomyocytes', *Biophysical reviews* **9**(3), 225–237.

Hanson, J. & Huxley, H. E. (1953), 'Structural basis of the cross-striations in muscle', *Nature* **172**(4377), 530–532.

Harford, J. J. & Squire, J. (1992), 'Evidence for structurally different attached states of myosin cross-bridges on actin during contraction of fish muscle', *Biophysical journal* **63**(2), 387–396.

Harris, S. P., Belknap, B., Van Sciver, R. E., White, H. D. & Galkin, V. E. (2016), 'C0 and c1 n-terminal ig domains of myosin binding protein c exert different effects on thin filament activation', *Proceedings of the National Academy of Sciences* **113**(6), 1558–1563.

Harris, S. P., Lyons, R. G. & Bezold, K. L. (2011), 'In the thick of it: Hcm-causing mutations in myosin binding proteins of the thick filament', *Circulation research* **108**(6), 751–764.

Haselgrove, J. (1975), 'X-ray evidence for conformational changes in the myosin filaments of vertebrate striated muscle', *Journal of molecular biology* **92**(1), 113–143.

Hayes, D., Huang, M. & Zobel, C. R. (1971), 'Electron microscope observations on thick filaments in striated muscle from the lobster homarus americanus', *Journal of ultrastructure research* **37**(1-2), 17–30.

He, Z.-H., Bottinelli, R., Pellegrino, M. A., Ferenczi, M. A. & Reggiani, C. (2000), 'Atp consumption and efficiency of human single muscle fibers with different myosin isoform composition', *Biophysical journal* **79**(2), 945–961.

Heinrich, B. & Bartholomew, G. A. (1971), 'An analysis of pre-flight warm-up in the sphinx moth, manduca sexta', *Journal of Experimental Biology* **55**(1), 223–239.

Herman, D. S., Lam, L., Taylor, M. R., Wang, L., Teekakirikul, P., Christodoulou, D., Conner, L., DePalma, S. R., McDonough, B., Sparks, E. et al. (2012), 'Truncations of titin causing dilated cardiomyopathy', *New England Journal of Medicine* **366**(7), 619–628.

Herwig, M., Kolijn, D., Lódi, M., Hölper, S., Kovács, Á., Papp, Z., Jaquet, K., Haldenwang, P., Dos Remedios, C., Reusch, P. H. et al. (2020), 'Modulation of titin-based stiffness in hypertrophic cardiomyopathy via protein kinase d', *Frontiers in Physiology* **11**, 240.

Herzberg, O. & James, M. N. (1985), 'Structure of the calcium regulatory muscle protein troponin-c at 2.8 å resolution', *Nature* **313**(6004), 653–659.

Hochachka, P. (1999), 'The metabolic implications of intracellular circulation', *Proceedings of the National Academy of Sciences* **96**(22), 12233–12239.

Holmes, K., Trentham, D., Simmons, R., Lombardi, V., Piazzesi, G., Reconditi, M., Linari, M., Lucii, L., Stewart, A., Sun, Y.-B. et al. (2004), 'X-ray diffraction studies of the contractile mechanism in single muscle fibres', *Philosophical Transactions of the Royal Society of London. Series B: Biological Sciences* **359**(1452), 1883–1893.

Homsher, E. (1987), 'Muscle enthalpy production and its relationship to actomyosin atpase', *Annual Review of Physiology* **49**(1), 673–690.

Hoshijima, M. (2006), 'Mechanical stress-strain sensors embedded in cardiac cytoskeleton: Z disk, titin, and associated structures', *American Journal of Physiology-Heart and Circulatory Physiology* **290**(4), H1313–H1325.

Houdusse, A., Love, M. L., Dominguez, R., Grabarek, Z. & Cohen, C. (1997), 'Structures of four ca2+-bound troponin c at 2.0 å resolution: further insights into the ca2+-switch in the calmodulin superfamily', *Structure* **5**(12), 1695–1711.

Hoyle, G. (1967), 'Diversity of striated muscle', *American zoologist* **7**(3), 435–449.

Hoyle, G., McNeill, P. A. & Selverston, A. I. (1973), 'Ultrastructure of barnacle giant muscle fibers', *The Journal of cell biology* **56**(1), 74–91.

Hu, Z., Taylor, D. W., Reedy, M. K., Edwards, R. J. & Taylor, K. A. (2016), 'Structure of myosin filaments from relaxed lethocerus flight muscle by cryo-em at 6 å resolution', *Science advances* **2**(9), e1600058.

Huxley, A. (1974), 'Muscular contraction.', *The Journal of physiology* **243**(1), 1.

Huxley, A. (1980), *Reflections on muscle*, Vol. 14, Liverpool University Press Liverpool.

Huxley, A. F. (1957), 'Muscle structure and theories of contraction', *Prog. Biophys. Biophys. Chem* **7**, 255–318.

Huxley, A. F. & Niedergerke, R. (1954), 'Structural changes in muscle during contraction: interference microscopy of living muscle fibres', *Nature* **173**(4412), 971–973.

Huxley, A. F. & Simmons, R. M. (1971), 'Proposed mechanism of force generation in striated muscle', *Nature* **233**(5321), 533–538.

Huxley, A. & Taylor, R. (1958), 'Local activation of striated muscle fibres', *The Journal of physiology* **144**(3), 426.

Huxley, H. E. (2004), 'Fifty years of muscle and the sliding filament hypothesis', *European journal of biochemistry* **271**(8), 1403–1415.

Huxley, H. E., Brown, W. & Holmes, K. C. (1965), 'Constancy of axial spacings in frog sartorius muscle during contraction', *Nature* **206**(4991), 1358–1358.

Huxley, H. E., Stewart, A. & Irving, T. (1998), Spacing changes in the actin and myosin filaments during activation, and their implications, *in* 'Mechanisms of Work Production and Work Absorption in Muscle', Springer, pp. 281–288.

Huxley, H. E., Stewart, A., Sosa, H. & Irving, T. (1994), 'X-ray diffraction measurements of the extensibility of actin and myosin filaments in contracting muscle', *Biophysical journal* **67**(6), 2411–2421.

Huxley, H., Faruqi, A., Bordas, J., Koch, M. & Milch, J. (1980), 'The use of synchrotron radiation in time-resolved x-ray diffraction studies of myosin layer-line reflections during muscle contraction', *Nature* **284**(5752), 140–143.

Huxley, H. & Hanson, J. (1954), 'Changes in the cross-striations of muscle during contraction and stretch and their structural interpretation', *Nature* **173**(4412), 973–976.

Huxley, H., Reconditi, M., Stewart, A. & Irving, T. (2006), 'X-ray interference studies of crossbridge action in muscle contraction: evidence from quick releases', *Journal of molecular biology* **363**(4), 743–761.

Irving, T. C. (2006), X-ray diffraction of indirect flight muscle from drosophila in vivo, *in* 'Nature's Versatile Engine: Insect Flight Muscle Inside and Out', Springer, pp. 197–213.

Irving, T. & Maughan, D. (2000), 'In vivo x-ray diffraction of indirect flight muscle from drosophila melanogaster', *Biophysical journal* **78**(5), 2511–2515.

Irving, T., Wu, Y., Bekyarova, T., Farman, G. P., Fukuda, N. & Granzier, H. (2011), 'Thick-filament strain and interfilament spacing in passive muscle: effect of titin-based passive tension', *Biophysical journal* **100**(6), 1499–1508.

Iwamoto, H. (2019), 'Synchrotron radiation x-ray diffraction studies on muscle: past, present, and future', *Biophysical reviews* pp. 1–12.

Iwamoto, H. & Yagi, N. (2013), 'The molecular trigger for high-speed wing beats in a bee', *Science* **341**(6151), 1243–1246.

Jahromi, S. & Atwood, H. (1969), 'Structural features of muscle fibres in the cockroach leg', *Journal of Insect Physiology* **15**(12), 2255–2262.

Jain, M. (2018*a*), 'Hyperparameter-tuning-in-xgboost-using-genetic-algorithm'.
URL: *https://github.com/mjain72/Hyperparameter-tuning-in-XGBoost-using-genetic-algorithm/blob/master/LICENSE*

Jain, M. (2018*b*), '*Hyperparameter tuning in XGBoost using genetic algorithm*'.
URL: *https://towardsdatascience.com/hyperparameter-tuning-in-xgboost-using-genetic-algorithm-17bd2e581b17*

Jiratrakanvong, J., Shao, J., Menendez, M., Li, X., Li, J., Ma, W., Agam, G. & Irving, T. (2018), 'Musclex: software suite for diffraction x-ray imaging v1. 13.1'.

Kaya, M. & Higuchi, H. (2010), 'Nonlinear elasticity and an 8-nm working stroke of single myosin molecules in myofilaments', *Science* **329**(5992), 686–689.

Kekenes-Huskey, P. M., Liao, T., Gillette, A. K., Hake, J. E., Zhang, Y., Michailova, A. P., McCulloch, A. D. & McCammon, J. A. (2013), 'Molecular and subcellular-scale modeling of nucleotide diffusion in the cardiac myofilament lattice', *Biophysical journal* **105**(9), 2130–2140.

Kellermayer, M. S., Smith, S. B., Granzier, H. L. & Bustamante, C. (1997), 'Folding-unfolding transitions in single titin molecules characterized with laser tweezers', *Science* **276**(5315), 1112–1116.

Kentish, J. C., McCloskey, D. T., Layland, J., Palmer, S., Leiden, J. M., Martin, A. F. & Solaro, R. J. (2001), 'Phosphorylation of troponin i by protein kinase a accelerates relaxation and crossbridge cycle kinetics in mouse ventricular muscle', *Circulation research* **88**(10), 1059–1065.

Keren, K., Yam, P. T., Kinkhabwala, A., Mogilner, A. & Theriot, J. A. (2009), 'Intracellular fluid flow in rapidly moving cells', *Nature cell biology* **11**(10), 1219–1224.

Kinsey, S. T., Locke, B. R. & Dillaman, R. M. (2011), 'Molecules in motion: influences of diffusion on metabolic structure and function in skeletal muscle', *Journal of Experimental Biology* **214**(2), 263–274.

Konhilas, J. P., Irving, T. C. & De Tombe, P. P. (2002), 'Myofilament calcium sensitivity in skinned rat cardiac trabeculae: role of interfilament spacing', *Circulation research* **90**(1), 59–65.

Koser, F., Loescher, C. & Linke, W. A. (2019), 'Posttranslational modifications of titin from cardiac muscle: how, where, and what for?', *The FEBS journal* **286**(12), 2240–2260.

Kreutziger, K. L., Piroddi, N., Scellini, B., Tesi, C., Poggesi, C. & Regnier, M. (2008), 'Thin filament ca2+ binding properties and regulatory unit interactions alter kinetics of tension development and relaxation in rabbit skeletal muscle', *The Journal of physiology* **586**(15), 3683–3700.

Kushmerick, M. J. & Davies, R. E. (1969), 'The chemical energetics of muscle contraction. ii. the chemistry, efficiency and power of maximally working sartorius muscles', *Proceedings of the Royal Society of London. Series B. Biological Sciences* **174**(1036), 315–347.

Lange, S., Ehler, E. & Gautel, M. (2006), 'From a to z and back? multicompartment proteins in the sarcomere', *Trends in cell biology* **16**(1), 11–18.

Li, J., Gresham, K. S., Mamidi, R., Doh, C. Y., Wan, X., Deschenes, I. & Stelzer, J. E. (2018), 'Sarcomere-based genetic enhancement of systolic cardiac function in a murine model of dilated cardiomyopathy', *International journal of cardiology* **273**, 168–176.

Lin, B. L., Li, A., Mun, J. Y., Previs, M. J., Previs, S. B., Campbell, S. G., Dos Remedios, C. G., Tombe, P. d. P., Craig, R., Warshaw, D. M. et al. (2018), 'Skeletal myosin binding protein-c isoforms regulate thin filament activity in a ca 2+-dependent manner', *Scientific reports* **8**(1), 1–13.

Linari, M., Brunello, E., Reconditi, M., Fusi, L., Caremani, M., Narayanan, T., Piazzesi, G., Lombardi, V. & Irving, M. (2015), 'Force generation by skeletal muscle is controlled by mechanosensing in myosin filaments', *Nature* **528**(7581), 276–279.

Linari, M., Caremani, M., Piperio, C., Brandt, P. & Lombardi, V. (2007), 'Stiffness and fraction of myosin motors responsible for active force in permeabilized muscle fibers from rabbit psoas', *Biophysical journal* **92**(7), 2476–2490.

Linari, M., Piazzesi, G., Dobbie, I., Koubassova, N., Reconditi, M., Narayanan, T., Diat, O., Irving, M. & Lombardi, V. (2000), 'Interference fine structure and sarcomere length dependence of the axial x-ray pattern from active single muscle fibers', *Proceedings of the National Academy of Sciences* **97**(13), 7226–7231.

Lindstedt, S. & Nishikawa, K. (2017), 'Huxleys' missing filament: form and function of titin in vertebrate striated muscle', *Annual review of physiology* **79**, 145–166.

Linke, W. A. (2018), 'Titin gene and protein functions in passive and active muscle', *Annual review of physiology* **80**, 389–411.

Linke, W. A. & Hamdani, N. (2014), 'Gigantic business: titin properties and function through thick and thin', *Circulation research* **114**(6), 1052–1068.

Linke, W. A., Ivemeyer, M., Mundel, P., Stockmeier, M. R. & Kolmerer, B. (1998), 'Nature of pevk-titin elasticity in skeletal muscle', *Proceedings of the National Academy of Sciences* **95**(14), 8052–8057.

Linke, W. A., Ivemeyer, M., Olivieri, N., Kolmerer, B., Rüegg, C. J. & Labeit, S. (1996), 'Towards a molecular understanding of the elasticity of titin', *Journal of molecular biology* **261**(1), 62–71.

Luby-Phelps, K. (1994), 'Physical properties of cytoplasm', *Current opinion in cell biology* **6**(1), 3–9.

Luther, P. K. (2009), 'The vertebrate muscle z-disc: sarcomere anchor for structure and signalling', *Journal of muscle research and cell motility* **30**(5-6), 171–185.

Luther, P. K., Padron, R., Ritter, S., Craig, R. & Squire, J. M. (2003), 'Heterogeneity of z-band structure within a single muscle sarcomere: implications for sarcomere assembly', *Journal of molecular biology* **332**(1), 161–169.

Ma, W., Gong, H., Kiss, B., Lee, E.-J., Granzier, H. & Irving, T. (2018), 'Thick-filament extensibility in intact skeletal muscle', *Biophysical Journal* **115**(8), 1580 – 1588.

Maheshwari, A. J., Sunol, A. M., Gonzalez, E., Endy, D. & Zia, R. N. (2019), 'Colloidal hydrodynamics of biological cells: A frontier spanning two fields', *Physical Review Fluids* **4**(11), 110506.

Malingen, S. A., Asencio, A. M., Cass, J. A., Ma, W., Irving, T. C. & Daniel, T. L. (2020), 'In vivo x-ray diffraction and simultaneous emg reveal the time course of myofilament lattice dilation and filament stretch', *Journal of Experimental Biology* **223**(17).

Mann, C. K., Lee, L. C., Campbell, K. S. & Wenk, J. F. (2020), 'Force-dependent recruitment from myosin off-state increases end-systolic pressure–volume relationship in left ventricle', *Biomechanics and modeling in mechanobiology* pp. 1–10.

Marcucci, L., Washio, T. & Yanagida, T. (2017), 'Titin-mediated thick filament activation, through a mechanosensing mechanism, introduces sarcomere-length dependencies in mathematical models of rat trabecula and whole ventricle', *Scientific reports* **7**(1), 1–10.

Marcucci, L., Washio, T. & Yanagida, T. (2019), 'Proposed mechanism for the length dependence of the force developed in maximally activated muscles', *Scientific reports* **9**(1), 1–13.

Marszalek, P. E., Lu, H., Li, H., Carrion-Vazquez, M., Oberhauser, A. F., Schulten, K. & Fernandez, J. M. (1999), 'Mechanical unfolding intermediates in titin modules', *Nature* **402**(6757), 100–103.

Mártonfalvi, Z., Bianco, P., Linari, M., Caremani, M., Nagy, A., Lombardi, V. & Kellermayer, M. (2014), 'Low-force transitions in single titin molecules reflect a memory of contractile history', *Journal of cell science* **127**(4), 858–870.

Maruyama, K., Matsubara, S., Natori, R., Nonomura, Y., Kimura, S., Ohashi, K., Murakami, F., Handa, S. & Eguchi, G. (1977), 'Connectin, an elastic protein of muscle: characterization and function', *The Journal of biochemistry* **82**(2), 317–337.

Maruyama, K., Natori, R. & Nonomura, Y. (1976), 'New elastic protein from muscle', *Nature* **262**(5563), 58–60.

Matsuda, T. & Podolsky, R. J. (1986), 'Ordering of the myofilament lattice in muscle fibers', *Journal of molecular biology* **189**(2), 361–365.

Maughan, D. W. & Godt, R. E. (1999), 'Parvalbumin concentration and diffusion coefficient in frog myoplasm', *Journal of Muscle Research & Cell Motility* **20**(2), 199–209.

McKillop, D. & Geeves, M. A. (1993), 'Regulation of the interaction between actin and myosin subfragment 1: evidence for three states of the thin filament', *Biophysical journal* **65**(2), 693–701.

McNamara, J. W., Li, A., dos Remedios, C. G. & Cooke, R. (2015), 'The role of super-relaxed myosin in skeletal and cardiac muscle', *Biophysical reviews* **7**(1), 5–14.

McNamara, J. W. & Sadayappan, S. (2018), 'Skeletal myosin binding protein-c: An increasingly important regulator of striated muscle physiology', *Archives of biochemistry and biophysics* **660**, 121–128.

McNamara, J. W., Singh, R. R. & Sadayappan, S. (2019), 'Cardiac myosin binding protein-c phosphorylation regulates the super-relaxed state of myosin', *Proceedings of the National Academy of Sciences* **116**(24), 11731–11736.

Metzger, J. M. & Moss, R. L. (1987), 'Shortening velocity in skinned single muscle fibers. influence of filament lattice spacing', *Biophysical Journal* **52**(1), 127–131.

Mijailovich, S. M., Kayser-Herold, O., Stojanovic, B., Nedic, D., Irving, T. C. & Geeves, M. A. (2016), 'Three-dimensional stochastic model of actin–myosin binding in the sarcomere lattice', *Journal of General Physiology* **148**(6), 459–488.

Millman, B. M. (1998), 'The filament lattice of striated muscle', *Physiological reviews* **78**(2), 359–391.

Millman, B. M., Wakabayashi, K. & Racey, T. J. (1983), 'Lateral forces in the filament lattice of vertebrate striated muscle in the rigor state.', *Biophysical journal* **41**(3), 259.

Moeendarbary, E., Valon, L., Fritzsche, M., Harris, A. R., Moulding, D. A., Thrasher, A. J., Stride, E., Mahadevan, L. & Charras, G. T. (2013), 'The cytoplasm of living cells behaves as a poroelastic material', *Nature materials* **12**(3), 253–261.

Mogilner, A. & Manhart, A. (2018), 'Intracellular fluid mechanics: Coupling cytoplasmic flow with active cytoskeletal gel', *Annual Review of Fluid Mechanics* **50**.

Mogre, S., Brown, A. I. & Koslover, E. F. (2020), 'Getting around the cell: physical transport in the intracellular world', *Physical Biology* .

Moisescu, D. (1973), 'Interfilament forces in striated muscle', *Bulletin of mathematical biology* **35**(5-6), 565–575.

Molloy, J., Burns, J., Kendrick-Jones, J., Tregear, R. & White, D. (1995), 'Movement and force produced by a single myosin head', *Nature* **378**(6553), 209–212.

Morel, J. E., Pinset-Härström, I. & Gingold, M. P. (1976), 'Muscular contraction and cytoplasmic streaming: a new general hypothesis', *Journal of theoretical biology* **62**(1), 17–51.

Moss, R. L. & Fitzsimons, D. P. (2002), 'Frank-starling relationship: long on importance, short on mechanism', *Circulation research* **90**, 11–13.

Moss, R. L., Fitzsimons, D. P. & Ralphe, J. C. (2015), 'Cardiac mybp-c regulates the rate and force of contraction in mammalian myocardium', *Circulation research* **116**(1), 183–192.

Mun, J. Y., Previs, M. J., Hope, Y. Y., Gulick, J., Tobacman, L. S., Previs, S. B., Robbins, J., Warshaw, D. M. & Craig, R. (2014), 'Myosin-binding protein c displaces tropomyosin to activate cardiac thin filaments and governs their speed by an independent mechanism', *Proceedings of the National Academy of Sciences* **111**(6), 2170–2175.

Nag, S., Sommese, R. F., Ujfalusi, Z., Combs, A., Langer, S., Sutton, S., Leinwand, L. A., Geeves, M. A., Ruppel, K. M. & Spudich, J. A. (n.d.), 'Contractility parameters of human b-cardiac myosin with the hypertrophic cardiomyopathy mutation r403q show loss of motor function'.

Nag, S., Trivedi, D. V., Sarkar, S. S., Adhikari, A. S., Sunitha, M. S., Sutton, S., Ruppel, K. M. & Spudich, J. A. (2017), 'The myosin mesa and the basis of hypercontractility caused by hypertrophic cardiomyopathy mutations', *Nature structural & molecular biology* **24**(6), 525.

Needham, D. (1950), 'Myosin and adenosinetriphosphate in relation to muscle contraction', *Biochimica et biophysica acta* **4**, 42–49.

Nie, X., Chen, S., Robbins, M. et al. (2004), 'A continuum and molecular dynamics hybrid method for micro-and nano-fluid flow', *Journal of Fluid Mechanics* **500**, 55.

Nishikawa, K. C., Monroy, J. A., Uyeno, T. E., Yeo, S. H., Pai, D. K. & Lindstedt, S. L. (2012), 'Is titin a 'winding filament'? a new twist on muscle contraction', *Proceedings of the royal society B: Biological sciences* **279**(1730), 981–990.

Osborne, M. (1967), 'Supercontraction in the muscles of the blowfly larva: an ultrastructural study', *Journal of Insect Physiology* **13**(10), 1471–1482.

Oster, G. (2002), 'Brownian ratchets: Darwin's motors', *Nature* **417**(6884), 25–25.

Padding, J. & Louis, A. (2006), 'Hydrodynamic interactions and brownian forces in colloidal suspensions: Coarse-graining over time and length scales', *Physical Review E* **74**(3), 031402.

Palmer, B. M., Swank, D. M., Miller, M. S., Tanner, B. C., Meyer, M. & LeWinter, M. M. (2020), 'Enhancing diastolic function by strain-dependent detachment of cardiac myosin crossbridges', *Journal of General Physiology* **152**(4).

Papadopoulos, S., Endeward, V., Revesz-Walker, B., Jürgens, K. D. & Gros, G. (2001), 'Radial and longitudinal diffusion of myoglobin in single living heart and skeletal muscle cells', *Proceedings of the National Academy of Sciences* **98**(10), 5904–5909.

Pertici, I., Caremani, M. & Reconditi, M. (2019), 'A mechanical model of the half-sarcomere which includes the contribution of titin', *Journal of muscle research and cell motility* **40**(1), 29–41.

Perz-Edwards, R. J., Irving, T. C., Baumann, B. A., Gore, D., Hutchinson, D. C., Kržič, U., Porter, R. L., Ward, A. B. & Reedy, M. K. (2011), 'X-ray diffraction evidence for myosin-troponin connections and tropomyosin movement during stretch activation of insect flight muscle', *Proceedings of the National Academy of Sciences* **108**(1), 120–125.

Perz-Edwards, R. J. & Reedy, M. K. (2011), 'Electron microscopy and x-ray diffraction evidence for two z-band structural states', *Biophysical journal* **101**(3), 709–717.

Piazzesi, G., Caremani, M., Linari, M., Reconditi, M. & Lombardi, V. (2018), 'Thick filament mechano-sensing in skeletal and cardiac muscles: a common mechanism able to adapt the energetic cost of the contraction to the task', *Frontiers in physiology* **9**, 736.

Piazzesi, G., Lucii, L. & Lombardi, V. (2002), 'The size and the speed of the working stroke of muscle myosin and its dependence on the force', *The Journal of physiology* **545**(1), 145–151.

Piazzesi, G., Reconditi, M., Linari, M., Lucii, L., Bianco, P., Brunello, E., Decostre, V., Stewart, A., Gore, D. B., Irving, T. C. et al. (2007), 'Skeletal muscle performance determined by modulation of number of myosin motors rather than motor force or stroke size', *Cell* **131**(4), 784–795.

Piazzesi, G., Reconditi, M., Linari, M., Lucii, L., Sun, Y.-B., Narayanan, T., Boesecke, P., Lombardi, V. & Irving, M. (2002), 'Mechanism of force generation by myosin heads in skeletal muscle', *Nature* **415**(6872), 659–662.

Pinzauti, F., Pertici, I., Reconditi, M., Narayanan, T., Stienen, G. J., Piazzesi, G., Lombardi, V., Linari, M. & Caremani, M. (2018), 'The force and stiffness of myosin motors in the isometric twitch of a cardiac trabecula and the effect of the extracellular calcium concentration', *The Journal of physiology* **596**(13), 2581–2596.

Polilov, A. A. (2015), 'Small is beautiful: features of the smallest insects and limits to miniaturization', *Annual review of entomology* **60**.

Powers, J. D., Bianco, P., Pertici, I., Reconditi, M., Lombardi, V. & Piazzesi, G. (2020), 'Contracting striated muscle has a dynamic i-band spring with an undamped stiffness 100 times larger than the passive stiffness', *The Journal of Physiology* **598**(2), 331–345.

Powers, J. D., Williams, C. D., Regnier, M. & Daniel, T. L. (2018), 'A spatially explicit model shows how titin stiffness modulates muscle mechanics and energetics', *Integrative and comparative biology* **58**(2), 186–193.

Powers, J. D., Yuan, C.-C., McCabe, K. J., Murray, J. D., Childers, M. C., Flint, G. V., Moussavi-Harami, F., Mohran, S., Castillo, R., Zuzek, C. et al. (2019), 'Cardiac myosin activation with 2-deoxy-atp via increased electrostatic interactions with actin', *Proceedings of the National Academy of Sciences* **116**(23), 11502–11507.

Previs, M. J., Prosser, B. L., Mun, J. Y., Previs, S. B., Gulick, J., Lee, K., Robbins, J., Craig, R., Lederer, W. & Warshaw, D. M. (2015), 'Myosin-binding protein c corrects an intrinsic inhomogeneity in cardiac excitation-contraction coupling', *Science Advances* **1**(1), e1400205.

Pyle, W. G. & Solaro, R. J. (2004), 'At the crossroads of myocardial signaling: the role of z-discs in intracellular signaling and cardiac function', *Circulation research* **94**(3), 296–305.

Ratcliffe, J. M., Elemans, C. P., Jakobsen, L. & Surlykke, A. (2013), 'How the bat got its buzz', *Biology Letters* **9**(2), 20121031.

Razumova, M. V., Bezold, K. L., Tu, A.-Y., Regnier, M. & Harris, S. P. (2008), 'Contribution of the myosin binding protein c motif to functional effects in permeabilized rat trabeculae', *The Journal of general physiology* **132**(5), 575–585.

Razumova, M. V., Bukatina, A. E. & Campbell, K. B. (2000), 'Different myofilament nearest-neighbor interactions have distinctive effects on contractile behavior', *Biophysical journal* **78**(6), 3120–3137.

Razumova, M. V., Shaffer, J. F., Tu, A.-Y., Flint, G. V., Regnier, M. & Harris, S. P. (2006), 'Effects of the n-terminal domains of myosin binding protein-c in an in vitro motility assay evidence for long-lived cross-bridges', *Journal of Biological Chemistry* **281**(47), 35846–35854.

Reconditi, M. (2006), 'Recent improvements in small angle x-ray diffraction for the study of muscle physiology', *Reports on Progress in Physics* **69**(10), 2709.

Reconditi, M., Brunello, E., Linari, M., Bianco, P., Narayanan, T., Panine, P., Piazzesi, G., Lombardi, V. & Irving, M. (2011), 'Motion of myosin head domains during activation and force development in skeletal muscle', *Proceedings of the National Academy of Sciences* **108**(17), 7236–7240.

Reconditi, M., Caremani, M., Pinzauti, F., Powers, J. D., Narayanan, T., Stienen, G. J., Linari, M., Lombardi, V. & Piazzesi, G. (2017), 'Myosin filament activation in the heart is tuned to the mechanical task', *Proceedings of the National Academy of Sciences* **114**(12), 3240–3245.

Reconditi, M., Koubassova, N., Linari, M., Dobbie, I., Narayanan, T., Diat, O., Piazzesi, G., Lombardi, V. & Irving, M. (2003), 'The conformation of myosin head domains in rigor muscle determined by x-ray interference', *Biophysical journal* **85**(2), 1098–1110.

Reconditi, M., Linari, M., Lucii, L., Stewart, A., Sun, Y.-B., Boesecke, P., Narayanan, T., Fischetti, R. F., Irving, T., Piazzesi, G. et al. (2004), 'The myosin motor in muscle generates a smaller and slower working stroke at higher load', *Nature* **428**(6982), 578–581.

Reedy, M., Squire, J., Baumann, B., Stewart, A. & Irving, T. (2000), 'X-ray fibre diffraction of the indirect flight muscle of lethocerus indicus', *Advanced Photon Source User Activity: Report* .

Regnier, M. & Homsher, E. (1998), 'The effect of atp analogs on posthydrolytic and force development steps in skinned skeletal muscle fibers', *Biophysical journal* **74**(6), 3059–3071.

Regnier, M., Lee, D. & Homsher, E. (1998), 'Atp analogs and muscle contraction: mechanics and kinetics of nucleoside triphosphate binding and hydrolysis', *Biophysical journal* **74**(6), 3044–3058.

Regnier, M., Rivera, A. J., Wang, C.-K., Bates, M. A., Chase, P. B. & Gordon, A. M. (2002), 'Thin filament near-neighbour regulatory unit interactions affect rabbit skeletal muscle steady-state force-ca2+ relations', *The Journal of physiology* **540**(2), 485–497.

Rief, M., Gautel, M., Oesterhelt, F., Fernandez, J. M. & Gaub, H. E. (1997), 'Reversible unfolding of individual titin immunoglobulin domains by afm', *science* **276**(5315), 1109–1112.

Risi, C., Belknap, B., Forgacs-Lonart, E., Harris, S. P., Schröder, G. F., White, H. D. & Galkin, V. E. (2018), 'N-terminal domains of cardiac myosin binding protein c cooperatively activate the thin filament', *Structure* **26**(12), 1604–1611.

Rivas-Pardo, J. A., Eckels, E. C., Popa, I., Kosuri, P., Linke, W. A. & Fernández, J. M. (2016), 'Work done by titin protein folding assists muscle contraction', *Cell Reports* **14**(6), 1339–1347.

Rome, E. (1968), 'X-ray diffraction studies of the filament lattice of striated muscle in various bathing media', *Journal of molecular biology* **37**(2), 331–344.

Rome, L. C., Syme, D. A., Hollingworth, S., Lindstedt, S. L. & Baylor, S. M. (1996), 'The whistle and the rattle: the design of sound producing muscles', *Proceedings of the National Academy of Sciences* **93**(15), 8095–8100.

Rose, H. H. (2008), 'Optics of high-performance electron microscopes', *Science and Technology of Advanced Materials* **9**(1), 014107.

Royuela, M., Fraile, B., Arenas, M. I. & Paniagua, R. (2000), 'Characterization of several invertebrate muscle cell types: a comparison with vertebrate muscles', *Microscopy research and technique* **48**(2), 107–115.

Schoenberg, M. (1980), 'Geometrical factors influencing muscle force development. i. the effect of filament spacing upon axial forces', *Biophysical Journal* **30**(1), 51–67.

Sellers, J. R. (2004), 'Fifty years of contractility research post sliding filament hypothesis', *Journal of Muscle Research & Cell Motility* **25**(6), 475–482.

Shaffer, J. F., Kensler, R. W. & Harris, S. P. (2009), 'The myosin-binding protein c motif binds to f-actin in a phosphorylation-sensitive manner', *Journal of Biological Chemistry* **284**(18), 12318–12327.

Shear, D. B. (1970), 'Electrostatic forces in muscle contraction', *Journal of theoretical biology* **28**(3), 531–546.

Shih, Y.-H., Dvornikov, A. V., Zhu, P., Ma, X., Kim, M., Ding, Y. & Xu, X. (2016), 'Exon-and contraction-dependent functions of titin in sarcomere assembly', *Development* **143**(24), 4713–4722.

Shimomura, T., Iwamoto, H., Doan, T. T. V., Ishiwata, S., Sato, H. & Suzuki, M. (2016), 'A beetle flight muscle displays leg muscle microstructure', *Biophysical journal* **111**(6), 1295–1303.

Shorten, P. & Sneyd, J. (2009), 'A mathematical analysis of obstructed diffusion within skeletal muscle', *Biophysical journal* **96**(12), 4764–4778.

Sia, S. K., Li, M. X., Spyracopoulos, L., Gagné, S. M., Liu, W., Putkey, J. A. & Sykes, B. D. (1997), 'Structure of cardiac muscle troponin c unexpectedly reveals a closed regulatory domain', *Journal of Biological Chemistry* **272**(29), 18216–18221.

Smith, D. A. (2014), 'Electrostatic forces or structural scaffolding: what stabilizes the lattice spacing of relaxed skinned muscle fibers?', *Journal of theoretical biology* **355**, 53–60.

Smith, L., Tainter, C., Regnier, M. & Martyn, D. (2009), 'Cooperative cross-bridge activation of thin filaments contributes to the frank-starling mechanism in cardiac muscle', *Biophysical journal* **96**(9), 3692–3702.

Smith, N. P., Barclay, C. J. & Loiselle, D. S. (2005), 'The efficiency of muscle contraction', *Progress in biophysics and molecular biology* **88**(1), 1–58.

Solaro, R. J., Rosevear, P. & Kobayashi, T. (2008), 'The unique functions of cardiac troponin i in the control of cardiac muscle contraction and relaxation', *Biochemical and biophysical research communications* **369**(1), 82–87.

Sotavalta, O. (1953), 'Recordings of high wing-stroke and thoracic vibration frequency in some midges', *The Biological Bulletin* **104**(3), 439–444.

Spudich, J. A. (2001), 'The myosin swinging cross-bridge model', *Nature reviews Molecular cell biology* **2**(5), 387–392.

Spudich, J. A. (2014), 'Hypertrophic and dilated cardiomyopathy: four decades of basic research on muscle lead to potential therapeutic approaches to these devastating genetic diseases', *Biophysical journal* **106**(6), 1236–1249.

Spudich, J. A. (2015), 'The myosin mesa and a possible unifying hypothesis for the molecular basis of human hypertrophic cardiomyopathy', *Biochemical Society Transactions* **43**(1), 64–72.

Squire, J. (2012), *The structural basis of muscular contraction*, Springer Science & Business Media.

Squire, J. M. (1997), 'Architecture and function in the muscle sarcomere', *Current opinion in structural biology* **7**(2), 247–257.

Squire, J. M. (2016), 'Muscle contraction: Sliding filament history, sarcomere dynamics and the two huxleys', *Global cardiology science & practice* **2016**(2).

Squire, J. M. & Knupp, C. (2005), 'X-ray diffraction studies of muscle and the crossbridge cycle', *Advances in protein chemistry* **71**, 195–255.

Squire, J. M. & Morris, E. P. (1998), 'A new look at thin filament regulation in vertebrate skeletal muscle', *The FASEB Journal* **12**(10), 761–771.

Stelzer, J. E., Dunning, S. B. & Moss, R. L. (2006), 'Ablation of cardiac myosin-binding protein-c accelerates stretch activation in murine skinned myocardium', *Circulation research* **98**(9), 1212–1218.

Stelzer, J. E., Fitzsimons, D. P. & Moss, R. L. (2006), 'Ablation of myosin-binding protein-c accelerates force development in mouse myocardium', *Biophysical journal* **90**(11), 4119–4127.

Sugi, H., Iwamoto, H., Akimoto, T. & Kishi, H. (2003), 'High mechanical efficiency of the cross-bridge powerstroke in skeletal muscle', *Journal of experimental biology* **206**(7), 1201–1206.

Syme, D. A. & Josephson, R. K. (2002), 'How to build fast muscles: synchronous and asynchronous designs', *Integrative and comparative biology* **42**(4), 762–770.

Takada, F., Vander Woude, D. L., Tong, H.-Q., Thompson, T. G., Watkins, S. C., Kunkel, L. M. & Beggs, A. H. (2001), 'Myozenin: an α-actinin-and γ-filamin-binding protein of skeletal muscle z lines', *Proceedings of the National Academy of Sciences* **98**(4), 1595–1600.

Tanner, B. C., Daniel, T. L. & Regnier, M. (2007), 'Sarcomere lattice geometry influences cooperative myosin binding in muscle', *PLoS Comput Biol* **3**(7), e115.

Tanner, B. C., Daniel, T. L. & Regnier, M. (2012), 'Filament compliance influences cooperative activation of thin filaments and the dynamics of force production in skeletal muscle', *PLoS Comput Biol* **8**(5), e1002506.

Tanner, B. C., Regnier, M. & Daniel, T. L. (2008), 'A spatially explicit model of muscle contraction explains a relationship between activation phase, power and atp utilization in insect flight', *Journal of Experimental Biology* **211**(2), 180–186.

Tidball, J. G. & Daniel, T. L. (1986), 'Myotendinous junctions of tonic muscle cells: structure and loading', *Cell and tissue research* **245**(2), 315–322.

Tobacman, L. S. (1996), 'Thin filament-mediated regulation of cardiac contraction', *Annual review of physiology* **58**(1), 447–481.

Tonino, P., Kiss, B., Strom, J., Methawasin, M., Smith, J. E., Kolb, J., Labeit, S. & Granzier, H. (2017), 'The giant protein titin regulates the length of the striated muscle thick filament', *Nature communications* **8**(1), 1–11.

Tregear, R. & Squire, J. (1973), 'Myosin content and filament structure in smooth and striated muscle', *Journal of Molecular Biology* **77**(2), 279–290.

Trinick, J. (1996), 'Cytoskeleton: titin as a scaffold and spring', *Current Biology* **6**(3), 258–260.

Tskhovrebova, L. & Trinick, J. (2012), 'Making muscle elastic: the structural basis of myomesin stretching', *PLoS Biol* **10**(2), e1001264.

Tskhovrebova, L., Trinick, J., Sleep, J. & Simmons, R. (1997), 'Elasticity and unfolding of single molecules of the giant muscle protein titin', *Nature* **387**(6630), 308.

Tu, M. S. & Daniel, T. L. (2004), 'Cardiac-like behavior of an insect flight muscle', *Journal of Experimental Biology* **207**(14), 2455–2464.

Tune, T. C., Ma, W., Irving, T. & Sponberg, S. (2020), 'Nanometer-scale structure differences in the myofilament lattice spacing of two cockroach leg muscles correspond to their different functions', *Journal of Experimental Biology* **223**(9).

Tyska, M., Hayes, E., Giewat, M., Seidman, C., Seidman, J. & Warshaw, D. (2000), 'Single-molecule mechanics of r403q cardiac myosin isolated from the mouse model of familial hypertrophic cardiomyopathy', *Circulation research* **86**(7), 737–744.

Wackerhage, H., Hoffmann, U., Essfeld, D., Leyk, D., Mueller, K. & Zange, J. (1998), 'Recovery of free adp, pi, and free energy of atp hydrolysis in human skeletal muscle', *Journal of applied physiology* **85**(6), 2140–2145.

Wakabayashi, K., Sugimoto, Y., Tanaka, H., Ueno, Y., Takezawa, Y. & Amemiya, Y. (1994), 'X-ray diffraction evidence for the extensibility of actin and myosin filaments during muscle contraction', *Biophysical journal* **67**(6), 2422–2435.

Wang, K., McClure, J. & Tu, A. (1979), 'Titin: major myofibrillar components of striated muscle', *Proceedings of the National Academy of Sciences* **76**(8), 3698–3702.

Wang, Y. & Fuchs, F. (1994), 'Length, force, and ca (2+)-troponin c affinity in cardiac and slow skeletal muscle', *American Journal of Physiology-Cell Physiology* **266**(4), C1077–C1082.

Warren, C. M., Kobayashi, T. & Solaro, R. J. (2009), 'Sites of intra-and intermolecular cross-linking of the n-terminal extension of troponin i in human cardiac whole troponin complex', *Journal of Biological Chemistry* **284**(21), 14258–14266.

Williams, C. D., Regnier, M. & Daniel, T. L. (2010), 'Axial and radial forces of cross-bridges depend on lattice spacing', *PLoS computational biology* **6**(12), e1001018.

Williams, C. D., Regnier, M. & Daniel, T. L. (2012), 'Elastic energy storage and radial forces in the myofilament lattice depend on sarcomere length', *PLoS computational biology* **8**(11), e1002770.

Williams, C. D., Salcedo, M. K., Irving, T. C., Regnier, M. & Daniel, T. L. (2013), 'The length–tension curve in muscle depends on lattice spacing', *Proceedings of the Royal Society B: Biological Sciences* **280**(1766), 20130697.

Williams, C. & Holt, N. (2018), 'Spatial scale and structural heterogeneity in skeletal muscle performance', *Integrative and Comparative Biology* **58**(2), 163–173.

Willis, M. S., Schisler, J. C., Portbury, A. L. & Patterson, C. (2009), 'Build it up–tear it down: protein quality control in the cardiac sarcomere', *Cardiovascular research* **81**(3), 439–448.

Winkelmann, D. A., Forgacs, E., Miller, M. T. & Stock, A. M. (2015), 'Structural basis for drug-induced allosteric changes to human β-cardiac myosin motor activity', *Nature communications* **6**(1), 1–10.

Woodhead, J. L., Zhao, F.-Q., Craig, R., Egelman, E. H., Alamo, L. & Padrón, R. (2005), 'Atomic model of a myosin filament in the relaxed state', *Nature* **436**(7054), 1195–1199.

Xu, C., Craig, R., Tobacman, L., Horowitz, R. & Lehman, W. (1999), 'Tropomyosin positions in regulated thin filaments revealed by cryoelectron microscopy', *Biophysical journal* **77**(2), 985–992.

Yotti, R., Seidman, C. E. & Seidman, J. G. (2019), 'Advances in the genetic basis and pathogenesis of sarcomere cardiomyopathies', *Annual review of genomics and human genetics* **20**, 129–153.

Young, P., Ferguson, C., Bañuelos, S. & Gautel, M. (1998), 'Molecular structure of the sarcomeric z-disk: two types of titin interactions lead to an asymmetrical sorting of α-actinin', *The EMBO journal* **17**(6), 1614–1624.

Yuan, C. C., Ma, W., Schemmel, P., Cheng, Y. S., Liu, J., Tsaprailis, G., Feldman, S., Southgate, A. A. & Irving, T. C. (2015), 'Elastic proteins in the flight muscle of manduca sexta', *Archives of biochemistry and biophysics* **568**, 16–27.

Zaunbrecher, R. J., Abel, A. N., Beussman, K., Leonard, A., von Frieling-Salewsky, M., Fields, P. A., Pabon, L., Reinecke, H., Yang, X., Macadangdang, J. et al. (2019), 'Cronos titin is expressed in human cardiomyocytes and necessary for normal sarcomere function', *Circulation* **140**(20), 1647–1660.

Zou, J., Tran, D., Baalbaki, M., Tang, L. F., Poon, A., Pelonero, A., Titus, E. W., Yuan, C., Shi, C., Patchava, S. et al. (2015), 'An internal promoter underlies the difference in disease severity between n-and c-terminal truncation mutations of titin in zebrafish', *Elife* **4**, e09406.

CHAPTER 2: SUPPLEMENT

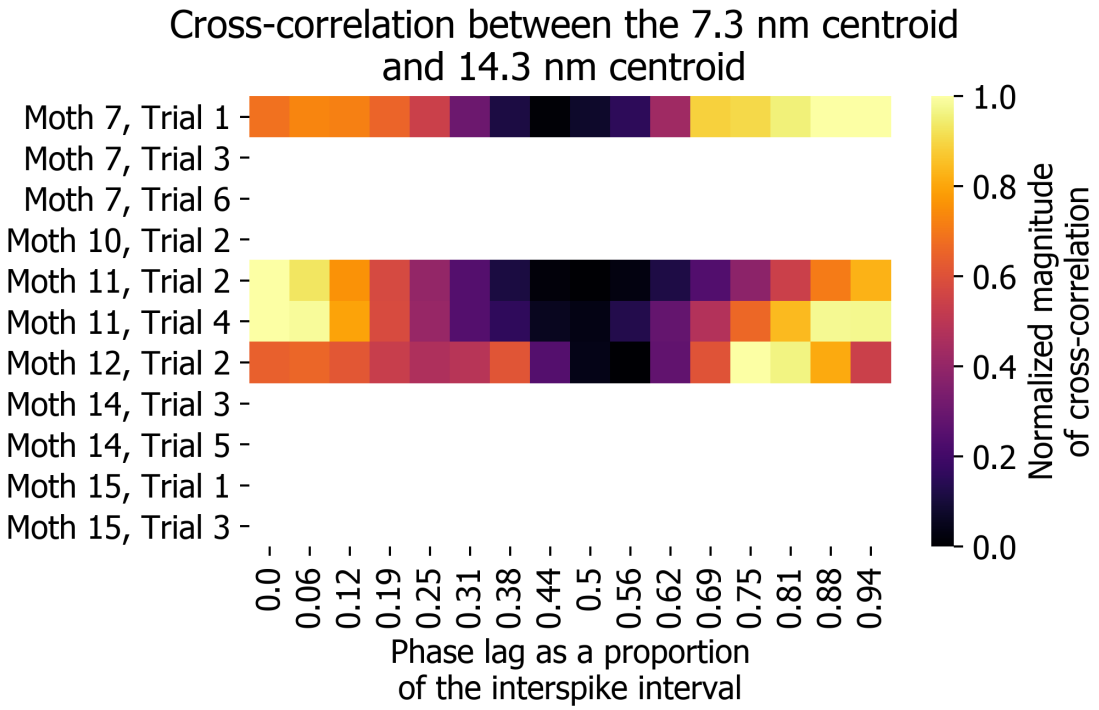

Figure 8: **The maximum correlation between the 7.3 nm repeat and 14.3 nm repeat occurs at small but variable phase offsets across trials.** The signals are minimally correlated at a phase offset midway through the interspike interval (the duration of time between one muscle activation and the next). The M6 and M3 may record different structures, explaining why signals are not perfectly phase locked. The reason why this is the case follows. X-ray diffraction takes a Fourier transform of the myofilament lattice. In short exposure images the intensities recorded by the detector due to periodic structures are hard to disambiguate from noise. By averaging many images strong traces from periodic structures emerge. Frame averaging is analogous to increasing the total photon count. Similarly, reflections close to the backstop are the composite of larger numbers of photons. Signal averaging is more important when there is a low signal to noise ratio. For labile structures like cross-bridges, a large photon count is needed to create a crisp signal that rises above the background noise. In contrast the more stable thick filament backbone's periodicity is less dependent on averaging. Hence, the intensity due to the myosin crown repeat predominates close to the backstop, but as the distance from the backstop increases, the signals from labile structures will become more diffuse, while those from stable structures retain their integrity. Therefore the M6 and M3 may record different structures, explaining why signals may not be perfectly phase-locked.

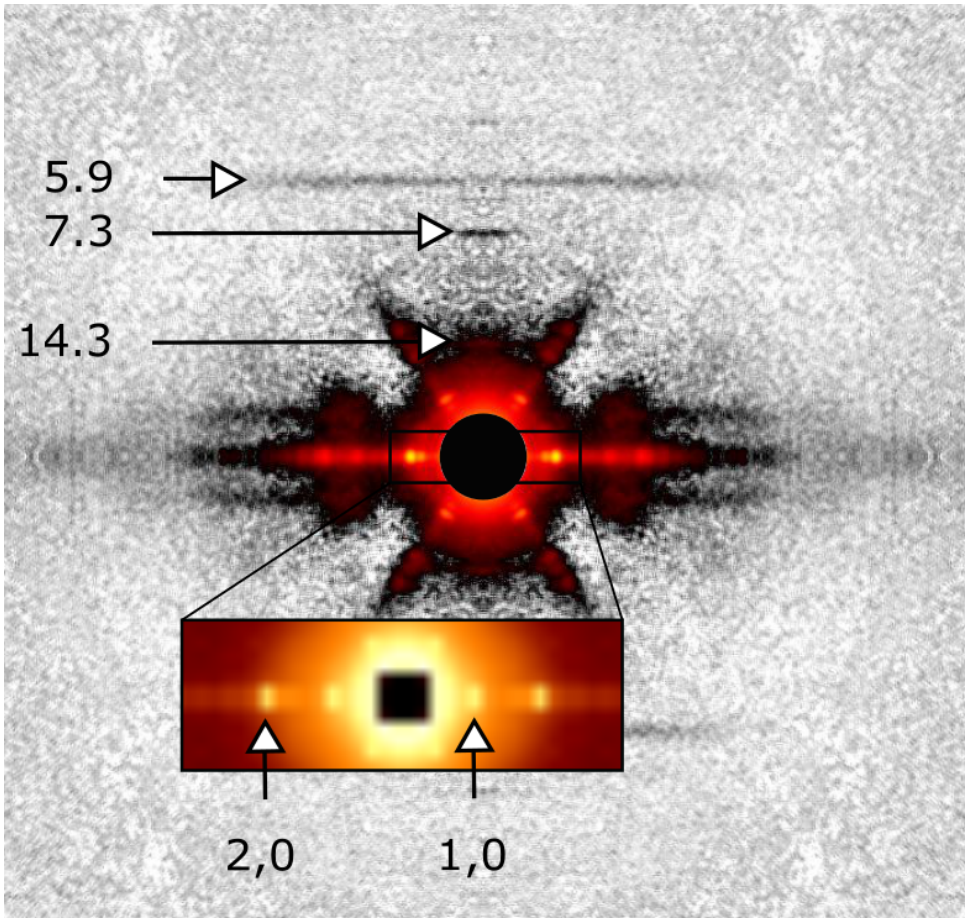

Figure 9: **A single, x-ray diffraction image from Moth 15 trial 1.** Greater clarity could have been gained from longer exposures at the expense of reduced time resolution. Since the conversion from pixel to nanometer space by Bragg's law is non-linear, error disproportionately effects data recorded close to the backstop. An error of one pixel corresponds to 0.04 nm for the 7.3 nm spacing, while for the 5.9 actin off meridional an error of one pixel corresponds to an error of 0.03 nm. Meanwhile for the 14.3 nm reflection and the lattice spacing, which are both closer to the center of the image, an error of one pixel corresponds to 0.17 nm and 1.68 nm respectively.

Table 2: The optimal hyperparameters determined by the genetic algorithm for each trial are listed. The white cells are those that were used for the case where the model was trained on 75% of the data and tested on the remaining 25% of the data within a trial. The gray cells are the the parameters that were used for the case where the model was trained on all trials except for the with-held trial upon which it was tested.

xGBoost model hyperparameters							
Trial	**learningrate**	**nestimators**	**maxdepth**	**minchildweight**	**gamma**	**subsample**	**colsamplebytree**
m07_t01_15	0.16	241.0	7.0	5.1	0.04	0.77	0.79
m07_t03_15	0.26	98.0	1.0	1.53	1.19	0.29	0.64
m07_t06_15	0.05	135.0	3.0	0.72	1.22	0.62	0.34
m10_t02_16	0.9	134.0	2.0	2.1	1.81	0.55	0.27
m11_t02_16	0.45	111.0	9.0	7.38	2.37	0.59	0.59
m11_t04_16	0.44	204.0	2.0	5.96	0.89	0.8	0.75
m12_t02_16	0.43	98.0	1.0	7.18	0.79	0.21	0.42
m14_t05_16	1.0	160.0	4.0	10.0	7.85	1.0	0.4
m14_t03_16	0.22	248.0	8.0	0.16	0.51	0.62	0.48
m15_t01_16	0.29	30.0	7.0	6.8	0.73	0.82	0.43
m15_t03_16	0.34	48.0	2.0	6.68	0.01	0.93	0.23
m07_t01_15	0.31	198.0	5.0	10.0	7.95	0.85	0.91
m07_t03_15	0.11	10.0	4.0	10.0	0.61	0.63	0.92
m07_t06_15	0.05	26.0	3.0	6.69	7.42	0.76	0.13
m10_t02_16	0.21	54.0	4.0	5.72	4.68	0.67	0.79
m11_t02_16	0.06	217.0	1.0	9.41	7.24	1.0	0.36
m11_t04_16	0.35	30.0	4.0	9.66	9.13	0.74	0.9
m12_t02_16	0.07	19.0	6.0	6.37	5.45	0.77	0.4
m14_t05_16	0.51	319.0	7.0	10.0	7.39	0.62	0.49
m14_t03_16	0.59	55.0	7.0	5.18	2.58	0.99	0.88
m15_t01_16	0.09	136.0	5.0	10.0	8.6	0.21	0.52
m15_t03_16	0.25	179.0	10.0	10.0	6.04	0.12	0.1

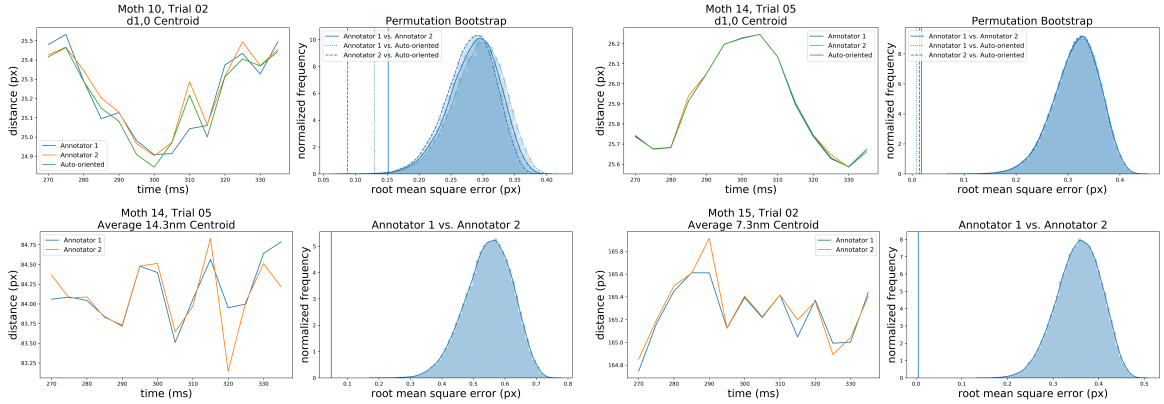

Figure 10: **Quantification of inter-annotator error.** To verify that there was not significant inter-annotator variation we compared their pixel space annotations for a time series (a stack of images). For the d1,0 data we also compared a version of Musclex with an auto-orienting patch to Musclex. To quantify the variation between annotators shown in the time series plots on the left hand side, we computed a Root Mean Square Goodness of Fit (RMS GOF) between the two annotated image stacks. This value was compared to the distribution of RMS GOFs for 10,000 random permutations of the time series. We performed this for 4 trials with 15 time points from the d1,0 centroid, the 7.3 nm centroid and the 14.3 nm centroid. Two of the 4 cross validated trials weren't used in the final analysis; in one case because the muscle activation couldn't be determined from the EMG, and in the other case because the moth quit flying in the middle of the trial. The right hand plots show the distribution of RMS values calculated from the permutation bootstrap, with vertical lines denoting the RMS value for each annotation comparison. The annotator-comparison RMS GOF values are outside of the permutation bootstrap distribution, suggesting that the results are not explained by chance. The low annotator-comparison RMS GOF values indicate that the variation between the annotators was low. In addition to the RMS GOF, we calculated a p-value for each trial. The p-value addresses the null hypothesis that the order of the data does not affect the RMS GOF value, with a low p-value indicating that the annotations are consistent in their placement within the series. A low RMS GOF value indicates low disparity in annotator recorded values. The distributions for our data were typically unimodal. The average RMS of the d1,0 centroid was 0.07, and the average p value was 0.0008. The average RMS of the 7.3 nm was 0.70 and the average p value was 0.02. The average RMS of the 14.3 nm was 0.41, while the p value was 0.03.

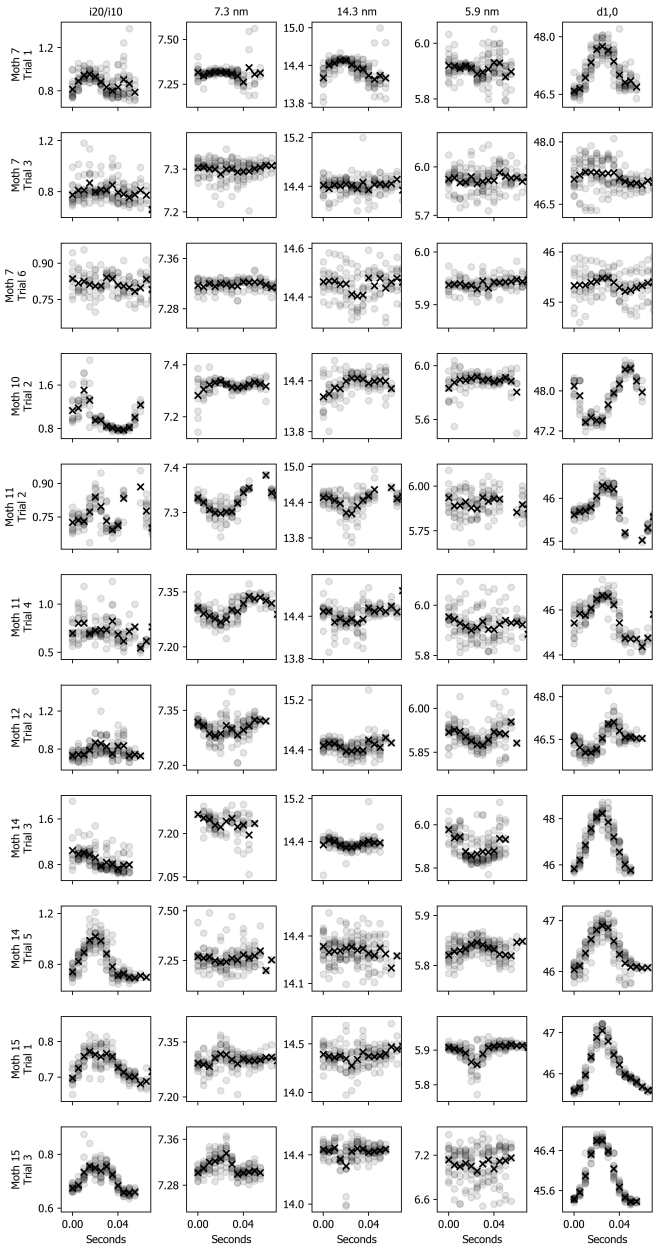

Figure 11: **All of the data we collected is shown in this panel of STAs.**

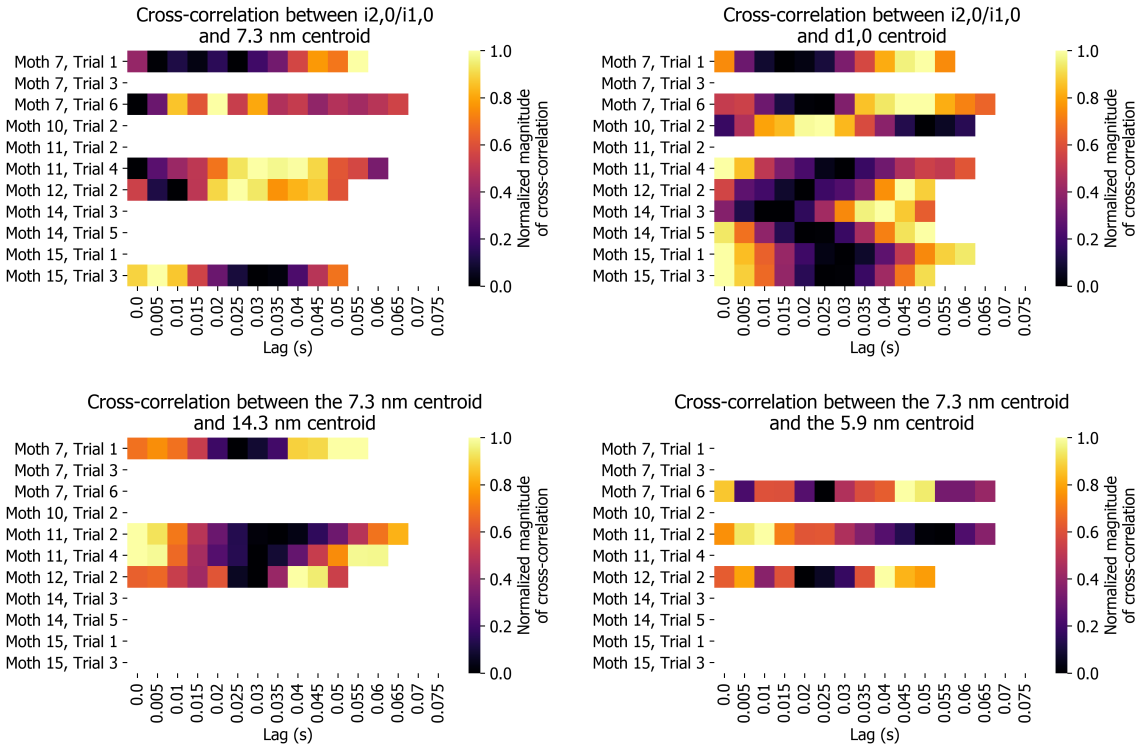

Figure 12: **The cross-correlation between a pair of signals given an offset of the signals measured in seconds shows inconsistent phase relationships across trials**. This is in contrast to the other plots of cross correlation as a function of proportion of interspike interval. In none of these cases does a given offset in seconds yield the maximum correlation across trials.